THE ORDERED COMPOUND V_6C_5 -- ITS STRUCTURE AND SUSCEPTIBILITY TO ELECTRON RADIATION DAMAGE

by

J. D. VENABLES

A dissertation submitted to the
University of Warwick
for admission to the degree of
Doctor of Philosophy

MEMORANDUM

This dissertation is submitted to the University of Warwick in support of my application for admission to the degree of Doctor of Philosophy. It contains an account of my own work performed at the Research Institute for Advanced Studies in the periods October 1967 to August 1968 and August 1969 to June 1970 under the supervision of Dr. A.R.C. Westwood, and at the School of Physics of the University of Warwick in the period August 1968 to August 1969 under the supervision of Dr. M. H. Lewis. No part of it has been used previously in a degree thesis submitted to this or any other university. The work described in this thesis is the result of my own independent research except where specifically acknowledged in the text.

June 1970

J. D. VENABLES

PUBLICATIONS

Certain parts of the work reported in this thesis have been published in scientific journals as follows:

(1) The paper "Structure of the Ordered Compound V_6C_5," Phil. Mag., 18, 177 (1968), written with D. Kahn and R. G. Lye contains an account of the ordering effects described in Part I of this thesis.

(2) The work described in Part II forms the basis of a paper "Radiation Damage of Ordered V_6C_5 by Electron Microscope Beam Bombardment," Phil. Mag., 19, 565 (1969), written with R. G. Lye.

Further parts of this thesis may be submitted for publication elsewhere in due course.

ACKNOWLEDGEMENTS

I am extremely grateful to Professor A. J. Forty, Dr. A.R.C. Westwood (Deputy Director of RIAS), and Mr. K. Jarmolow (Director of RIAS) for providing me the opportunity to undertake this joint course of study at the University of Warwick and the Research Institute for Advanced Studies (RIAS). To Dr. Westwood I owe further thanks for encouraging me to continue my education in this manner and for his advice and suggestions during the course of the work.

Many of my colleagues at RIAS and members of the School of Physics at the University have been available for discussions on a great variety of topics, but in particular I wish to thank Dr. M. H. Lewis, my advisor, Dr. D. Kahn, and Dr. J. P. Martin for their helpful suggestions.

To my assistant at RIAS, Mr. M. H. Meyerhoff I am deeply indebted for developing the technique used to prepare microscope foils and for his capable assistance on many other aspects of the work. Thanks are also due Mr. W. Precht who grew the single crystal specimens, and to Mrs. M. Stevens for her care and attention in typing the thesis.

The financial support provided by NASA Research Division, Code RRM, Materials Research Branch, under Contract NASw-1290, and the continued interest shown in this work by Dr. R. R. Nash and Dr. I. Weinberg of NASA Headquarters is greatly appreciated.

Finally, I owe a special debt of gratitude to Dr. R. G. Lye, RIAS, who taught me and counseled me during many hours of discussion, and who provided encouragement when it was most needed.

ABSTRACT

The crystallographic structure of vanadium carbide having a carbon-to-metal atom ratio close to 0.83 has been determined from electron diffraction and nuclear magnetic resonance (NMR) studies. Material of this composition occurs within the nominally cubic (rocksalt) phase field of the vanadium-carbon phase diagram, but in this investigation it is shown that the structure is modified substantially by an unusual type of ordering that is associated with the carbon sublattice. The ordered structure is based on two interpenetrating fcc lattices, only one of which (the metal lattice) is completely occupied. The other is only 83% filled, but the carbon atoms (and carbon vacancies) are distributed in an ordered manner on the available lattice sites. As a consequence of ordering, the electron diffraction patterns exhibit supplementary spots which may be analyzed to obtain information regarding the symmetry and size of the superlattice unit cell. Moreover, the NMR of the principal vanadium isotope, V^{51}, exhibit spectra which provide information about the disposition of carbon atoms within the unit cell.

In the proposed structure, which belongs to the trigonal space group $P3_1$, or its enantiomorph $P3_2$, the carbon atoms and carbon vacancies are arranged so that all the vanadium atoms have

exactly five nearest neighbor carbon atoms. The observation that ordering in material of this composition leads to a distribution of atoms that is homogeneous on an atomic scale is consistent with the electronic structure of vanadium carbide as it is currently understood, and suggests that it is appropriate to refer to the ordered compound as V_6C_5.

When the ordered compound is examined for extended periods of time in a 100 kV electron microscope, it is observed that the material becomes slowly disordered. Several possible explanations were considered for this effect, but it has been concluded that the disordering results from the displacement of carbon atoms by impinging electrons (i.e., by radiation damage). To determine the magnitude of the displacement threshold, studies have been made of the disordering rate under electron bombardment at energies from 33 keV to 100 keV, using a Faraday cup to measure superlattice spot intensities. The results have been compared with a theory for the damage process, from which it is concluded that the displacement energy of carbon atoms in V_6C_5 is 5.4 eV.

This value is unexpectedly low in comparison with the values that have been reported for most other materials, but it is consistent with a simple model for the displacement mechanism which appears to account for the threshold energy in this, and a number of other solids also. According to this model, observable damage will occur

in a solid only if the displaced atom has sufficient energy to (1) create a vacancy, (2) permit transferring the energy pulse for n interatomic distances through the lattice to a position at which the vacancy-interstitial pair is stable, and (3) form an interstitial at the terminal point of the disturbance. Calculations show that for most solids, the threshold energy is determined principally by mechanisms (2) and (3), but for V_6C_5 only the first process is important since a large number of vacant sites are available in the carbon sublattice to accept a displaced atom with the expenditure of very little energy.

The fact that V_6C_5 can be disordered <u>in situ</u> by electron microscope beam bombardment has presented an unusual opportunity to study the effect of electron channelling on radiation damage rates. It has long been a question whether significantly less damage occurs when a sample to be irradiated by energetic electrons is oriented for "anomalous transmission," a phenomenon which is similar to the Borrmann effect for x-rays and to channelling for ion beams. Experiments with ion beams have demonstrated that the damage rate in channelling orientations can be 10 times less than in random orientations, but no analogous experiments have been performed previously for electron damage because of the small angular separation between the channelling and de-channelling orientations. The

small divergence of the electron microscope beam, the ability to orient the crystal with great precision, and the fact that the full analytical capabilities of the electron microscope can be used to monitor the damage process in V_6C_5 have now made such an experiment possible.

Finally, studies have been made of the re-ordering kinetics of radiation damaged V_6C_5 to determine the activation energy for carbon diffusion. These measurements, which have been made in a temperature range about 1000°C below that for which previous values have been obtained, have important implications for the mechanical properties of V_6C_5 and provide an explanation for the extremely short time constant associated with the order-disorder transformation in this material.

CONTENTS

PART I

STRUCTURE OF V_6C_5

PART II

RADIATION DAMAGE OF V_6C_5

BY ELECTRON MICROSCOPE

BEAM BOMBARDMENT

PART III

AN OVERVIEW

PART I

STRUCTURE OF V_6C_5

CHAPTER ONE

INTRODUCTION

1.1 A brief review of ordering in the "cubic" carbides

The transition metal carbides belong to the class of refractory hard metals that are formed by reacting a Group IV, V, or VI transition element with one of the small nonmetals such as boron, carbon, nitrogen, or oxygen. The unusual properties of these compounds have been discussed by Schwarzkopf and Kieffer,[1] Kieffer and Benesovsky,[2] Storms,[3] Goldschmidt,[4] Hollox,[5] and Williams,[6] but generally they are characterized by their high melting points, extreme hardness, metallic reflectivity, and metallic electrical conductivities that are comparable to those of their parent metals. Within varying composition limits all of the Group IV and V carbides exhibit a nominally cubic structure in which the metal atoms occupy close packed fcc positions with the nonmetal atoms arranged in the octahedral interstices.[1-3] This structure is isomorphous with that of NaCl, but the metallic nature of the carbides suggests that it is more appropriate to consider them as fcc metals which are stabilized by the presence of carbon atoms.[7] This interpretation has received support from the description of bonding in TiC and VC derived by Lye[8-10] (to be discussed below) and the observation by William and Schaal[11] that the slip system

of TiC, {111} ⟨110⟩, corresponds to that of fcc metals, rather than to that of NaCl, in which slip on {111} planes is inhibited by the ionic character of its bonding.

Studies of the phase equilibrium in the MC carbides have shown that they retain their stabilized fcc structure over a relatively wide phase field. For example, Storms[3] phase diagram for the titanium-carbon system indicates that the range of homogeneity of TiC_x, where x is the carbon-to-metal atom ratio, extends from x = 0.53 to 0.96. The range for VC_x is somewhat more limited because of the presence of a V_2C phase at the low carbon end and a broad two phase VC + C region at high carbon concentrations, but as indicated by Adelsberg and Cadoff,[12] the carbon-to-metal ratio can vary from x = 0.67 to 0.89.

Lye[8-10] has proposed an explanation for the wide homogeneity range of VC and TiC which is based upon the current understanding of their unusual electronic structure. According to the results of his semi-empirical LCAO band structure calculations, the outer electrons of the six metal atoms surrounding a carbon atom overlap onto the carbon atom site depositing a negative charge there. This raises the potential energy of electrons on the carbon atoms enough to elevate electrons in the upper portion of the bands derived from carbon 2p states above those of vacant states in the 3d and 4s

bands associated with the metal atoms. To minimize their energy these electrons are redistributed into the lower lying bands, mostly 3d bands, where they occupy normally vacant states. Since these states make important contributions to the total cohesive energy,[9] their degree of occupancy plays a major role in determining the phase changes which accompany variations in stoichiometry.

In VC those d-states whose orbitals overlap in a bonding configuration become completely filled when the carbon-to-metal atom ratio is approximately 0.91.[13] Beyond this composition, additional carbon atoms contribute electrons to antibonding d-states, but to avoid this it might be expected that carbon would segregate to a more energetically favorable form. The presence of a transformation from single phase VC to VC + C at a carbon-to-metal atom ratio of approximately 0.89[12] suggests that the position of the upper phase boundary in VC can be accounted for by the tendency to avoid the occupation of antibonding states.

No such restriction is imposed upon the carbon concentration in TiC because the bonding states are not completely filled even at the stoichiometric limit.[13] This slight difference in the electronic structure of TiC, relative to that of VC, is reflected in the ability of TiC to attain a carbon-to-metal atom ratio which is very close to unity.[3] Whether TiC can be prepared at precisely the

stoichiometric composition remains a controversial question,[3] but in spite of this uncertainty, it appears that the position of the upper phase boundaries for these materials can be explained in a semi-quantitative manner on the basis of Lye's model for their electronic structure.

When the carbon concentration is decreased to a value well below that at the upper phase boundary, the number of electrons associated with metal atom states diminishes toward the normal value for the pure metal. In TiC the titanium atoms achieve their normal complement of electrons at a carbon-to-metal atom ratio of 0.6 and, as suggested by Lye,[8] it is not unreasonable to expect a phase transformation to the usual hcp structure at this composition. Support for this description of the behavior of TiC in terms of the occupation of metal atom electronic states is obtained from Storms[3] phase diagram which places the phase boundary between TiC and β - Ti + TiC at $x = 0.63$. Similar arguments undoubtedly apply to other carbides, but in some cases, e.g. VC, the situation is complicated by the presence of other phases. These phases may also be understood in terms of the electronic structure, but further discussion of this question will be deferred until Chapter Nine.

On the basis of these considerations, the large breadth of the homogeneity range and the significant deviation of the upper phase boundary from integral stoichiometry are readily explained as

intrinsic features of the carbides. Thus, the electronic structure of these compounds permits and sometimes enforces the presence of an unusually high (carbon) vacancy concentration, which can be orders of magnitude greater than that established normally by thermal equilibrium requirements. No study of the carbides would be complete unless the behavior imposed by such a large vacancy content were understood, and, in particular, it would seem reasonable to expect that some physical and mechanical properties would be sensitive to the degree of order exhibited by the carbon atoms and carbon vacancies on their sublattice.

Among the first reported attempts to look for ordering in non-stoichiometric carbides was the work of Gorbunov et al. in 1961.[14] Using neutron diffraction, to take advantage of the relatively large scattering cross-section of carbon atoms for this type of radiation, they concluded that the vacancies are distributed randomly in TiC_x throughout the entire composition range. Later, similar experiments by Goretzki[15] indicated that carbon vacancy ordering does occur in TiC but only in the composition range $x = 0.64$ to $x = 0.72$. Goretzki rationalized these somewhat divergent results by claiming that Gorbunov et al. had not examined material of the appropriate compositions.

Neutron diffraction techniques have also been applied to the study of $NbC_{0.75}$ and $TaC_{0.75}$ by Zubkov et al.[16] who observed superlattice lines that they attributed to ordering in the carbon

sublattice. Unfortunately, these studies were restricted to the one composition, x = 0.75, since the authors were attempting to demonstrate a particular point derived from energy considerations based on Bilz's[17] electronic band structure calculations, namely, that nearest neighbor carbon vacancy pairs should be unstable in the Group V carbides. (It can be shown[16] that the only way to avoid such pairs in an MC carbide having a carbon-to-metal ratio x = 0.75, is through ordering of the vacancies.) Thus, the degree of order exhibited throughout the remainder of the MC phase field for these materials is uncertain.

Conclusive evidence for ordering in vanadium carbide was reported in 1966 by de Novion, Lorenzelli and Costa,[18] who observed weak superlattice lines in Debye-Scherer X-ray patterns of $VC_{0.88}$ powders prepared by heating the metal hydride in contact with graphite. They attributed the supplementary lines to an ordered distribution of carbon vacancies, and, from an analysis of the observed systematic extinctions, concluded that $VC_{0.88}$ (V_8C_7) should be described in terms of a cubic unit cell with symmetry $P4_332$ or $P4_132$ and a parameter, $a_o = 8.33$ Å, twice that of the NaCl cell. In associated work, Froidevaux and Rossier[19] were able to confirm the vacancy ordering described by de Novion et al.[18] by investigating the nuclear magnetic resonance (NMR) of the principal vanadium isotope, V^{51}, in VC specimens. The resonance spectra exhibited a line

splitting characteristic of nuclei with a quadrupole moment that are situated in a non-cubic local environment. This observation was not unexpected since missing carbon atoms destroy the local cubic symmetry; however Froidevaux and Rossier were able to associate specific peaks in the spectra with nuclei in sites having 0,1,2, and 3 nearest neighbor carbon vacancies. The relative population of these sites differed substantially from that expected from a random distribution of vacancies, and on this basis they concluded that the carbon atoms were arranged in an ordered manner.

Although the presence of long range order in $VC_{0.88}$ was definitely established through combined X-ray diffraction and NMR measurements, the situation in material having a lower carbon concentration was somewhat less clear. According to de Novion et al.,[18] the cubic superlattice X-ray line intensities, which are functions of the long range order parameter, suffered a marked decrease as the carbon concentration was reduced below that of V_8C_7. On the other hand, the experimental distribution of vanadium sites having 0,1,2 and 3 nearest neighbor carbon vacancies (as determined by NMR[19]) differed substantially from a random distribution throughout the entire composition range. Since the NMR technique does not, in itself, readily distinguish between long and short range order, these apparently divergent results could be rationalized if it were assumed

that the distribution of additional vacancies in the low carbon material exhibited short range order only. In the following chapters, however, it will be shown that the situation is much more complex than this interpretation suggests and that another ordered structure, which is not readily detected by X-ray diffraction, forms when the carbon concentration is slightly below that of V_8C_7.

1.2 Scope of the present work

Transmission electron microscopy and selected area diffraction have, for many years, been successfully applied to the study of ordering in metal alloys but only recently have they been shown to be useful for studying ordered interstitial compounds. For example, the power of the techniques for sensing relatively light elements, even when they are present in a host matrix of heavier atoms, is illustrated by the work of Van Landuyt et al.[20] who investigated the distribution of (oxygen) interstitials in Nb. These authors observed supplementary electron diffraction spots and a domain structure in vacuum annealed Nb which they attributed to ordering of the interstitial oxygen atoms. From an analysis of the diffraction data, a unit cell having monoclinic symmetry was deduced for the superlattice and the domain structure was explained in terms of six equivalent orientations of the ordered lattice with respect to that of the host metal.

Until the present study these techniques had not been applied to the carbides because the materials generally available were either powders, sintered compacts, or small crystals that were not suitable for obtaining thinned sections. However, the successful production of large single crystals of the carbides in a crystal growing program associated with this investigation has made such a study feasible.[21]

In a sense the scope of this work must be considered somewhat limited since only one composition of vanadium carbide, $VC_{0.84}$, has been studied in detail. However, the impetus for the investigation was not simply to collect data on a large number of materials and compositions but, rather, its aim was to obtain an improved understanding of the unusual properties that make the transition metal carbides potentially useful materials for future technology. Thus, an attempt has been made to fully characterize the structure of one particular ordered compound, V_6C_5, in the hope that such information might contribute to an understanding of the driving forces, i.e. the electronic interactions, which establish the order. Moreover, since the long range ordering observed in V_6C_5 must be expected to modify its dislocation structure and thus influence the mobility of these dislocations, it was hoped that a knowledge

of the structure would also contribute to an understanding of the mechanical behavior. This investigation will be described in Part I.

During the course of the electron microscope studies it became evident that the superlattice and domain structure exhibited by the ordered compound V_6C_5 were being disrupted by electron microscope beam bombardment. This effect is interpreted as arising because carbon atoms are displaced by the incident electrons. However, the conclusion that a material as refractory as vanadium carbide can be damaged by relatively low energy electrons is somewhat surprising and has important implications, not only for the general problem of radiation damage in solids, but also for the stability of various refractory materials employed in nuclear reactor technology (e.g. actinide series carbides and nitrides). Accordingly, the disordering phenomenon has been subjected to a detailed analysis (described in Part II) in order to obtain a quantitative value for the threshold energy required to displace a carbon atom in V_6C_5.

REFERENCES

1. P. Schwartzkopf and R. Kieffer, "Refractory Hard Metals," (The Macmillan Co., New York, 1958).

2. R. Kieffer and F. Benesovsky, "Hartstoffe," (Springer-Verlag, Vienna, 1963).

3. E. K. Storms, "The Refractory Carbides," (Academic Press, New York, 1967).

4. H. J. Goldschmidt, "Interstitial Alloys," (Plenum Press, New York, 1967).

5. G. E. Hollox, Mat. Science Eng., 3, 121 (1968).

6. W. S. Williams, Science, 152, 34 (1966).

7. D. A. Robins, Powder Metallurgy, No. 1/2, 172 (1958).

8. R. G. Lye and E. M. Logothetis, Phys. Rev., 147, 622 (1966).

9. R. G. Lye, in "Atomic and Electronic Structure of Metals," (ASM, Cleveland, Ohio, 1967).

10. R. G. Lye, G. E. Hollox, and J. D. Venables, in "Anisotropy in Single Crystal Refractory Compounds," Vol. 2, ed. F. W. Vahldiek and S. A. Mersol, (Plenum Press, New York, 1968), p. 445.

11. W. S. Williams and R. D. Schaal, J. Appl. Phys., 33, 955 (1962).

12. L. M. Adelsberg and L. H. Cadoff, J. Am. Ceram. Soc., 51, 213 (1968).

13. R. G. Lye, Private communication.

14. N. S. Gorbunov, N. A. Shishakov, and C. G. Saidkov, Izv. Akad. Nauk. SSSR, 11, 2093 (1961).

15. H. Goretzki, Phys. Stat. Sol., 20, K141 (1967).

16. V. G. Zubkov, L. B. Dubrovskaya, P. V. Gel'd, V. A. Tskhai, and Y. A. Dorafeev, Dokl. Akad. Nauk. SSSR, 184, 874 (1969).

17. H. Bilz, Z. Physik, 153, 338 (1958).

18. C. H. de Novion, R. Lorzenelli, and P. Costa, Compt. Rend., 263, 775 (1966).

19. D. Froidevaux and D. Rossier, J. Phys. Chem. Solids, 28, 1197 (1967).

20. J. Van Landuyt, R. Gevers, and S. Amelinckx, Phys. Stat. Sol., 13, 467 (1966).

21. W. Precht and G. E. Hollox, J. Crystal Growth, 3-4, 818 (1968).

CHAPTER TWO

EXPERIMENTAL DETAILS

2.1 Crystal growth

The vanadium carbide single crystals employed in this study were grown by W. Precht of RIAS, who employed the floating zone technique described by Precht and Hollox.[1] Starting rods, 18 cm long and 2 cm in diameter, were prepared by isostatic pressing to 50,000 psi an aggregate containing $VC_{0.92}$ powders (supplied by Consolidated Astronautics), small additions of vanadium metal powder to achieve the desired carbon-to-metal ratio, and 0.5 weight percent of a binder consisting of 5% polyvinyl alcohol in distilled water. After sintering at 1700°C for 2 hours in a vacuum of 10^{-5} Torr, the rods were diamond ground to a constant diameter, see fig. 2.1(a), to ensure that a uniform molten zone could be maintained during crystal growth.

The crystal growing apparatus, fig. 2.2 and 2.3, is conventional except for the provision of a heavy stainless steel outer can that allows the furnace chamber to be pressurized with 10 atmospheres of helium. This inert gas blanket is required to reduce the preferential volatilization of vanadium which occurs at rapid rates above 2000°C. The sintered rod is held between two water cooled copper chucks which can be translated up or down to move the work past the

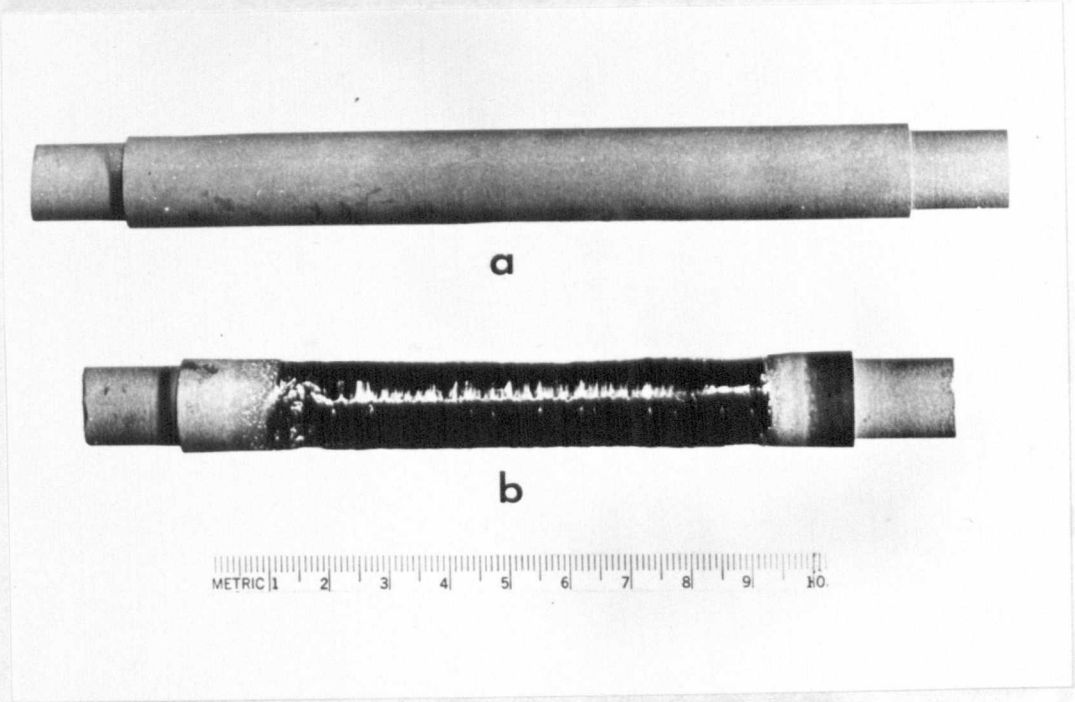

Fig. 2.1. Single crystals of $VC_{0.84}$ were prepared for this investigation by passing a molten zone along a sintered rod such as that shown in (a). The zone melted section, shown in (b), is polycrystalline near the starting end (right side of figure) but is single crystalline for the last 3/4 of its length. (After Precht and Hollox[1].)

Fig. 2.2. Float-zone apparatus used to grow single crystals of $VC_{0.84}$ employed in this investigation. Pressurized growing chamber is shown at A. (Photo courtesy of W. Precht, RIAS.)

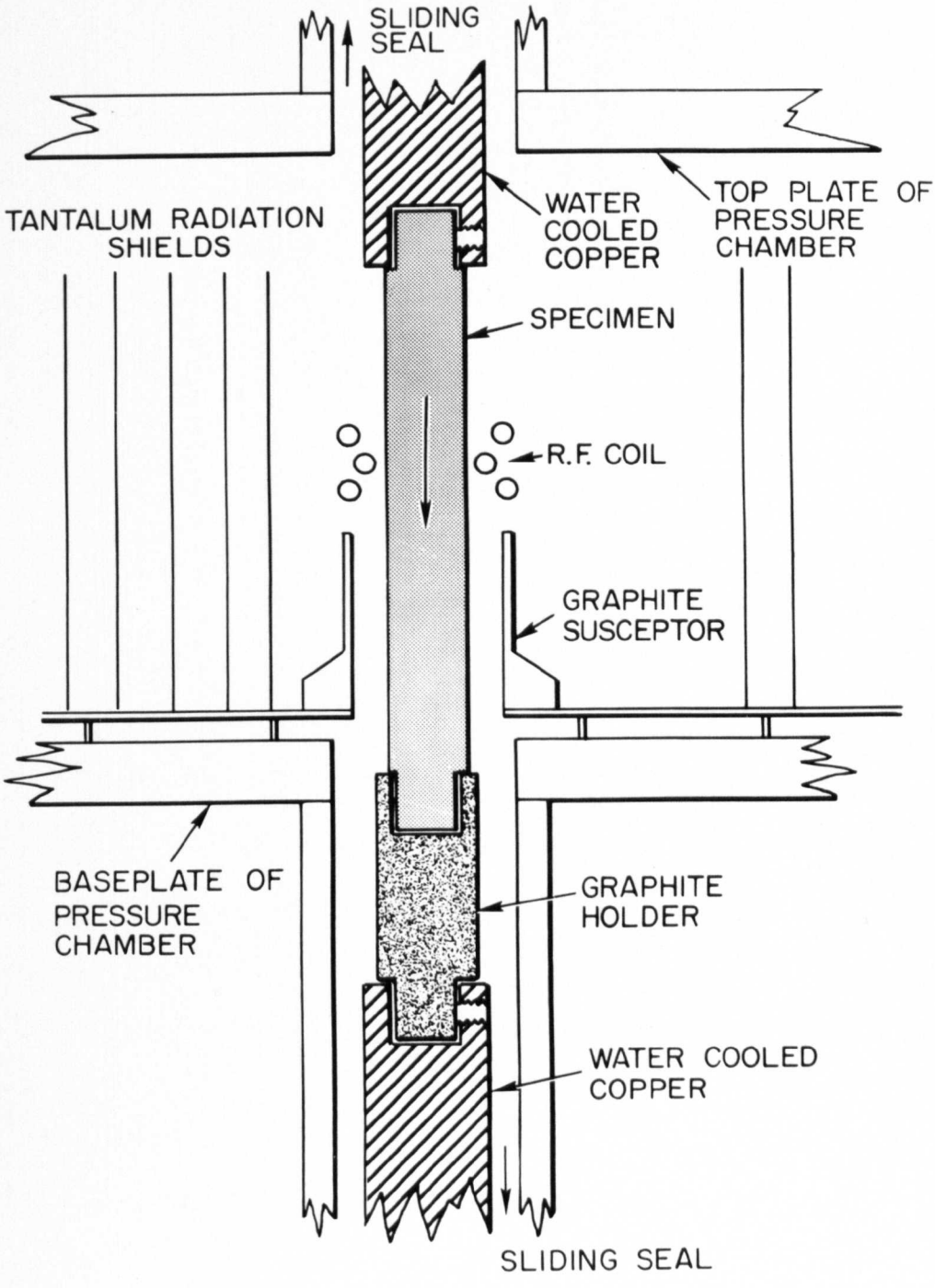

Fig. 2.3. Internal construction of pressurized crystal growing chamber. (After Precht and Hollox[1].)

the three-turn r.f. heater coil. The upper chuck can be translated independently of the lower one to compensate for density changes and to help maintain the stability of the zone, whereas the lower chuck can be rotated to compensate for any slight deviations from axial symmetry exhibited by the work coil. A 50 kVA r.f. generator operating near half power was sufficient to melt a stable zone approximately 1 cm high in the sintered rod. Best results were obtained when this zone was moved at a rate of 0.3 to 0.6 cm/hr from the bottom to the top of the rod, the freshly grown crystal passing directly into a graphite susceptor afterheater to reduce thermal shock cracking.

Single crystals of a desired carbon-to-metal ratio may be grown in this manner by properly adjusting the composition of the sintered rod, but as noted by Precht and Hollox,[1] due consideration must be given to the phase diagram,[2] fig. 2.4, in order to ensure a uniform composition along the entire length of crystal. For example, it was observed by these authors that when a rod having a nominal composition $VC_{0.75}$ is zone melted, the first zone to freeze has a composition close to $VC_{0.82}$, consistent with the separation between the liquidus and solidus lines in this region of the phase diagram. This situation leads to composition gradients along the length of the rod which persist until the composition of the liquid zone approaches a carbon-to-metal atom ratio $x = 0.62$ by zone refining action. It was demonstrated, however, that zone levelling

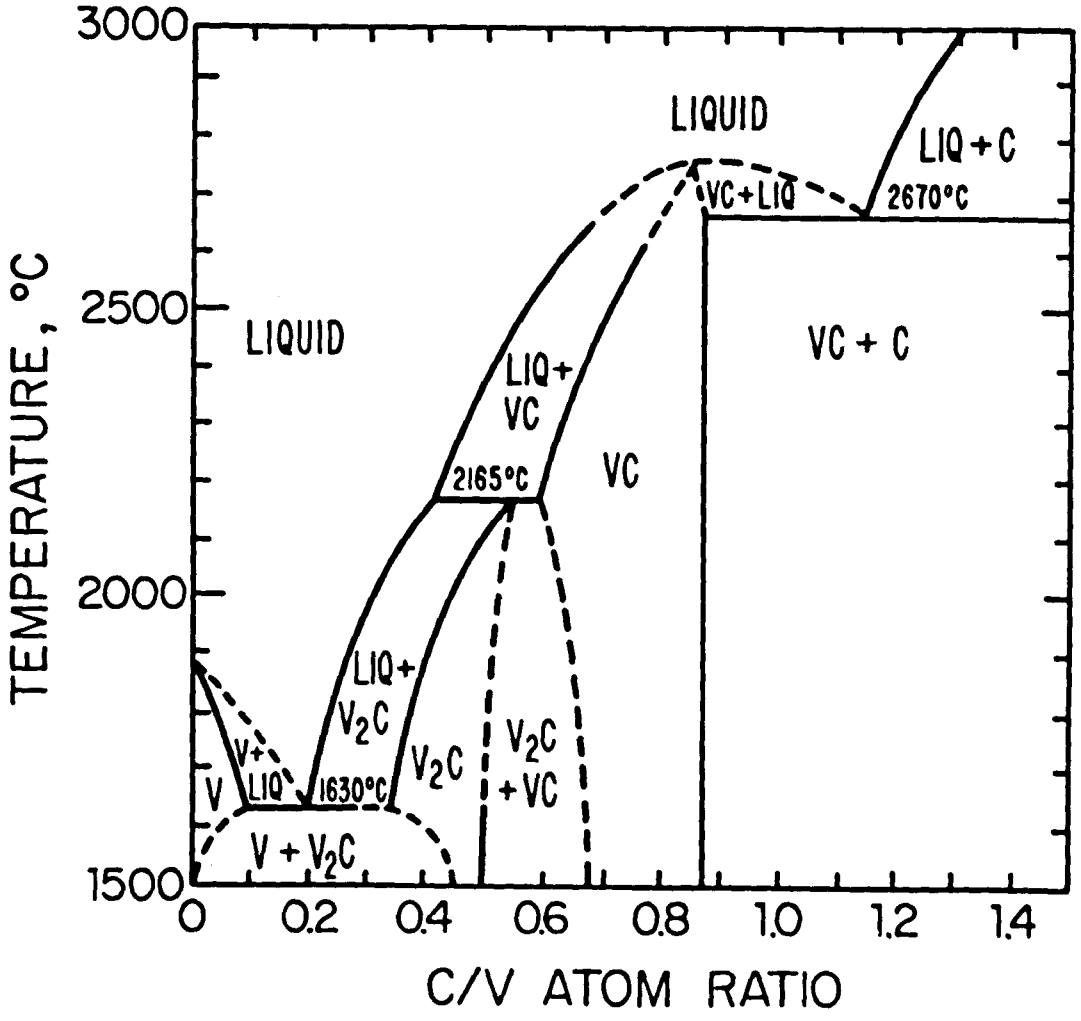

Fig. 2.4. Vanadium-carbon phase diagram. (After Adelsberg and Cadoff[2].)

conditions may be achieved at the start of crystal growth by incorporating an additional section into the lower end of the rod that has a composition close to $VC_{0.62}$ and a volume equal to that of the molten zone.

For the present study, single crystals having a carbon-to-metal ratio close to the integral composition V_6C_5 were desired and starting rods were made by adding 10% by weight of vanadium metal to the $VC_{0.92}$ powder. Because this composition lies close to the melting point maximum where the liquidus and solidus lines join, it was not necessary to take precuations against any zone refining action. Thus, in this case, zone levelling starts when the initial molten zone is formed and continues throughout the remainder of the traverse.

A V_6C_5 crystal similar to those employed in this investigation is shown in fig. 2.1(b). Typically, the zone melted section is polycrystalline and fine grained at the starting end, but, because preferential growth of one grain occurs during the freezing process, the last 3/4 of the rod is generally single crystal. Since the rods are not normally seeded, the growth directions do not usually lie parallel to low index crystallographic axes. However, this presents no problem since specific sample orientations may be readily obtained using ordinary X-ray diffraction techniques.

Chemical analysis, emission spectroscopy, and lattice parameter measurements based on Storm's[3] data have been used to characterize the crystals, Table 2.1. The carbon-to-metal ratios determined from chemical analysis (by a commercial analytical laboratory) are consistent with the more accurate results obtained by NMR measurements that will be described in Chapter 4, but disagree slightly with the values obtained by lattice parameter measurements. This suggests that the latter method of specifying the composition may be subject to a systematic error of approximately 0.01 in the values of x as first noted by Lowndes et al.[4]

TABLE 2.1

COMPOSITION OF V_6C_5 SINGLE CRYSTALS USED IN THIS INVESTIGATION

Carbon-to-metal atom ratio:

by chemical analysis	$x = 0.84$
by lattice parameter	$x = 0.851$
by NMR	$x = 0.838$

Impurity content:

Element	Weight percent
by spectrographic analysis	
Cr	< 0.1
Fe	< 0.1
Mo	< 0.1
Ti	0.1-1.0
Zr	0.1-1.0
by chemical analysis	
O	0.013
N	0.022-0.031
B	0.003-0.01

2.2 Preparation of thin foils

Thin foils for the transmission electron microscope studies were obtained by jet etching small disks of V_6C_5 with a 20% sulphuric acid - 80% methanol solution, followed by electrolytic polishing in the same solution. To prepare samples for thinning, the single crystal boules were oriented by standard Laue X-ray diffraction methods and sectioned with a diamond saw into 0.25mm thick slices having either {100}, {110}, or {111} faces. Disks, 3mm in diameter, were cut from the slices using an ultrasonic impact cutter and then mechanically polished with 3μ diamond paste in order to remove all coarse scratches, saw marks, etc.

The thinning apparatus, fig. 2.5 and 2.6, includes provisions for both jet etching and electrolytic polishing in one unit. In the jet operation a stream of electrolyte is directed against both sides of the sample by two jet nozzles made of 1mm inside diameter stainless steel tubing. The nozzles are made cathodic with respect to the sample by approximately 6-8 volts, the potential being adjusted to maintain a total current of 350 ma for optimum polishing conditions. Once well defined craters are formed on both sides of the disk, the sample is transferred to the electrolytic polishing bath where it is thinned to breakthrough using a current of 150 ma. The hole produced during polishing is kept small by switching off the

/

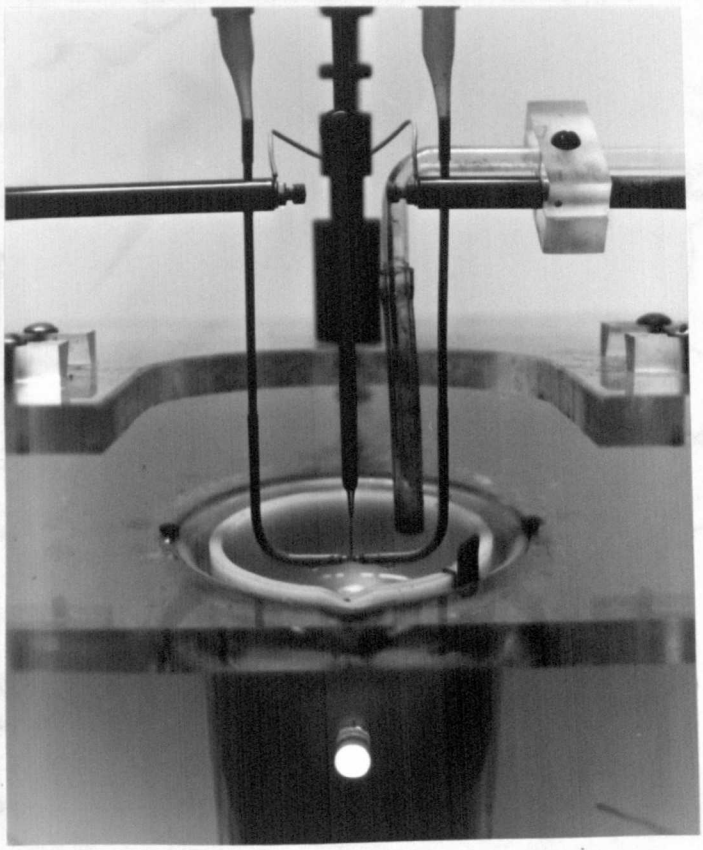

Fig. 2.5. Jet thinning apparatus used for preparing electron microscope foils.

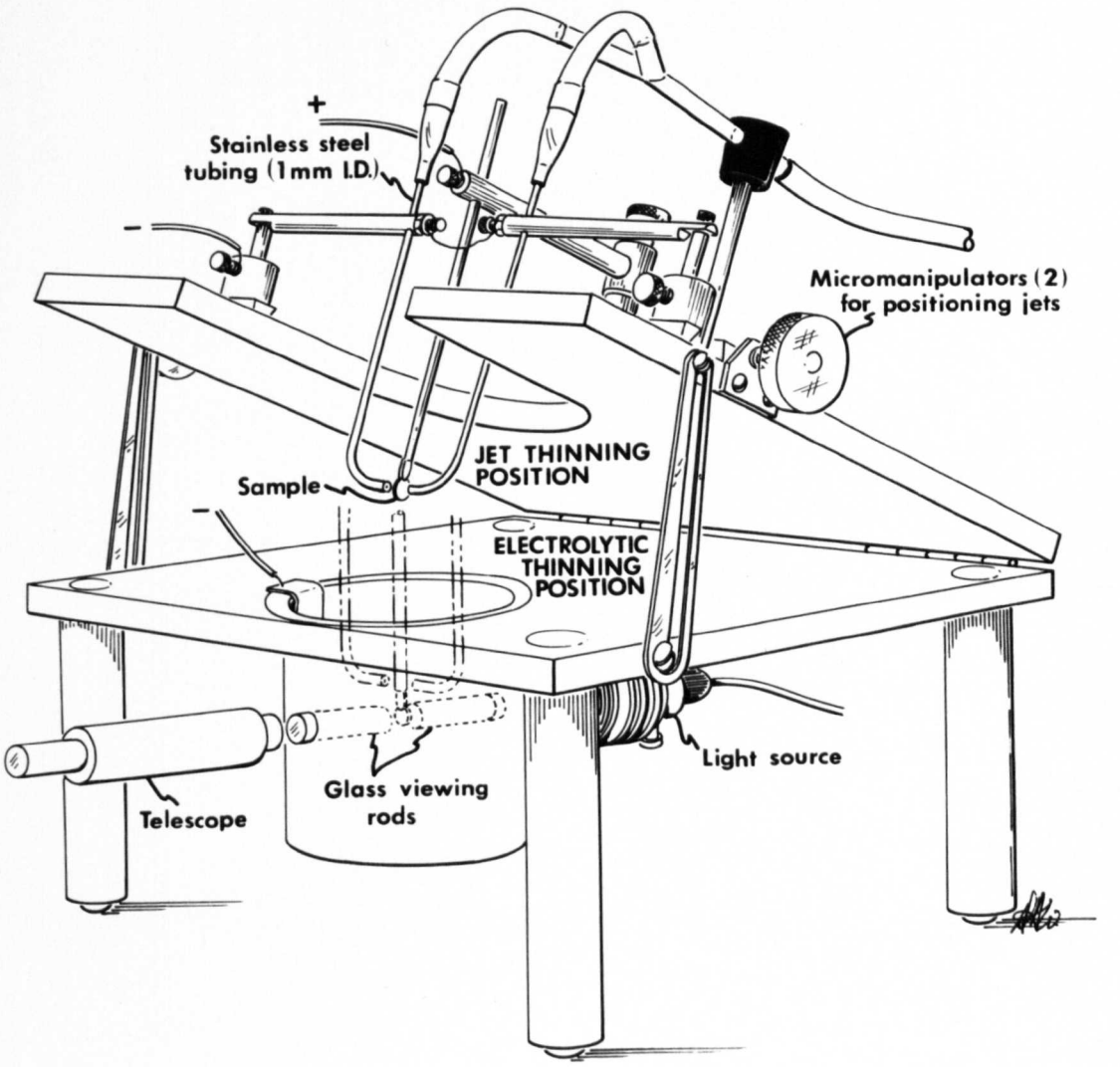

Fig. 2.6. Perspective view of the thinning apparatus in which microscope foils are prepared by a two-step process. In the first step, the sample is thinned by the jet technique to produce a convex profile near the center of the disk. The sample is then polished electrolytically until perforation occurs, at which time the current is shut off. The optical system provides a means of determining the instant of breakthrough.

current supply at the instant light is observed through the light pipe arrangement shown in fig. 2.6.

Samples prepared in this manner fit directly into the electron microscope holder without the need for further support. Furthermore, because they exhibit large transparent areas and are inherently rigid, the foils are suitable for both the general contrast and diffraction experiments discussed in Part I, as well as the radiation damage experiments discussed in Part II, which place stringent requirements upon sample stability.

REFERENCES

1. W. Precht and G. E. Hollox, J. Crystal Growth, 3,4, 818 (1968).

2. L. M. Adelsberg and L. H. Cadoff, J. Am. Ceram. Soc., 51, 213 (1968).

3. E. K. Storms, "The Refractory Carbides," (Academic Press, New York, 1967) p. 51.

4. D. H. Lowndes, L. E. Finegold, and R. G. Lye, Phil. Mag., 21, 245 (1970).

CHAPTER THREE

EVIDENCE FOR ORDERING

3.1 Observations with reflected polarized light

When a cleaved, or highly polished face of single crystal $VC_{0.84}$ is examined in reflected polarized white light, a domain type of substructure similar to that shown in fig. 3.1, is observed. Because matching freshly cleaved faces exhibit identical patterns which remain unchanged indefinitely at room temperature, the coloration can be attributed to optical anisotropy of the crystal rather than to a surface film. Thus the substructure is visible because each domain exhibits a color, due to birefringence, which contrasts with that of neighboring domains.

The presence of birefringence is surprising since vanadium carbide previously had been considered to be a cubic, isotropic material. Also surprising is the presence of domains, which have not been observed in any of the more widely studied, cubic transition metal carbides. It will be shown in the subsequent sections, however, that these unexpected findings may be understood in terms of the non-cubic superlattice which forms in $VC_{0.84}$ as a consequence of long range vacancy ordering.

Fig. 3.1. Optical micrograph of domain structure in $VC_{0.84}$ taken with polarized light between crossed Nicols on {100} cleavage plane. Average size of domains varies from sample to sample and is dependent upon prior thermal history of material.

3.2 Observations by electron microscopy

Figure 3.2 is a transmission electron micrograph of the domain substructure as observed in a (100) foil.‡ Accompanying the micrograph are two selected area diffraction patterns, one from each of the two domains marked A and B in the figure. Each pattern reveals supplementary, or superlattice spots in addition to the primary VC spots. The primary spot pattern which maps out the (100) reciprocal lattice plane, maintains an equivalent orientation in the two regions. The supplementary spot pattern, however, undergoes a rotation of 90° between domains A and B. Thus, each domain is associated with a specific orientation of the superlattice and, apparently, the domain structure results because the superlattice can assume several possible orientations within the nominally cubic vanadium carbide lattice.

To demonstrate that each domain is associated with a specific orientation of the superlattice, the micrograph in fig. 3.2 was taken in dark field, using a superlattice spot associated with domain A. Under these conditions, the domain at B remained dark. When a superlattice spot associated with domain B was employed, the contrast reversed, and domain A became dark.

---

‡Foil orientations are given with respect to the nominally cubic VC lattice.

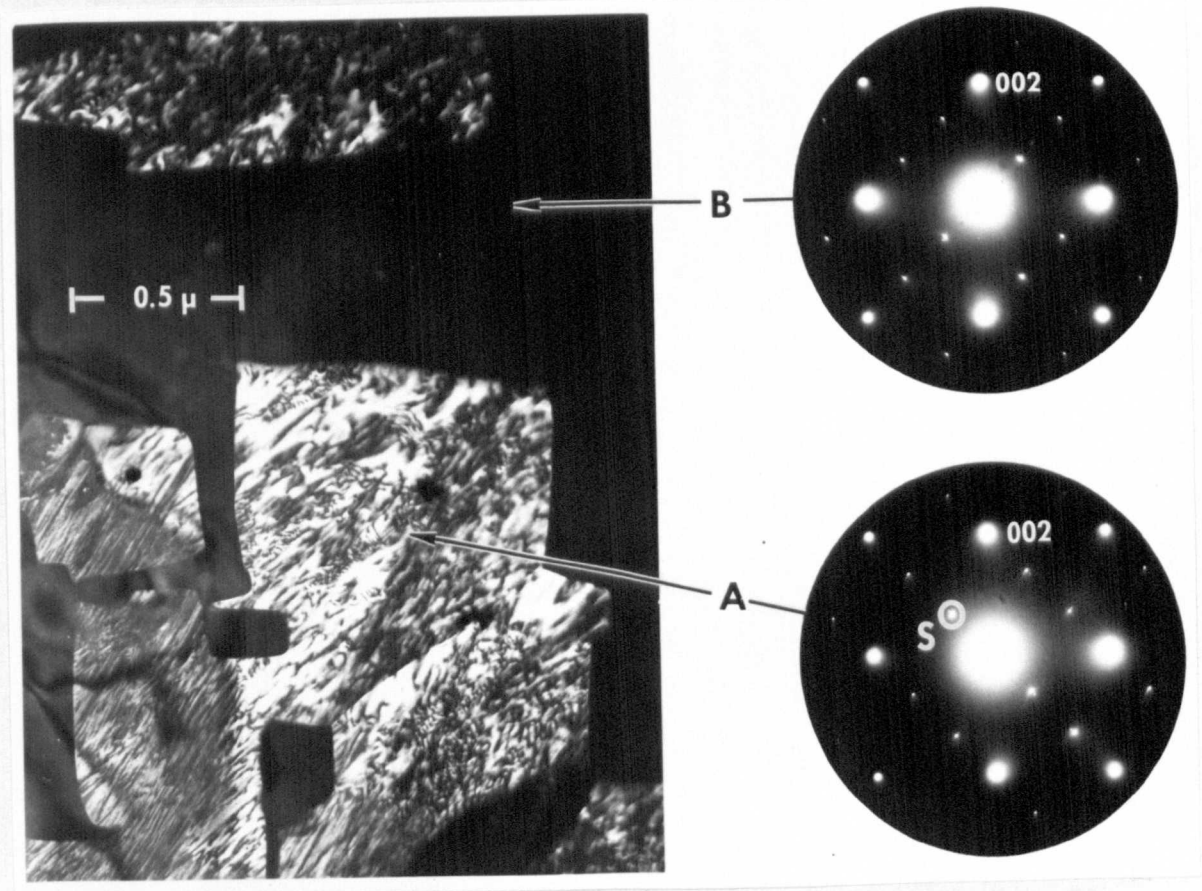

Fig. 3.2. Dark field transmission electron micrograph of domain structure in $VC_{0.84}$ taken with superlattice spot, S. Selected area diffraction patterns obtained from each of the two domains, A and B, demonstrate that primary VC pattern maintains equivalent orientation in two regions, but superlattice pattern undergoes 90° rotation. Plane of foil is (100).

Although the boundary walls between domains do not lie along well defined crystallographic planes, they do exhibit a tendency to lie parallel to {100} and {110} planes, as shown in fig. 3.3. From the nature of the contrast (asymmetrical in bright field), it is concluded that the boundaries at A and B are δ interfaces[1] that are similar to those observed in Nb by Van Landuyt et al.[2] The unusual contrast effects which have been observed within the domains (e.g., the mottled contrast of domain A in fig. 3.2 and the periodic fringes in fig. 3.3) are not completely understood but it is possible they may be a consequence of the unusual crystallographic structure of this material, as will be discussed in Chapter Four.

3.3 The superlattice unit cell

For the purpose of determining the symmetry and dimensions of the superlattice unit cell, selected area diffraction patterns were obtained from several foil orientations. A schematic diagram of all the observed diffraction patterns obtained from individual domains in (100), (110) and (111) foils is presented in fig. 3.4. In some foils, the patterns differ only with regard to the orientation of the superlattice spots relative to the primary spots. In other foils, superlattice patterns exhibiting different symmetry are observed. In all foils, however, the primary spot pattern remains essentially undeviated throughout the specimen, and to a first approximation it exhibits the symmetry and dimensions of a cubic structure having the parameter $a_o = 4.16$ Å.

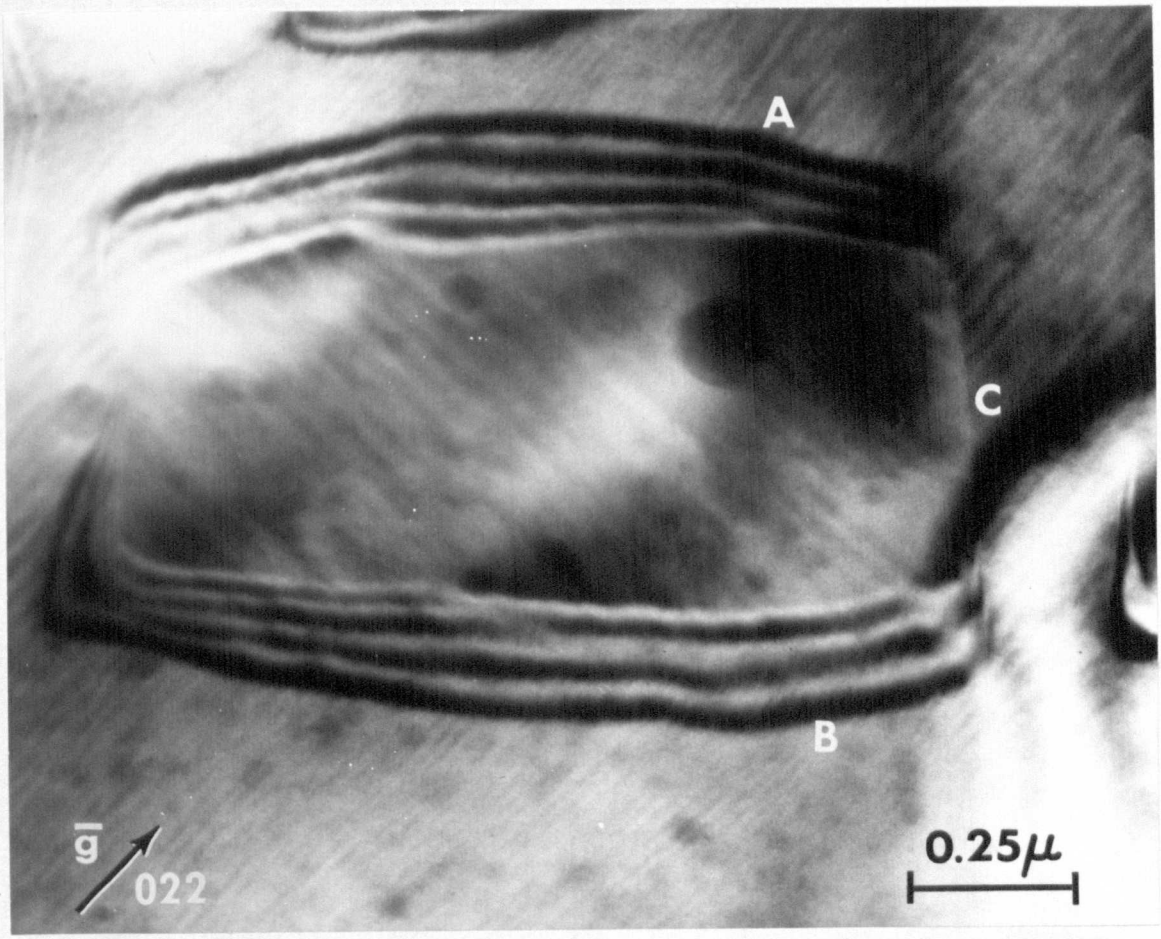

Fig. 3.3. Bright field transmission electron micrograph of a domain in (100) foil. Domain walls do not lie along well defined crystallographic planes, but those at A and B are roughly parallel to a {110} plane, whereas the wall at C is roughly parallel to a {100} plane. Fringe contrast of boundaries at A and B is asymmetrical indicating they are δ interfaces.

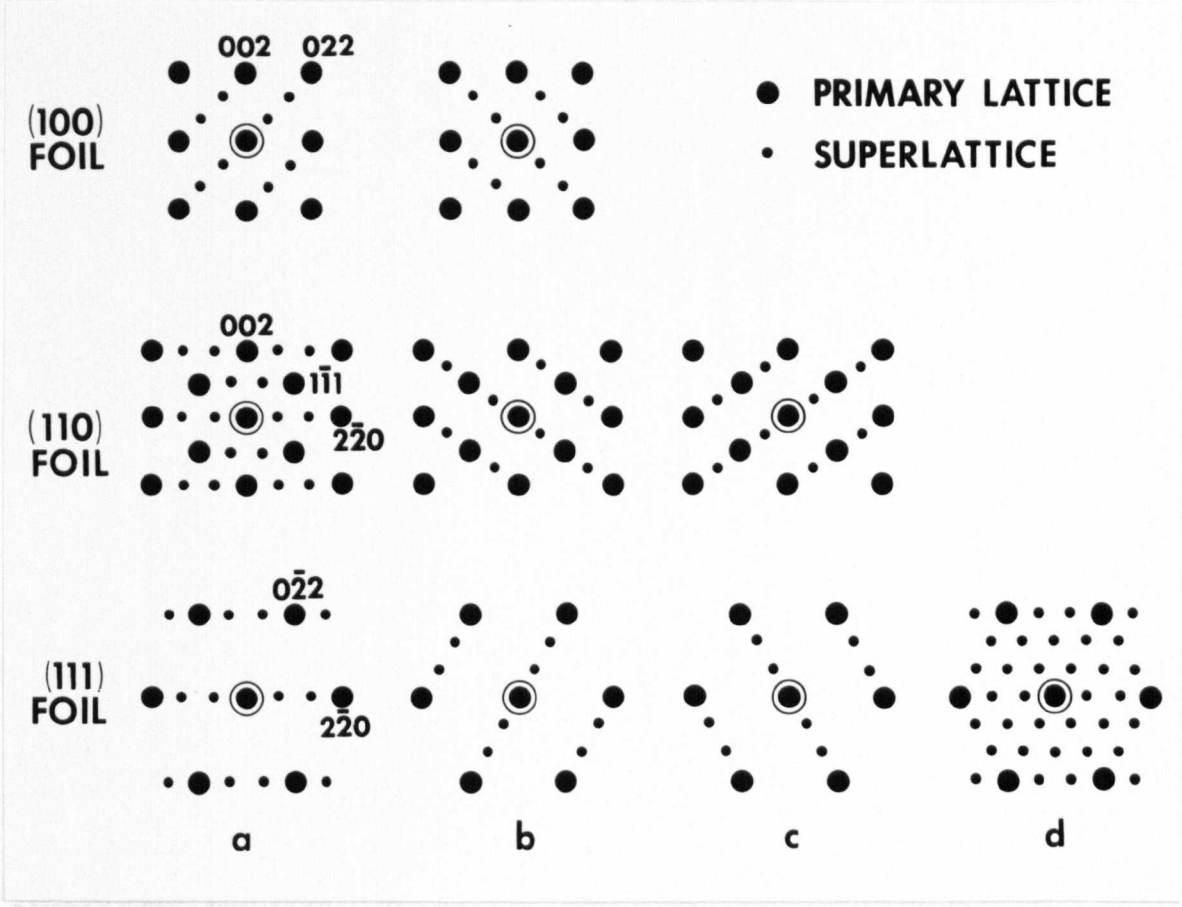

Fig. 3.4. Selected area diffraction patterns obtained from domains observed in three indicated foil orientations. In a given foil, primary spot pattern is continuous across all domain walls.

The symmetry of the superlattice unit cell may be deduced directly from fig. 3.4. The superlattice spots in pattern (111)d exhibit 6-fold symmetry, which indicates the presence of either a 3- or 6-fold axis in the unit cell. (A 3-fold axis in real space will give rise to a 6-fold symmetrical electron diffraction pattern because of the presence of positive and negative reflections [3].) The unit cell must, therefore, belong to either the hexagonal* or cubic crystal class because only these possess symmetry of this type. The orientation of the superlattice pattern with respect to the primary pattern dictates that the superlattice should give rise to a cubic pattern in (100) foils if its unit cell were cubic. Since such a pattern is not observed in this foil orientation, it is concluded that the unit cell must be hexagonal.

The dimensions of the unit cell can be obtained from the d-spacings which are associated with the various superlattice reflections observed in fig. 3.4. A summary of several important d-spacings obtained from the electron diffraction patterns is presented in Table 3.1. Included in the table are d-spacings obtained from two weak superlattice lines that have been observed in X-ray diffraction powder patterns from crushed single crystal samples. The X-ray diffraction data serve as a check on the electron diffraction d-values

*For the purposes of this discussion the trigonal class will be considered as a sub-group of the hexagonal class.

and also demonstrate that the important low index reflections, corresponding to d = 4.80 Å and 4.40 Å, are real reflections in the

TABLE 3.1

Measured Superlattice d-Values		d-Values calculated from Hex. Unit cell; a = 5.09 Å, c = 14.40 Å	
Electron Diff	X-Ray Diff	d	HKL
4.80 Å	4.80 Å	4.80 Å	003
4.40	4.42	4.42	100
3.77		3.79	102
2.78		2.79	104
2.40		2.40	006
2.21		2.20	200

electron diffraction patterns and do not arise, for example, because of multiple electron scattering. By using a Bunn chart for hexagonal structures, the parameters of the unit cell were found to be a = 5.09 Å and c = 14.40 Å.

The orientation of the superlattice unit cell with respect to the primary unit cell is as follows:

$$\langle 001 \rangle_{SL} \parallel \langle 111 \rangle_{PL}$$

$$\langle 2\bar{1}0 \rangle_{SL} \parallel \langle \bar{2}11 \rangle_{PL}.$$

The length of the c-axis corresponds to six complete {111} layers of atoms in the cubic lattice, and the length of the a-axis corresponds to the carbon-carbon (or metal-metal) atom spacing in the ⟨112⟩ direction of the primary cell.

Further analysis of the patterns shown in fig. 3.4 indicates that four orientations are possible for the superlattice, corresponding to the alignment of the c-axis parallel to any one of the four equivalent ⟨111⟩ directions in the primary cell. Only two distinguishable diffraction patterns are observed in a (100) foil because the reciprocal lattice projections of two orientations are exactly equivalent to the other two. In (110) foils, three distinguishable reciprocal lattice projections are possible, whereas in (111) foils all four superlattice orientations are distinguishable and may be detected separately.

REFERENCES

1. R. Gevers, J. Van Landuyt, and S. Amelinckx, Phys. Stat. Sol., 11, 689 (1965).

2. J. Van Landuyt, R. Gevers, and S. Amelinckx, Phys. Stat. Sol., 13, 467 (1966).

3. G. Thomas, Trans. Metall. Soc. A.I.M.E., 233, 1608 (1965).

CHAPTER FOUR

NATURE OF THE ORDERING

4.1 Nuclear Magnetic Resonance of V^{51} in $VC_{0.84}$*

Although the dimensions and symmetry of the superlattice unit cell can be derived from electron diffraction patterns as shown in Chapter 3, these data do not provide a description of the vacancy distribution within the cell. This information, however, can be obtained by NMR techniques.

The response of an atom to an oscillating magnetic field depends not only on the intrinsic properties of the atom but also on the local environment in which the atom is situated. For example, a displaced or missing atom destroys the local cubic symmetry in an otherwise perfect cubic crystal, and this disrupted symmetry can be expected to result in electric field gradients at the nuclei of atoms surrounding the defect. Such a situation occurs frequently in VC, of course, because the number of carbon atoms present is substantially less than the number of available sites in the carbon sublattice of this nominally rocksalt crystal. Furthermore, the principal vanadium isotope, V^{51} (~ 100% abundance), has a nuclear electric quadrupole moment (-0.052×10^{-24} cm^2),[1] so that the presence of an electric

*The NMR experiments described in this section were performed by D. Kahn and R. G. Lye of RIAS with the author as collaborator.

field gradient at the vanadium nucleus modifies the NMR behavior. In particular, the electric field gradient will split the single resonance line that is observed when the V^{51} atom is in a cubic environment into a central component and three pairs of satellite lines ($I = 7/2$) which are more or less symmetrically disposed about the central line. The central line also will be displaced by an amount which varies inversely with the strength of the applied dc magnetic field, H_o. Consequently, the NMR of VC specimens exhibit complex spectra which can be analyzed to yield information about the distribution of carbon vacancies within the crystal.

The VC specimens employed in this study were obtained by crushing the $VC_{0.84}$ single crystals so that the individual particles were smaller than the skin depth of the r.f. field used. The V^{51} NMR spectra obtained from the powdered specimens (powder patterns) could be resolved into central components, shown in fig. 4.1(a), and a satellite structure, shown in fig. 4.1(b).

Although some aspects of the identification require confirmation, the principle features can be accounted for on the following basis:

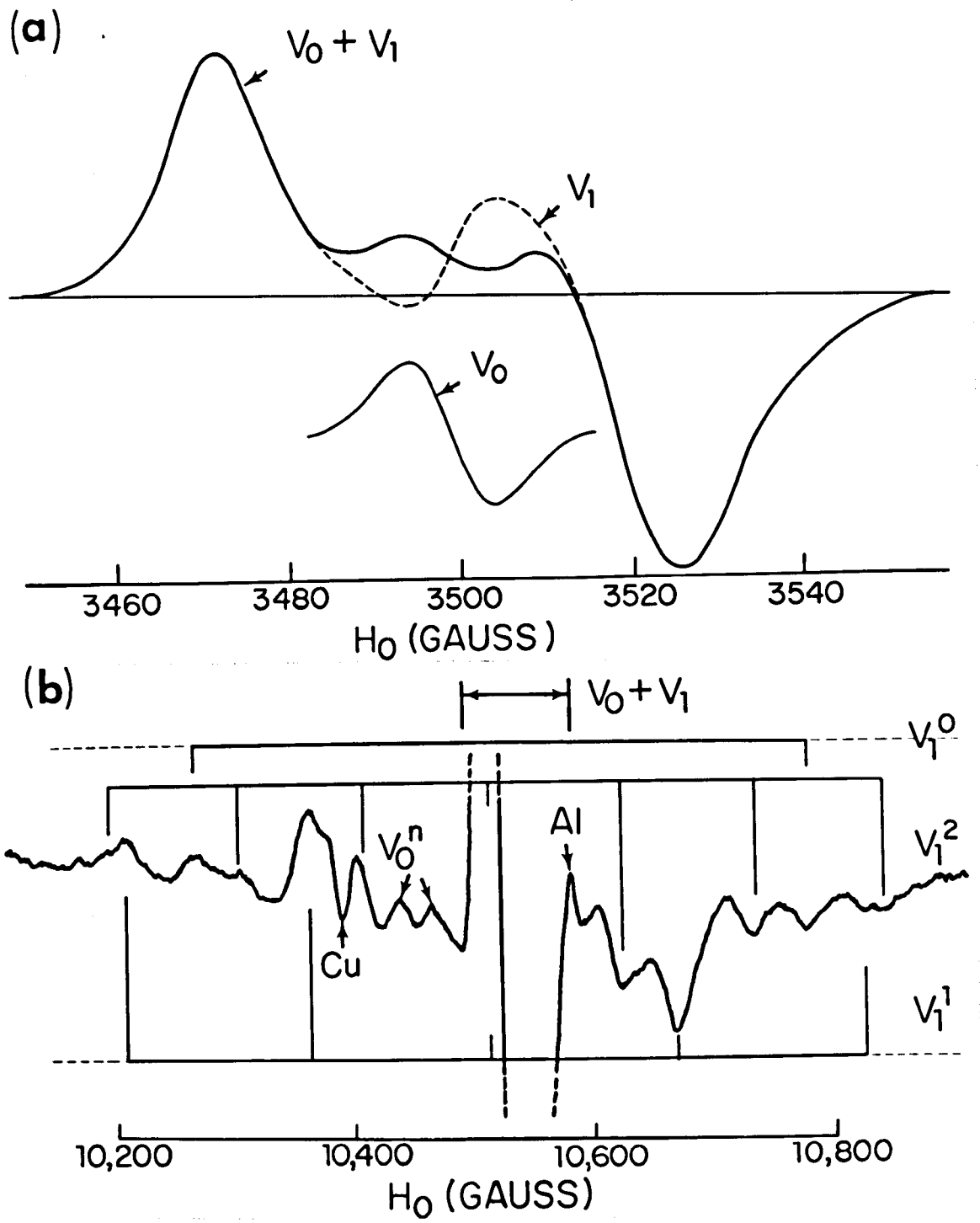

Fig. 4.1. Nuclear magnetic resonance curves of V^{51} nuclei in $VC_{0.84}$ obtained at 77°K. The central resonance, shown in (a), was separated into its two components, V_0 and V_1, by fitting a Gaussian line and a second order quadrupolar broadened line to the observed curve. The relative population of V_0 and V_1 sites was obtained by integrating the respective derivative curves twice. Most of the satellite structure shown in (b) is attributed to resonances from nuclei at three different V_1 sites, as explained in the text. The peaks labelled V_0^n are components of the partially resolved V_0 satellite structure. The Cu and Al lines arise from materials in the probe.

(1) A single line, V_0,* relatively weak and narrow is observed, with a width of approximately 10 gauss, almost independent of the strength of the dc magnetic field. This resonance is attributed to V^{51} atoms in a nearly perfect cubic environment, i.e. the vanadium atoms contributing to this spectrum must have no vacancies in the nearest shell of carbon atom neighbors. The line is displaced to the high field side of the resonance of an isolated V^{51} atom by an amount equivalent to a negative Knight shift of 0.32%. Close examination of the spectrum indicates, however, that this resonance is split and broadened by quadrupolar interactions, but only weakly. Two feeble lines, V_0^n, have been tentatively assigned to the satellite structure, and their splitting is consistent with the small quadrupolar broadening ($\lesssim$ 4 gauss at H_o = 3000 gauss) beyond the calculated dipolar breadth ($\cong$ 7 gauss) of the central line.

---

*The several components of the vanadium NMR spectrum are identified by a sequential set of suffixes. The first, a subscript, refers to the relevant Knight shift; the second, a superscript, refers to the quadrupolar splitting. For brevity, the same symbols are employed to designate the various inequivalent sites in the vanadium sublattice from which the corresponding spectral components originate. In the latter use of this notation, the subscript is intended to represent the number of vacancies in the nearest neighbor shell of carbon atoms surrounding the vanadium atom sites, and the superscript the number in the next-nearest-neighbor shell, as discussed subsequently in the text. No confusion should result from the use of the symbol V^{51} to identify the vanadium isotope.

(2) A strong broad resonance, V_1, is observed which comprises two spectra, V_1^1 and V_1^2, i.e. the central quadrupolar broadened line has two components (not resolved in the figure), and associated with them are two sets of satellite lines. These two resonances include by far the larger fraction of the V^{51} nuclei detected in the spectrum. The Larmor frequencies of both components are displaced from the resonance of an isolated atom by the same amount, corresponding to a negative Knight shift of 0.13%.

The central line has an extrapolated dipolar width near 7 gauss, and additional quadrupolar broadening (proportional to $1/H_o$) that is consistent with the average of the separations of the two sets of satellite lines ($\nu_q \cong 280$ kHz). This broadening and splitting of the resonance indicates the presence of strong electric field gradients at the V^{51} nuclei involved. The principal component of this gradient is attributed to the presence of a single vacancy in the nearest neighbor shell of carbon atoms surrounding these nuclei, in agreement with the assignment made by Froidevaux and Rossier[2] for a similar resonance observed in their NMR studies of VC.

(3) A third series of lines is present, but only the innermost pair of satellite lines, V_1^0, has been resolved. The central component of this spectrum is too faint to be resolved under the much more intense central lines discussed in (2), but the satellite lines

indicate a displacement of the resonance to the high field side. The magnitude of the Knight shift cannot be measured accurately for this series, but it is negative and approximately equal to the shifts of the lines discussed in (2). The satellite splitting of this series is larger than for the spectra discussed in (2), and thus corresponds to an even larger electric field gradient at the V^{51} nuclei involved. For reasons to be discussed later, this spectrum is attributed to V^{51} nuclei with one carbon vacancy in their nearest neighbor shell, but with no vacancies in the next nearest neighbor shell of carbon atoms.

According to the present analysis of the NMR spectra, almost all of the vanadium atoms are on V_1 sites (with one carbon vacancy in the nearest neighbor shell), as might be expected from the fact that the composition of the $VC_{0.84}$ material studied is close to the integral composition V_6C_5. Only a small fraction of the vanadium atoms are on V_0 sites (with no carbon vacancies in the nearest neighbor shell). The integrated intensities, I_0 and I_1, of the central components of the spectra associated with these sites are in the ratio $I_0/I_1 = 0.035$. Because each carbon vacancy in the lattice has six vanadium atoms surrounding it, the addition of a carbon atom into a vacant site would convert all six of the neighboring vanadium sites to V_0 sites. Thus, because most of the V^{51} atoms

appear to occupy V_1 sites, the ratio $I_0/I_1 = 3.5\%$ implies that the carbon/metal atom ratio in the vanadium carbide under study exceeds that of V_6C_5 by approximately $0.035/6 \cong 0.5\%$. That is, the NMR spectra indicate that the composition of this vanadium carbide is $VC_{0.838}$, in good agreement with the results of chemical analysis ($VC_{0.84}$), Table 2.1.

The conclusion that all but a very small fraction of the V^{51} nuclei in vanadium carbide are surrounded by precisely five carbon atoms in the nearest neighbor shell, coupled with the electron diffraction data, has allowed a crystal structure to be deduced for V_6C_5. The result, which will be described in the next section, provides a reasonable interpretation for the two components of the V_1 spectrum. In the proposed model of V_6C_5, all the vanadium atoms have one vacancy in the nearest neighbor shell of carbon atoms, but two-thirds of them have also a single vacancy in the next nearest neighbor shell, whereas one-third have two vacancies in this shell. The geometries of these two inequivalent sites are illustrated in fig. 4.2. Because the intensities of the V_1^1 and V_1^2 spectra are also in the ratio 2:1, the V_1^1 spectrum can be associated with vanadium sites of the first kind, and the V_1^2 spectrum with sites of the second kind. Although this assignment is tentative, it is consistent with other characteristics of the NMR spectrum. In particular, if an extra carbon atom were incorporated into the V_6C_5 crystal, it

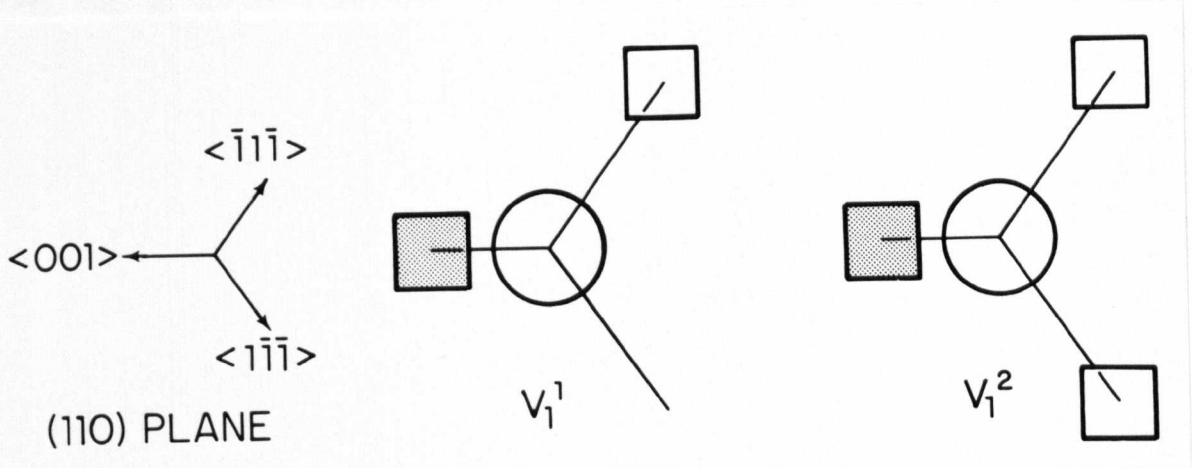

Fig. 4.2. The two types of vanadium atom sites predicted by the proposed structure of V_6C_5. Circles are vanadium atoms, shaded squares represent nearest neighbor carbon vacancies, and open squares are next nearest neighbor carbon vacancies.

would convert the six nearest neighbor V_1 sites to V_0 sites, but the V_0 sites formed in this way would be of two kinds, V_0^1 and V_0^2, corresponding to the two possible configurations of vacancies in the next nearest neighbor shells of carbon atoms surrounding the original V_1 sites. Thus, the small quadrupolar broadening of the V_0 NMR line can be attributed to electric field gradients caused by second nearest neighbor carbon vacancies.

This extra carbon atom also converts vanadium atom sites in its next nearest neighbor shell from V_1^1 and V_1^2 to V_1^0 and V_1^1 sites, respectively. Thus, the presence of an excess of carbon should lead to the occurrence of a third NMR V_1 spectrum due to V_1^0 sites, which are not present in the perfect V_6C_5 crystal. The incomplete group of satellites labeled V_1^0 in fig. 4.1 is assigned tentatively to this site.

4.2. Proposed Crystal Structure of $VC_{0.84}$ (V_6C_5)

Data obtained from electron diffraction, NMR, and chemical analysis have been employed to deduce the superlattice structure of $VC_{0.84}$ crystals under the assumption that the vanadium atoms form a fcc array and that the carbon atoms occupy specific octahedral interstices within the metal atom lattice. Thus, the proposed crystal structure differs from the commonly assumed rocksalt lattice of VC

only in that carbon vacancies are distributed in an ordered manner through the carbon lattice.

A model of the proposed structure is shown in fig. 4.3(a). It will be noted that carbon atoms have been removed from certain {111} carbon planes so that each vacant site is separated by a ⟨112⟩ distance, i.e. 5.09 Å, from its six nearest neighbor vacancies in the plane. In this manner, all the vanadium atom sites on the adjacent {111} planes are converted from V_0 to V_1 sites. By repeating this construction in every other carbon layer, all the vanadium atom sites are converted to V_1 configurations, and the resulting carbon/metal ratio corresponds to the integral composition V_6C_5.

The symmetry of the resulting carbon lattice is no longer fcc but must be described in terms of an hexagonal unit cell, fig. 4.3(b), whose dimensions, and orientation relative to the vanadium lattice, are completely consistent with the electron diffraction results. For simplicity, only the vacancy positions have been shown in fig. 4.3(b). However, the complete carbon lattice may be constructed upon this framework by placing an appropriate grouping of five carbon atoms around each vacancy site. The unit cell contains three screw triads and possesses the symmetry of the hexagonal (trigonal) class $P3_1$ or its enantiomorph, $P3_2$. In this figure the

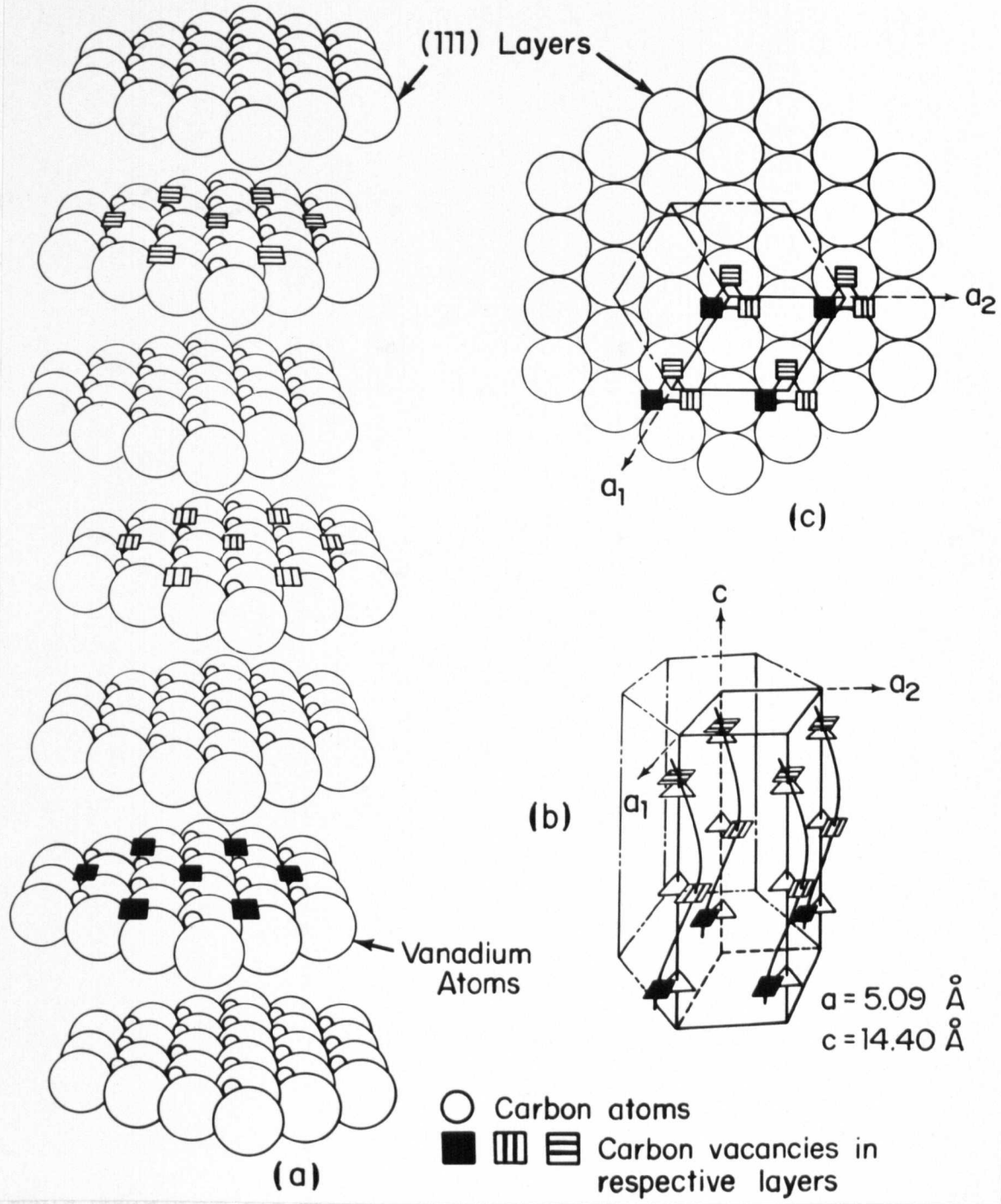

Fig. 4.3. The structure of V_6C_5, showing: (a) location of ordered carbon atom vacancies (c-axis expanded for clarity), (b) hexagonal superlattice formed by vacancy ordering, and (c) projection of superlattice on a {111} plane of vanadium atoms. Symmetry of superlattice corresponds to trigonal class $P3_1$, or its enantiomorph $P3_2$. The material studied, $VC_{0.84}$, exhibits this structure, but contains a slight excess of carbon atoms over the integral composition.

right handed modification, $P3_1$, is shown, however the left handed form, $P3_2$, is an equally probable configuration.

The structure of V_6C_5 may be viewed, therefore, in terms of two interpenetrating lattices; a vanadium atom lattice which, neglecting some distortions that may arise because of the carbon vacancies, is essentially fcc, and an hexagonal superlattice containing all the carbon atoms present. On this basis, it is apparent that the domain structure results because the c-axis of the superlattice can be oriented parallel to any one of the four ⟨111⟩ directions in the vanadium lattice.

For many purposes, it is convenient to describe the structure in terms of a primary lattice and a superlattice. However, this description tends to under-emphasize the anisotropic nature of the material, which leads, for example, to the strong birefringence observed in reflected polarized light. An alternative description that places greater emphasis on the anisotropy of the structure is obtained by considering V_6C_5 as an hexagonal (trigonal), ordered compound possessing the symmetry $P3_1$ or $P3_2$. On this basis, a molecule containing six vanadium atoms and five carbon atoms forms the "building block" of the structure. The right handed modification, $P3_1$, is illustrated in fig. 4.4. All the atoms (as well as

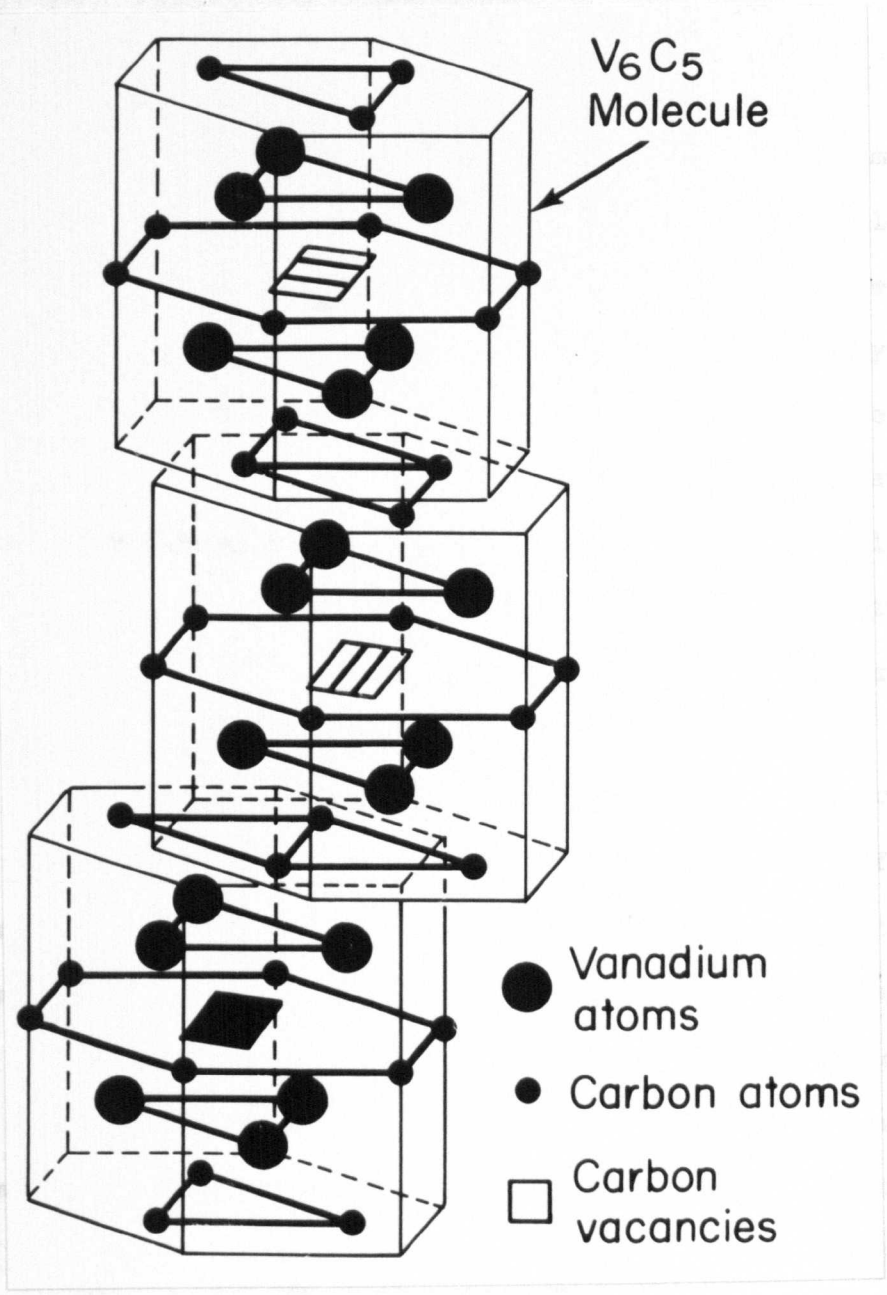

Fig. 4.4. The structure of V_6C_5, viewed in terms of spiralling chains of V_6C_5 molecules. At the center of each molecule is a vacant carbon site which corresponds to a vacancy on one of the screw triad axes shown in fig. 4.3(b). A complete unit cell consists of nine such molecules, and, thus, contains 54 vanadium atoms and 45 carbon atoms.

carbon vacancies) occupy the point position 3(a), with the parameters* listed in Table 4.1. A complete unit cell consists of 9 molecules which are disposed in such a manner that the center of each molecule coincides with a carbon vacancy site. Thus, each of the vacancy sites shown in fig. 4.3(b) denotes the position of one V_6C_5 molecule, and the complete structure consists of "chains of molecules" that spiral about a direction parallel to the c-axis of the unit cell, fig. 4.4. From this point of view, of course, the domain structure arises because the directions of the spiral axes may be different in various regions of the crystal.

By considering V_6C_5 as an hexagonal compound, the birefringence may be rationalized, but the precise orgins of the effect are not understood. Although the obvious anisotropy is associated with the carbon lattice, the nominally cubic vanadium lattice may be distorted by the ordering of the carbon vacancies. Thus, de Novion et al.[3] have noted that a slight displacement (~ 2%) of the vanadium atoms from their cubic sites is necessary to account for the intensities of the superlattice lines observed by X-ray diffraction in V_8C_7. The corresponding displacements have not been determined for

---

*Values of the parameters are approximate because possible distortions of the parent rocksalt structure have not been included.

TABLE 4.1

PARAMETERS OF THE ATOMS IN V_6C_5

ATOM	x	y	z
V(1)	4/9	-1/9	1/4
V(2)	-2/9	-4/9	1/4
V(3)	1/9	2/9	1/4
V(4)	-2/9	-1/9	1/12
V(5)	4/9	2/9	1/12
V(6)	1/9	-4/9	1/12
C(1)	1/9	-4/9	1/3
C(2)	-2/9	-1/9	1/3
C(3)	4/9	2/9	1/3
C(4)	-2/9	2/9	1/6
C(5)	4/9	5/9	1/6
C	1/9	-1/9	1/6

V_6C_5, but the magnitudes may be similar in the two compounds. Birefringence could arise, therefore, from the anisotropy of the carbon lattice, from the associated distortion of the vanadium lattice, or from a combination of both effects. A detailed interpretation must await identification of the electronic excitations that are responsible for the optical properties in the visible region of the spectrum.

4.3. Discussion of ordering effects

This investigation has shown that single crystal vanadium carbide grown from the melt with a carbon-to-metal ratio close to the integral composition V_6C_5 is an ordered hexagonal (trigonal) compound belonging to the space group $P3_1$ or $P3_2$. This structure is very different from that reported by de Novion et al.[3] for powdered material prepared by reacting the metal hydride with graphite. To determine whether the difference is a consequence of the two different methods of preparation, single crystal specimens with a composition close to V_8C_7 have been grown from the melt and examined by transmission electron microscopy. A detailed interpretation is beyond the scope of this work, but the results indicate that these specimens also exhibit ordering in the carbon sublattice and their electron diffraction patterns are consistent with the cubic superlattice unit cell proposed by de Novion et al.[3] Accordingly,

/

it is concluded that at least two superlattice structures are stable within the "cubic" phase field of the vanadium-carbon phase diagram and are established because of differences in composition -- not necessarily because of different methods of preparation.

Although there is no essential disagreement between the two results it should be noted that de Novion et al.[3] did not anticipate a change in structure as the carbon concentration was decreased below that of V_8C_7. They observed that the superlattice X-ray lines diminished in intensity with decreasing carbon content and concluded that the distribution of additional vacancies did not exhibit long range order. The weak superlattice X-ray lines derived from the V_6C_5 structure were apparently overlooked in their investigation.

The proposed structure of V_6C_5 is generally consistent with the results of NMR and electron diffraction, but the fine striations observed under certain reflecting conditions, fig. 3.3, remain to be explained. These striations have not been investigated in detail, however the similarity between their appearance and the contrast effect observed by Pashley and Presland[4] in ordered CuAu II suggest that they arise from the presence of periodic planar faulting within the crystal.

The perfect V_6C_5 structure may be modified to include planar faults while simultaneously satisfying the NMR spectra from which the V_1 population as well as the relative population of V_1^1 and V_1^2 sites

have been determined. In the perfect structure, carbon vacancies are arranged on alternating carbon layers (parallel to the basal plane) in two-dimensional hexagonal nets that are, in turn, sequentially positioned so as to define either a right handed or left handed triad screw axis, fig. 4.3. This sequence is disrupted if one or more of the carbon layers that contain vacancies (C_v layers) is displaced by any vector in the basal plane that connects nearest neighbor carbon atoms. Such displacements do not change the V_1^1 or V_1^2 populations and for this reason it is expected that faults of this type would be low energy configurations with a high probability for forming in the V_6C_5 structure.

Two basic types of lamellar defects can be generated by the indicated displacements. If several successive C_v layers are all shifted according to the same displacement vectors, an antiphase region, bounded by antiphase boundaries (APB's), is formed in the manner shown schematically in fig. 4.5(a). If only one out of every three C_v layers associated with a unit cell is displaced in this fashion, the result is a change of handedness of the screw triad as illustrated in fig. 4.5(b). In principle, it should be possible to distinguish between the two configurations using standard diffraction contrast techniques[5,6] and the analytical method employed by McLaren and Phakey[7] in the study of enantiomorphic boundaries

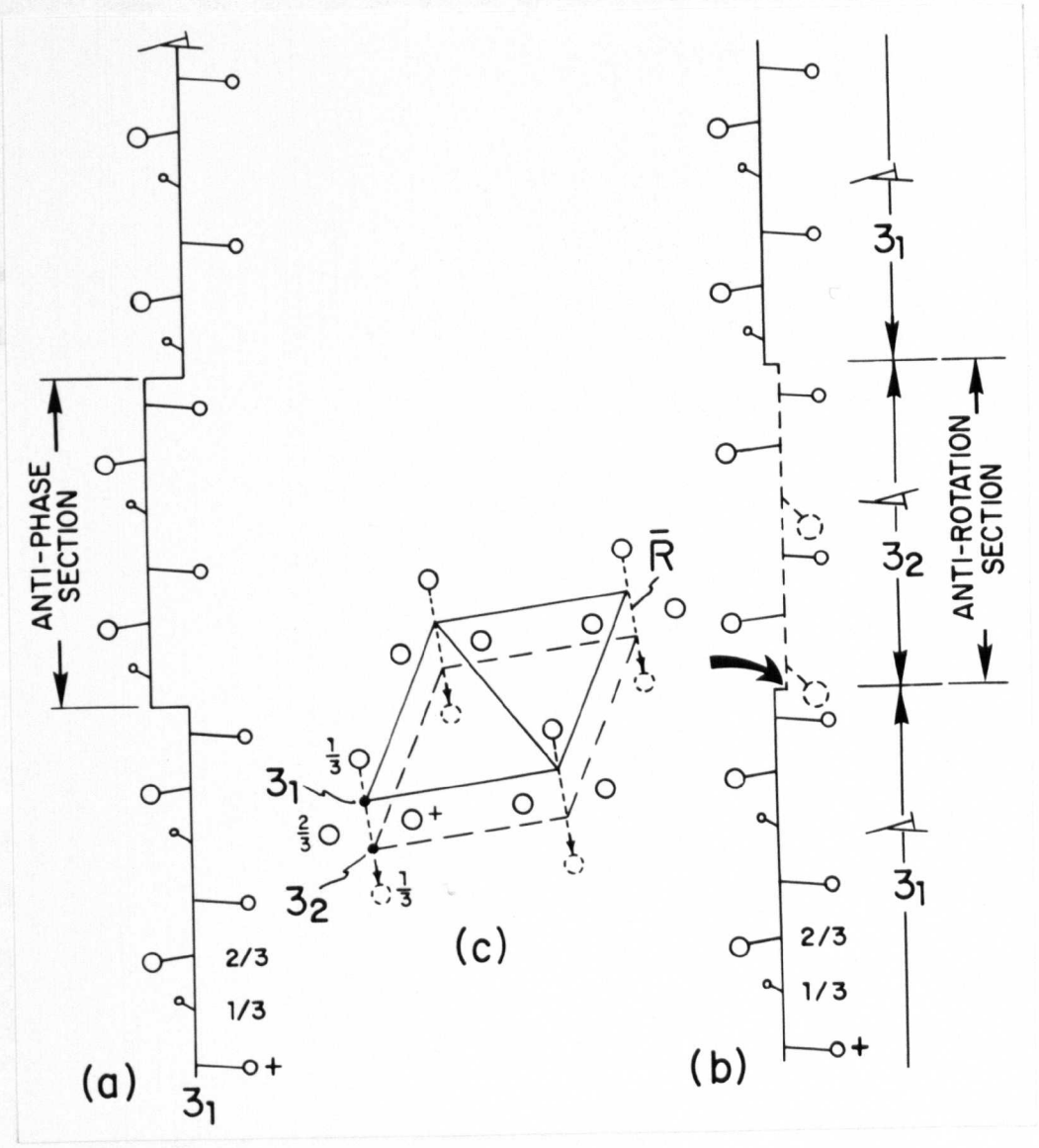

Fig. 4.5. Schematic representation of two types of lamellar defects which may occur in V_6C_5. In (a) an antiphase section is formed when several successive C_v layers (carbon layers that contain vacancies and lie parallel to the basal plane) are displaced by vector $\bar{R}$, where $\bar{R}$ is any vector in the basal plane that connects nearest neighbor carbon atoms. Depicted in (b) is the change-of handedness, or anti-rotation section that results when only one out of the three C_v layers associated with a unit cell is displaced by a vector $\bar{R}$. The basal plane projection (c) illustrates that the crystal axis does not remain coincident across an anti-rotation boundary, but is displaced by $\bar{R}/3$.

in quartz. The situation is complicated in the present case, however, by the narrow spacing between the faults which obscures details of the extinction fringe contrast.

REFERENCES

1. W. J. Childs, Phys. Rev., 156, 71 (1967).

2. D. Froidevaux and D. Rossier, J. Phys. Chem. Solids, 28, 1197 (1967).

3. C. H. de Novion, R. Lorenzelli, and P. Costa, Compt. Rend., 263, 775 (1966).

4. D. W. Pashley and A.E.B. Presland, J. Inst. Metals, 87, 419 (1959).

5. H. Hashimoto, A. Howie, and M. J. Whelan, Proc. Roy. Soc., A269, 80 (1962).

6. J. van Landuyt, R. Gevers, and S. Amelinckx, Phys. Stat. Sol., 7, 519 (1964).

7. A. C. McLaren and P. P. Phakey, Phys. Stat. Sol., 13, 413 (1966).

PART II

RADIATION DAMAGE OF V_6C_5 BY ELECTRON MICROSCOPE BEAM BOMBARDMENT

CHAPTER FIVE

LATTICE DISORDERING BY ELECTRON BOMBARDMENT

5.1 Evidence for disordering in V_6C_5 during electron bombardment

When a sample of the ordered compound V_6C_5 is examined for extended periods of time in a 100 kV electron microscope, both the superlattice diffraction spots and the domain structure diminish in intensity as illustrated in fig. 5.1. During the initial stages of observation, fig. 5.1(a), the domain structure and superlattice spot pattern remain visible, but after a 10-20 min. exposure to the 100 keV electron beam the domains and supplemental spots disappear entirely, fig. 5.1(b), although the intensity of the primary pattern increases slightly*. Similar effects are observed at other accelerating potentials, and in particular, even at the lowest potential employed in this study, 33 kV.

This disordering phenomenon is attributed to the displacement of carbon atoms by impinging electrons, and will be subjected to a detailed analysis in subsequent sections. That the effect

---

*The increased intensity of the primary pattern is not clearly depicted in fig. 5.1(b) because of the photographic reproduction difficulties, but it is apparent on the microscope viewing screen. This increase results from redistribution of the diffracted electrons into the primary spot pattern as the supplemental pattern decreases in intensity.

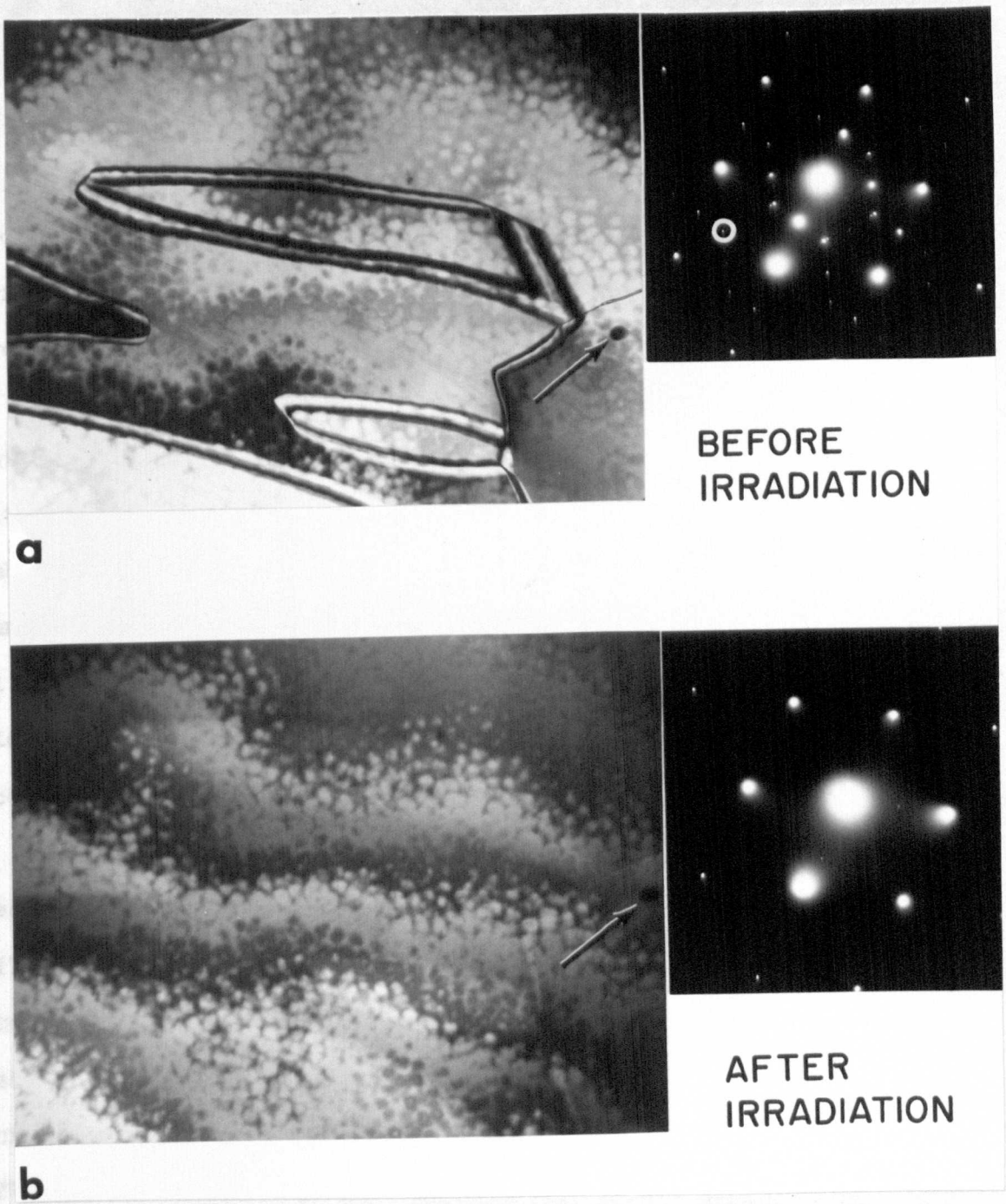

Fig. 5.1. Transmission electron micrographs and selected area diffraction patterns from a (110) foil (indices referred to cube axes) of V_6C_5, (a) before extensive irradiation with electron beam and (b) after 1/2 hour exposure to 100 keV electrons. (The fiducial mark indicated by arrows shows that the two micrographs were taken from the same region.) The domain structure and superlattice spots have disappeared in (b) due to radiation damage by the incident electron beam. Quantitative measurements of the rate of disordering were obtained by monitoring the intensity of diffraction spots derived from superlattice planes of the form $\{20\bar{2}0\}$. A typical spot of this type is circled in (a) above.

is due to radiation damage caused by electron bombardment was not obvious immediately, however, and several alternative explanations were explored and dismissed on the basis of the following arguments:

1. The effect is not due to the formation of a surface contamination film. It is observed that the intensity of the superlattice spots relative to that of the primary spots changes during bombardment, whereas the formation of a contamination film would cause a uniform decrease in the intensity of all the spots. Furthermore, all the present experiments were performed with a highly efficient cold finger positioned close to the sample area, and no evidence for a contamination film was noted at any time.

2. The effect is not due to ion bombardment. Pashley and Presland[1] have reported that defect clusters form in gold foils while under observation in the electron microscope. Because gold atoms are too heavy to be displaced by 100 keV electrons, they proposed that (oxygen) ion bombardment was responsible, and performed a critical experiment that supported their proposal. Using magnetic deflection, they separated the electrons from the much heavier ions, and observed that the defect clusters were formed at the point of impact of the ions. The opposite result was obtained, however, when this technique was employed in the present work on V_6C_5. The damaged region in V_6C_5 was always associated with the electron beam, which is

consistent with the proposal that the effect is, principally, due to electron bombardment.

3. The effect is not due to thermal disordering. Watanabe et al.[2] have demonstrated that the temperature of a metallic foil increased by less than 100°C when it was bombarded with a beam of 100 keV electrons focussed to a 5μ spot at a current density of 2 amp/cm^2. The present experiments on vanadium carbide, which also exhibits metallic thermal conductivity, were performed at current densities between 0.5 amp/cm^2 and 1.4 amp/cm^2. Thus, the sample temperature should have been far below the order-disorder transformation temperature of 1250°C reported for this material by Hollox and Venables.[3]

4. The effect is not due to injection of carbon vacancies. Dobson et al.[4] have observed that, under appropriate conditions, vacancies can be injected into specimens of aluminum alloys while they are under observation in the microscope. Thus, it might be argued that, if a specimen of V_6C_5 attained a sufficiently high temperature during bombardment, carbon atoms could unite with residual oxygen at the surface to form CO gas, possibly leaving behind a supply of vacancies sufficient to destroy the vacancy ordering in the lattice. It is observed, however, that when a previously disordered region of the sample is beam-heated in the microscope (by shutting off the second condenser lens, removing the condenser aperture and increasing

the beam intensity), it can be caused to re-order at an extremely rapid rate. This rapid (less than 1 sec.) disorder-to-order transformation is inconsistent with the long range diffusion that would be required to eliminate injected vacancies. For example, calculations utilizing the self-diffusion coefficients reported by Torkar et al.[5] for carbon in vanadium carbide indicate that 10 min. would be required for carbon atoms to diffuse into the 2μ diameter disordered region from the surrounding sample volume at 1250°C, the order-disorder temperature.

It is concluded, therefore, that the phenomenon illustrated in fig. 5.1 arises primarily because of the displacement of carbon atoms by the incident electrons, and a model for the disordering mechanism will be developed in Chapter Six following a brief review of the theory of electron damage in metals in the next section.

5.2 Theoretical considerations for disordering by electron bombardment

Historically the electron microscope has played a vital part in the study of radiation damage processes in solids, but its use has been confined generally to a somewhat passive role in the post irradiation examination of defects introduced by energetic particles. In this investigation the electron microscope assumes an active role, serving as a source of energetic particles and at

the same time providing a means for analyzing the resulting damage. This use of the electron microscope for studying radiation damage represents a distinct departure from those methods that have been commonly employed in this field, but the basic concepts which relate to the physics of the process are the same. Thus, before discussing the disordering in V_6C_5 by electron microscope beam bombardment specifically, it will be desirable to review some of the general theoretical considerations for lattice disordering by electron irradiation.

5.2.1 The displacement cross-section

An energetic electron incident upon a solid can displace atoms by various processes which depend upon the nature of the solid. In molecular and ionic crystals, atomic displacements can arise indirectly when energy is transferred from the incident electron to the electronic system of the crystal. Three basic mechanisms have been proposed whereby ionization effects lead to the formation of displacement damage. In one, the Varley[6] mechanism, it is proposed that a normally stable negative ion may be multiply ionized by electronic excitations leaving it positively charged and thus highly unstable in its normal lattice site. To minimize its energy, it is forced to occupy a more favorable (interstitial) position within the crystal. In the

Seitz[7] mechanism, it is suggested that excitons, which are formed by the energetic electrons, migrate freely through the lattice until they become trapped at dislocations where they recombine, releasing their energy in a "burst of lattice vibrations." The third mechanism involves only the single ionization of a negative ion to form a neutral atom and a free electron. Because the neutral atom is no longer bound electrostatically, it is at liberty to diffuse away from its lattice site into an interstitial position.[8] Unfortunately, it is difficult to devise experiments that will distinguish between these mechanisms, but, in any event, the data that are available suggest that ionization processes, rather than direct knock-on collisions with the nucleus, are important in promoting displacement damage by electrons in ionic crystals. (For a discussion of this subject see, e.g., the review article by Amelinckx.[9]

The situation is quite different for valence crystals and metallic solids, however, and there appears to be no experimental evidence to indicate that atom displacements can be generated by ionization processes alone.[10,11] In semiconductors such as germanium and silicon the recombination energy of electrons and holes is small compared with the heat of formation. Moreover, it has been shown by Seitz and Koehler[10] that in metals the coupling between excited s- or p-electrons and the lattice is so weak that

sufficient energy cannot be transferred to produce displacements. These authors have, however, suggested the possibility that excited d-electrons (which are more tightly coupled) may come to equilibrium with the lattice in such a manner to form thermal spikes and local disorder. Since vanadium carbide contains a transition element, this must be considered as a possible source of displacement damage but, as will be discussed in Chapter Seven, the experimental evidence in this case is not consistent with such a mechanism. Therefore, it will be assumed that the same displacement process that is applicable to most metals, i.e. coulomb encounters between the incident electron and the nucleus, accounts for the disordering in V_6C_5. The cross-section for the energy interchange resulting from such encounters may be derived on the following basis:

An energetic electron incident upon an atom interacts with the atom's nucleus through the coulomb potential

$$V(r) = \frac{Ze^2}{r}, \qquad (5.1)$$

where Z is the nuclear charge (Z = 6 for carbon). As a consequence of the encounter, an amount of energy is transferred to the atom which may be conveniently expressed in terms of the scattering angle, θ, in the center of gravity system (CGS) as follows: In the CGS, fig. 5.2(b), the center of mass moves with velocity

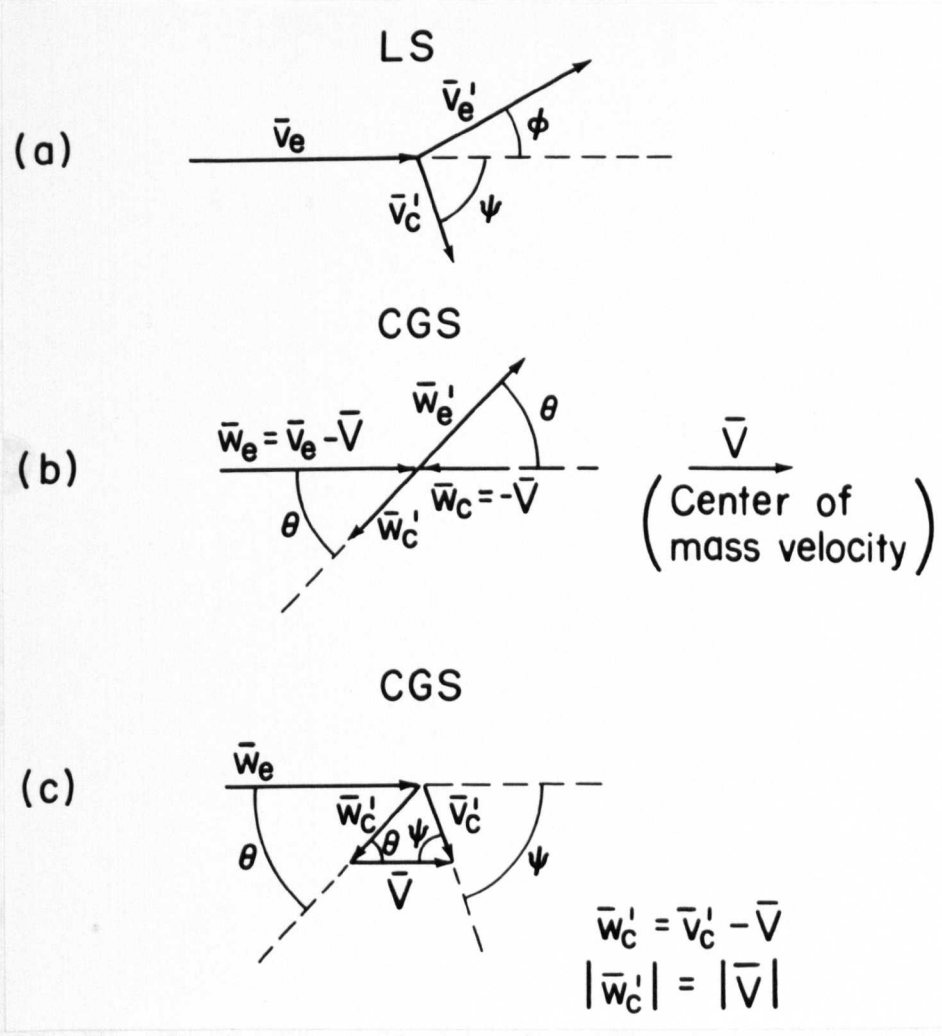

Fig. 5.2. Electron-atom collision in (a) the laboratory and (b) the center-of-gravity coordinate systems. The subscripts e and c refer to electron and atom velocities, respectively, and the primes refer velocities after collision. The relation between the velocities and scattering angles in the two systems is shown in (c). Since $|\bar{w}_c'| = |\bar{V}|$ it is apparent from (c) that $\psi = \frac{\pi}{2} - \frac{\theta}{2}$.

$$\bar{V} = \frac{m_e}{m_e + M_c} \bar{v}_e, \tag{5.2}$$

where m_e and M_c are the mass of the electron and atom, respectively, and $\bar{v}_e$ is the (non-relativistic) velocity of the incident electron in the laboratory system (LS), fig. 5.2(a). An observer in the CGS observes velocities

$$\bar{w} = \bar{v} - \bar{V}, \tag{5.3}$$

as graphically portrayed in fig. 5.2(c) for the velocities, $\bar{w}_c'$ and $\bar{v}_c'$, of the atom after collision. Because the conservation of momentum and energy insures that only the direction of the velocities is changed by the collision in the CGS, it is apparent that

$$|\bar{w}_c'| = |\bar{V}| \tag{5.4}$$

and that therefore

$$|\bar{v}_c'| = 2V \sin \frac{\theta}{2} \tag{5.5}$$

from inspection of fig. 5.2(c). Thus, the kinetic energy of the atom after collision is given by

$$E_c = E_m \sin^2 \frac{\theta}{2}, \tag{5.6}$$

where E_m is the maximum energy that can be transmitted to the atom from an incident electron having energy E_e, i.e.,

$$E_m = [(4m_eM_c)/(m_e + M_c)^2]E_e \approx (4m_e/M_c)E_e. \qquad (5.7)$$

The statistical distribution of atoms scattered into an annular cone of width $d\theta$, about θ, by non-relativistic classical electrons is given by the Rutherford[12] differential cross-section

$$d\sigma_R = \pi\left(\frac{Ze^2}{m_e v_e^2}\right)^2 \cos\frac{\theta}{2}\csc^3\frac{\theta}{2}\,d\theta \qquad (5.8)$$

where the reduced mass of the two particles has been approximated by the electron mass. Using equation (5.6) the cross-section may be expressed in terms of the energy distribution of the scattered atoms, and equation (5.8) becomes,

$$d\sigma_R = \pi\left(\frac{Ze^2}{m_e v_e^2}\right)^2 E_m \frac{dE_c}{E_c^2}. \qquad (5.9)$$

For relativistic electrons, equation (5.9) must be modified by expressing the mass as $m_e = m_o\gamma$, where $\gamma = (1 - \beta^2)^{-1/2}$ and $\beta = v/c$. Upon substitution, the expression for the cross-section becomes,

$$d\sigma_R = \pi\left(\frac{Ze^2}{m_o c^2}\right)^2\left(\frac{1}{\beta^4\gamma^2}\right) E_m \frac{dE_c}{E_c^2} \qquad (5.10)$$

where E_m must also be expressed relativistically as

$$E_m = \left(\frac{4m_o}{M_c}\right)(1 + E_e/2m_oc^2)E_e. \qquad (5.11)$$

Thus, for relativistic Rutherford scattering the probability that an atom receives an energy in the interval dE_c at E_c is proportional to E_c^{-2}.

Although equation (5.10) includes relativistic effects, it is still classical in the sense that it does not include the spin of the electron and its interaction with the nuclear potential. Mott[13] has taken account of this purely quantum effect to derive a formula for the scattering of Dirac electrons by a point nucleus. His exact result is difficult to handle analytically, however, and for the present purposes it will suffice to use an approximation derived by McKinley and Feshbach[14] which is valid for elements below copper in the periodic table. In this formulation, a correction factor, R, is applied to equation (5.10) as follows,

$$d\sigma_{MF} = R d\sigma_R \qquad (5.12)$$

where R is given by

$$R = \left[1 - \beta^2 E_c/E_m + \pi\alpha\beta\left((E_c/E_m)^{1/2} - E_c/E_m\right)\right] \qquad (5.13)$$

and $\alpha = Z/137$.

The total scattering cross-section may be obtained by integrating equation (5.12) but because the expression diverges for low energies it is necessary to restrict the range of integration at the low energy limit. Physically, low angle scattering is cut off by the screening effect of the orbital electrons surrounding the nucleus and by choosing an appropriate model for the screened nuclear potential, a reasonable estimate for the minimum energy transfer may be obtained. Seitz and Koehler[10] have shown that this minimum energy, although dependent upon the nuclear mass and charge, is of the order 10^{-2} eV and is therefore far below the energy, $E_d \sim 10\text{-}30$ eV, required to displace an atom in a typical solid. It follows that equation (5.12) is valid to a high degree of accuracy when only those collisions resulting in atomic displacements are considered. Thus, equation (5.12) may be integrated over the range from E_d to E_m to provide an expression for the total displacement cross-section,

$$\sigma_d = \pi \left(\frac{Ze^2}{m_o c^2}\right)^2 \left(\frac{1}{\beta^4 \gamma^2}\right) \left[\left(\frac{E_m}{E_d} - 1\right) - \beta^2 \ell n\left(\frac{E_m}{Ed}\right) + \pi\alpha\beta \left\{ 2\left[\left(\frac{E_m}{E_d}\right)^{1/2} - 1\right] - \ell n\left(\frac{E_m}{E_d}\right)\right\}\right], \tag{5.14}$$

where σ_d has the units of area and the meaning that its product

with the magnitude of the incident electron flux (electrons/cm^2sec) gives the number of atomic displacements/second.

5.2.2 Secondary displacements

When the energy of an atom that has been displaced by an incident electron is in excess of E_d, it may dislodge other atoms from the lattice. The problem of determining the number of secondary displacements produced per primary has been treated by Snyder and Neufeld[15,16] and Harrison and Seitz.[17] Seitz and Koehler[10] combined certain features of the two similar methods and concluded that the total number of atoms, g, which are displaced when a primary atom is produced with an energy E_c may be described by the following relations,

$$\begin{aligned} g_1(x) &= 1 && 0 \leq x \leq 1 \\ g_2(x) &= 1 + \ell nx && 1 < x \leq 3 \\ g_3(x) &= 0.561\ (1+x) && x > 3 \end{aligned} \qquad (5.15)$$

where x is the energy of the atom in excess of that required to displace it from its lattice site and is expressed in units of the displacement energy, i.e.,

$$x = (E_c - E_d)/E_d. \qquad (5.16)$$

It will be noted that g(x) includes the primary atom and, therefore, has a minimum value of unity.

The mean number of atoms displaced per primary is obtained by weighting g(x) with the energy distribution function appropriate to the primary atoms and averaging over the energy range of the primaries. To a reasonable approximation the distribution given by equation (5.10) may be employed, in which case the weighting factor is $1/E_c^2 \propto 1/(1 + x)^2$. The mean number of displaced atoms is then given by either,

$$\bar{\nu} = 1 \tag{5.17}$$

if $0 \leq x_m \leq 1$, or

$$\bar{\nu} = \left[1.19 + \frac{(x_m-1)}{2(x_m+1)} - \frac{\ell n x_m}{(x_m+1)} - \ell n(x_m+1)/x_m\right] \frac{(x_m+1)}{x_m} \tag{5.18}$$

if $1 < x_m \leq 3$, or

$$\bar{\nu} = \left[0.881 + 0.561\ \ell n(x_m+1)/4\right] \frac{(x_m+1)}{x_m} \tag{5.19}$$

if $x_m > 3$, where x_m, the maximum value of x, is given by

$$x_m = (E_m - E_d)/E_d. \tag{5.20}$$

It is apparent that the total cross-section, σ_d, must be multiplied by the factor, $\bar{\nu}$, to take account of the secondary displacements.

The theory of atomic displacements in solids has now been developed sufficiently to treat the disordering phenomenon observed in V_6C_5. In the next two chapters, the results of this theory will be employed in the development of a model for the disordering process and in the interpretation of experimental observations to obtain a value for the carbon atom displacement energy, E_d.

REFERENCES

1. D. W. Pashley and A.E.B. Presland, Phil. Mag., 6, 1003 (1961).

2. M. Watenabe, T. Someya, and Y. Nagahama, "Fifth Intl. Congress for Electron Microscopy", Paper A-8, (Academic Press, New York, 1962).

3. G. E. Hollox and J. D. Venables, Proc. Intl. Conf. on Strength of Metals and Alloys, Tokyo, in Suppl. Trans. Japan Inst. Metals, 9, 295 (1968).

4. P. S. Dobson, S. Kritzinger, and R. E. Smallman, Phil. Mag., 17, 769 (1968).

5. K. Torkar, H. Oel, and A. Illingen, Berichte der Deutchen Keramischen Gesellshaft, 43, 162 (1966).

6. J.H.O. Varley, J. Nuclear Energy, 1, 30 (1954).

7. F. Seitz, Rev. Mod. Phys., 26, 81 (1954).

8. J. H. Schulman and W. D. Compton, "Color Centers in Solids", (Pergamon Press, New York, 1962) p. 213.

9. S. Amelinckx, in "Radiation Damage in Solids", ed. D. S. Billington, (Academic Press, New York, 1962) p. 421.

10. F. Seitz and J. S. Koehler, in "Solid State Physics", ed. F. Seitz and D. Turnbull, Vol. 2, (Academic Press, New York, 1956).

11. J. W. Corbett, ibid, supplement to Vol. 7, (1966).

12. E. Rutherford, Phil. Mag., 21, 669 (1911).

13. N. F. Mott, Proc. Roy. Soc., A124, 426 (1929).

14. W. A. McKinley and H. Feshbach, Phys. Rev., 74, 1759 (1948).

15. W. S. Snyder and J. Neufeld, Phys. Rev., 97, 1636 (1955).

16. J. Neufeld and W. S. Snyder, Phys. Rev., 99, 1326 (1955).

17. W. Harrison and F. Seitz, Phys. Rev., 98, 1530 (1955).

CHAPTER SIX

A MODEL FOR THE DISORDERING IN V_6C_5

6.1 The displacement process

The threshold energy required to displace an atom in a solid from its equilibrium lattice site by an energetic incident particle is expected to have a value near 25 eV,[1] but in fact it varies from ~ 10 eV to ~ 30 eV in different materials.[2] For example, Corbett et al.[3] determined the value 22 ± 3 eV for copper, and Denney[4] found a threshold energy of 27 eV for displacing Fe atoms in a Cu-Fe alloy. Thus, the threshold energy for displacing vanadium atoms in vanadium carbide is expected to be approximately 25 eV also. Consequently, if the bombarding particles are electrons, they must have energies in excess of 420 keV in order to displace the vanadium atoms by direct collisions. At this incident energy, however, the relatively low mass of the carbon atoms allows some of them to receive as much as 110 eV from the electrons, and these carbon atoms in turn can transmit up to 65 eV to vanadium atoms in secondary collisions. Thus, the radiation damage caused by high energy electrons is expected to be a complex superposition of primary and secondary effects involving both kinds of atoms.

The problem is much simpler when the incident electrons have energies less than 220 keV, for then the vanadium atoms would not be

displaced either by the incident electrons or by the most energetic primary displaced carbon atoms. It follows that only the carbon atoms will be displaced by electrons having energies in the range employed in the present investigation (33 keV to 100 keV). Of course, the vanadium atoms will absorb energy from the electron beam and thereby increase the temperature of the specimen. In addition, they will scatter the displaced carbon atoms, modifying their kinetic energies and terminal displacements, but otherwise they will remain unaffected.

If the threshold energy for displacing carbon atoms in vanadium carbide were also 25 eV, bombardment by electrons would be expected to cause little rearrangement of the atoms unless the incident energy were greater than 122 keV. However, the observations reported in Chapter Five indicate that the spots in the diffraction pattern that are associated with ordering in the C-lattice become degraded at a significant rate during electron bombardment at energies as low as 33 keV, which implies that the threshold energy for displacing carbon atoms must be less than 6.22 eV. To obtain a more quantitative estimate for the displacement energy, the experimental results have been analyzed according to the following model*:

---

*The development of this model was accomplished with R. G. Lye of RIAS. Those features of the model discussed in (3) and (4) below are due principally to his efforts, and are reproduced here with his kind permission.

1. The elastic collisions between the incident electrons and the carbon atoms satisfy the relativistic Rutherford scattering relation given by equation (5.10) to a good approximation*. Thus, the probability that a carbon atom receives an energy in the interval dE_c at E_c is proportional to E_c^{-2} for $E_c \leq E_m$, where E_m is given by equation (5.11). The conditions employed in the electron microscope ensure that the energy of the bombarding electrons decreases by an insignificant fraction during their passage through the specimen. (For example, 51 keV electrons lose approximately 310 eV by electron-electron collisions in traversing a foil of V_6C_5 1000 Å in thickness.) Consequently, the distribution in initial energies of the carbon atoms also remains uniform throughout the foil.

2. The structure of the ordered compound V_6C_5 can be represented in a useful approximation as two interpenetrating fcc lattices, one of which (the V-lattice) is completely occupied by the vanadium atoms, whereas the other (the C-lattice) is only partially occupied by by the carbon atoms. It will be assumed that the carbon atoms lie in spherically symmetric potential wells of uniform depth, E_d, the same for all sites in the C-lattice. Thus, no carbon atom can be displaced unless it receives an energy greater than E_d from the incident electron.

---

*This simplifying assumption is made for the arguments presented in this section. The experimental data, however, will be compared with the more accurate McKinley and Feshbach relation given by equation (5.12).

3. Those carbon atoms that receive energies $E_c > E_d$ are displaced initially from their equilibrium positions into the forward cone bounded by the half angle $\psi = \pi/2 - \theta_m/2$, where $\sin^2(\theta_m/2) = E_d/E_m$, see fig. 5.2. As will become evident later, the cone is somewhat restricted, ψ varying from approximately 59° for 100 keV electrons to 22° for 33 keV electrons. If only the portion $(E_c - E_d)$ of the energy received by the carbon atoms from the incident electrons is available as kinetic energy of motion of the displaced atoms, their mean initial kinetic energy is $(\langle E_c \rangle - E_d)$ where $\langle E_c \rangle$ is given by

$$\frac{\langle E_c \rangle}{E_d} = \frac{1}{E_d} \left[\int_{E_d}^{E_m} \left(\frac{1}{E_c^2} \right) E_c \, dE_c \right] \Bigg/ \left[\int_{E_d}^{E_m} \left(\frac{1}{E_c^2} \right) dE_c \right]$$
$$= (1 + x_m) x_m^{-1} \ell n (1 + x_m) \qquad (6.1)$$

in which $x_m = (E_m - E_d)/E_d$. Because the energy of the bombarding electrons is rather small, $(\langle E_c \rangle - E_d)/E_d < 1$ throughout the range of the present study. Moreover, the fraction of the displaced carbon atoms that receive kinetic energies greater than E_d also is small:

$$\frac{n(E_c > 2E_d)}{n(E_c > E_d)} = \left[\int_{2E_d}^{E_m} \left(\frac{1}{E_c^2} \right) dE_c \right] \Bigg/ \left[\int_{E_d}^{E_m} \left(\frac{1}{E_c^2} \right) dE_c \right]$$
$$= (x_m - 1)/2x_m, \; x_m \geq 1,$$
$$= 0 \qquad , \; x_m < 1. \qquad (6.2)$$

Thus, significant multiplication of the displaced carbon atoms by secondary collisions is expected to occur only near the upper limit of bombarding energies employed in this study. According to the analysis presented in section 5.2.2, the multiplication factor, $\bar{\nu}$, obtained by averaging over the initial energy distribution, has the value unity when the maximum energy received by the displaced atoms lies between E_d and twice this threshold energy. It increases slowly at higher energies, and attains a value near 1.15 at $x_m = 2.72$, which corresponds to bombardment by 100 keV electrons if the energy lost in collisions with the vanadium atoms is neglected.

4. The displaced carbon atoms undergo hard-sphere collisions with the neighboring atoms in their line of flight.(1) If the cone of initial displacements is sufficiently broad, the atoms will be scattered isotropically, losing on the average 0.31 of their energy in each collision with a vandium atom and 0.5 of their energy in each collision with a carbon atom. The mean energy lost in the first of such collisions, $\langle \delta E_{cj} \rangle$, may be obtained from

$$\langle \delta E_{cj} \rangle = \left[\int_0^{E_{jcm}} E_{jc} N(E_{jc}) dE_{jc} \right] \Big/ \left[\int_0^{E_{jcm}} N(E_{jc}) dE_{jc} \right], \quad (6.3)$$

where $N(E_{jc})$ is the energy distribution function of the secondary atoms that have maximum energies,

$$E_{jcm} = C_j(E_m - E_d)$$

where

$C_j = C_c \equiv 1$ for collisions with C atoms,

and

$C_j = C_v \equiv 4\, M_c M_v (M_c + M_v)^{-2} = 0.618$ for collisions with V atoms,

in which M_c and M_v are the masses of the carbon and vanadium atoms, respectively. The distribution function, $N(E_{jc})$, is proportional to,

$$\int_{E_c = (E_{jc}/C_j) + E_d}^{E_m} \left(\frac{1}{E_c 2}\right) \frac{1}{C_j(E_c - E_d)}\, dE_c,$$

where the term $1/[C_j(E_c - E_d)]$ is the probability that a C or V atom receives an energy in the interval dE_{jc} at E_{jc} when hit by a primary carbon atom having an initial energy E_c (isotropic scattering), and the term $1/E_c^2$ is proportional to the energy distribution function of the primary carbon atoms. When the resultant expression for $N(E_{jc})$ is substituted into equation (6.3), there is obtained upon integration,

$$((\delta E_{cj})/E_d) = (C_j/2)[(1+x_m)x_m^{-1}\ln(1+x_m) - (1+x_m)^{-1}]. \quad (6.4)$$

If the first collisions are with vanadium atoms, the mean energy loss is less than the excess over E_d of the initial mean energy, i.e.,

$$\frac{\langle \delta E_{cv} \rangle}{\langle E_c \rangle - E_d} = \frac{(C_v/2)[(1+x_m)x_m^{-1}\ell n(1+x_m) - (1+x_m)^{-1}]}{[(1+x_m)x_m^{-1}\ell n(1+x_m) - 1]} < 1. \qquad (6.5)$$

Thus, on the average, a primary displaced carbon atom can make at least one collision with a vanadium atom in the nearest neighbor shell before its energy falls below E_d. Most of the displaced carbon atoms, therefore, can penetrate beyond the nearest neighbor shell of vanadium atoms, and the resultant scattering will broaden the distribution of velocity vectors to encompass a greater fraction of the sites in the nearest neighbor shell of the C-lattice than was accessible in the initial cone. This scattering will also change the distribution in energy of the displaced atoms as they approach the nearest neighbor shell of the C-lattice, and the reduction in the mean energy will, in turn, decrease the probability of multiplication by subsequent collisions with carbon atoms.

The energy loss ratio for collisions with carbon atoms, $\langle \delta E_{cc} \rangle / (\langle E_c \rangle - E_d)$, remains greater than unity throughout most of the range of energies employed in these studies, becoming less than unity only for $x_m \gtrsim 2.15$ ($E_e \gtrsim 85$ keV). The ratio decreases very

slowly at higher energies, however, and only attains a value near 0.96 for $x_m = 2.72$, which corresponds to an incident electron energy of 100 keV if changes in the energy distribution caused by prior scattering from vanadium atoms are neglected. Accordingly, the displaced atoms are scattered strongly by the nearest neighbor shell of carbon atoms, and subsequent scattering by the second shell of vanadium atoms ensures that few of the displaced atoms reach the second shell of the C-lattice. It follows, therefore, that the carbon atoms have a high probability of being permanently displaced only if a vacant site is accessible in the nearest neighbor shell of the C-lattice.

5. The displaced carbon atoms are trapped at vacant sites within the C-lattice, not at the tetrahedral interstitial positions within the metal lattice. The latter possibility was investigated experimentally by comparing the intensities of the 111 and 222 sets of primary lattice spots, which are sensitive to the fraction of carbon atoms in the tetrahedral sites. In particular, computer calculations by Kahn[5] show that the ratio of intensity of the 111 spot to that of the 222 spot would increase by the factor 1.20 if 10% of the carbon atoms were transferred from octahedral to tetrahedral sites, whereas no change would be expected from a simple redistribution within the octahedral sites. During the bombardment,

the intensities of both 111 and 222 spots were found to increase, as expected, but the ratio of their intensities remained constant within approximately 15%. It can be concluded, therefore, that at most a small fraction (< 10%) of the displaced atoms are trapped at tetrahedral sites under the experimental conditions employed here. Thus, the principal effect of the damage process is to rearrange the carbon atoms so that they become more randomly distributed over the octahedral sites as suggested schematically in fig. 6.1.

6. In the C-lattice, there are N sites per unit volume, of which the fraction $r = 5/6$ is occupied in the ordered compound and the fraction (1-r) is vacant. Following a common convention, the sites that are occupied in the perfectly ordered compound will be designated the α sites, and the vacant sites will be designated β sites. If the ordered compound has its stoichiometric composition, there will be rN carbon atoms per unit volume in the C-lattice. In the perfectly ordered state, all of the rN carbon atoms will be on the rN α sites, and all of the (1-r)N β sites will be vacant. Otherwise, there will be a smaller number, n_a, of carbon atoms per unit volume on the α sites, and the remainder, $n_b = rN - n_a$, will be distributed over the β sites.

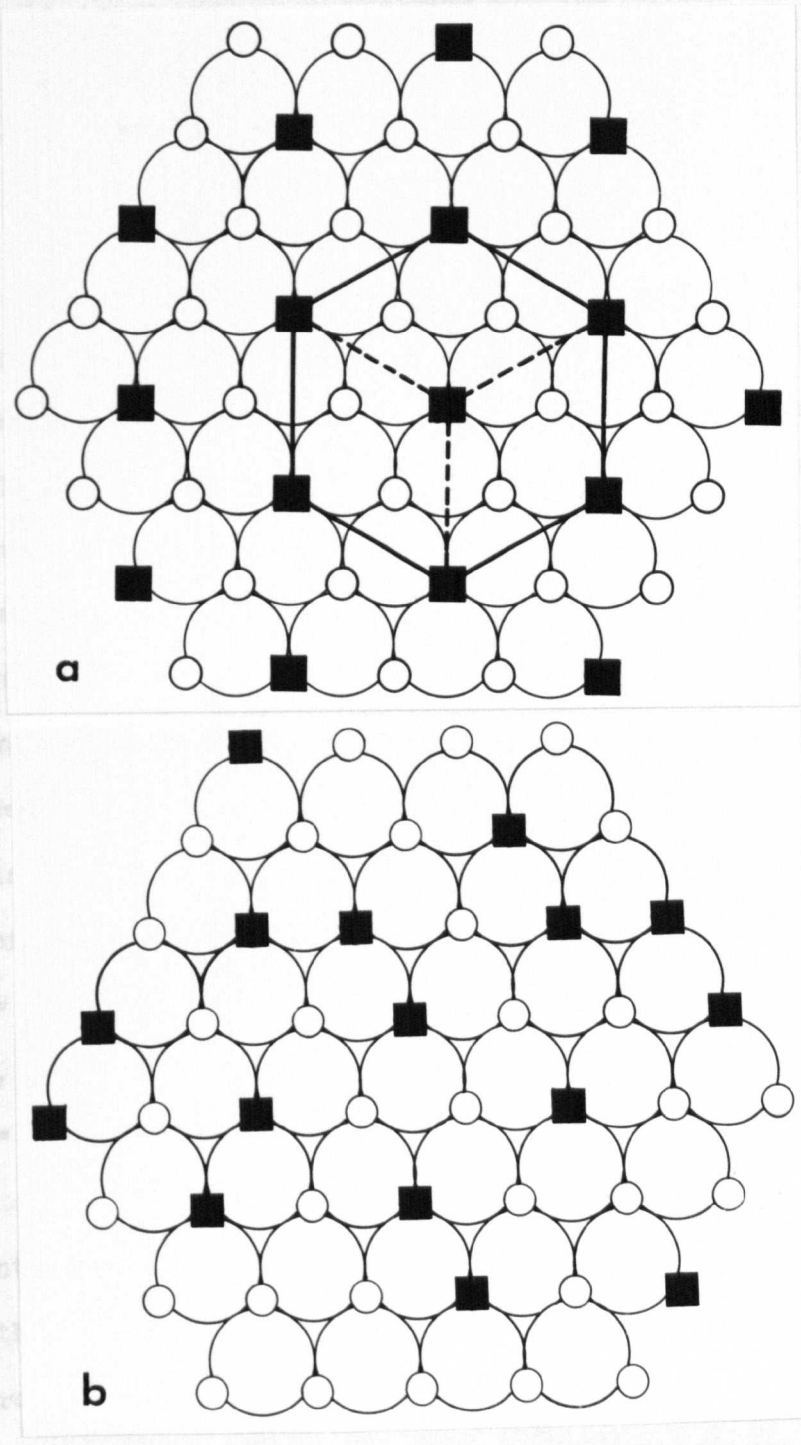

Fig. 6.1. Comparison of (a) ordered V_6C_5 structure as viewed along trigonal c-axis, and (b) structure after it has been disordered by electron bombardment. Based on considerations described in the text, electrons having energies in the range employed in this study displace only the carbon atoms, causing them to become randomly distributed over sites in the fcc carbon sublattice as suggested in (b). (Large circles, small circles, and squares represent vanadium atoms, carbon atoms, and carbon vacancies, respectively.)

It is assumed that when a low-energy displaced atom approaches a vacant site in the C-lattice it will be captured with equal likelihood whether the site belongs to the α- or the β- sublattice. Thus, a displaced atom has probabilities of being captured by α- and β- sites that depend only on the concentrations of the two kinds of sites accessible to it from its initial position in the lattice. Two kinds of α sites can be distinguished in V_6C_5 according to the concentrations of β sites in the nearest neighbor shell of the C-lattice: 3/5 of the α sites have 2 β sites among the 12 positions in this shell; the remaining 2/5 have 3 β sites. Thus, the fraction of β sites surrounding an α site has the average value $f_{\beta/\alpha} = 1/5$. Only one kind of β site can be distinguished on this basis, and it has only α sites in its nearest neighbor shell, i.e., $f_{\alpha/\beta} = 1$.

It will be also assumed that these fractions represent the concentrations of α or β sites available to a displaced atom from the other kind of site regardless of the energy of the impinging electron beam or of its orientation relative to the crystallographic axes. At energies somewhat greater than those employed here, it appears probable that the range of the primary displaced carbon atoms will become sufficiently great that their probabilities

of being captured by α and β sites will approach the average concentrations of the two kinds of sites in the C-lattice, i.e. $f_{\beta/\alpha} \rightarrow 1/6$ and $f_{\alpha/\beta} \rightarrow 5/6$, under high energy electron bombardment. The behavior of the carbon atoms is more difficult to describe when they are displaced by low-energy bombarding electrons having energies near the threshold. It seems likely that under these circumstances the orientation of the beam may influence not only the distribution of α and β sites accessible to the displaced atom, but also the effective value of the energy required for displacement as discussed by Brown and Augustyniak[6] and Walker.[7] These complexities will not be considered here. Instead, it will be assumed for simplicity that all of the sites in the nearest neighbor shell are equally accessible throughout the range of energies investigated, and that the displaced atoms reach the second shell of the C-lattice in such small numbers that they have little effect on the fractions $f_{\alpha/\beta}$ and $f_{\beta/\alpha}$.

6.2 The rate of disordering

According to the above description, the rate of change of the number of carbon atoms on α sites is the difference between the rate of displacement from α to β sites that results from electron bombardment and the rate of the reverse displacements that occur when some of the β sites are occupied:

$$dn_a/dt = J\sigma_d\bar{\nu}[-f_1 n_a + f_2 n_b], \qquad (6.6)$$

where J is the incident electron flux (electrons/cm^2sec.);

σ_d is the cross-section for displacement of a carbon atom by the incident electrons, assumed to be the same for both α and β sites;

f_1 is the fraction of displacement collisions with atoms on α sites that result in transfer to β sites, $f_1 = f_{\beta/\alpha}(1-n_b/N_b)$;

f_2 is the fraction of displacement collisions with atoms on β sites that result in transfer to α sites, $f_2 = f_{\alpha/\beta}(1-n_a/N_a)$;

and $\bar{\nu}$ is the factor required to account for the multiplication that may occur if the primary displaced atom has an energy sufficient to effect a secondary displacement and is given by either equation (5.17), (5.18), or (5.19), depending upon the value of x_m.

Equation (6.6) can be integrated directly to yield

$$p_a = n_a/rN = r + (1-r)\exp-(fJ\sigma_d\bar{\nu})t, \qquad (6.7)$$

if it is assumed that the crystal is perfectly ordered at $t = 0$. The coefficient f in the exponential has the value $6/5$ for V_6C_5 if

the displaced atoms have access only to the nearest neighbor shell of the C-lattice, the limitation that is expected to prevail in the present study. At somewhat higher bombarding energies, f is expected to decrease gradually toward unity as the range of the primary displaced atoms approaches the radius of the second shell in the C-lattice.

This result may be used to interpret the experimental observations of electron bombardment disordering, because the probability that an α site is occupied by a carbon atom, $p_a = n_a/rN$, may be related in a simple manner to the measured intensity of a superlattice diffraction spot. According to the present model, the Bragg-Williams[8] long-range order parameter, S, defined by the relation

$$S \equiv (p-r)/(1-r), \tag{6.8}$$

assumes the simple form

$$S = \exp - (fj\sigma_d\bar{\nu})t. \tag{6.9}$$

On the other hand, the geometrical structure factor of a superlattice diffraction spot in V_6C_5 is related to S in the following manner:

The general expression for the structure factor corresponding to reflecting planes (h,k,ℓ) is given by,[9]

$$|F(h,k,\ell)|^2 = [\sum_r f_r A_r]^2 + [\sum_r f_r B_r]^2 \qquad (6.10)$$

where f_r is the atomic scattering factor for the atom at the site $\underline{r}$,

$$A_r = \sum_j \cos 2\pi(hx_j + ky_j + \ell z_j), \qquad (6.11)$$

$$B_r = \sum_j \sin 2\pi(hx_j + ky_j + \ell z_j), \qquad (6.12)$$

and x_j, y_j, z_j are the coordinates of any one of the equivalent sites for the atom which has the scattering factor f_r. The summations in A_r and B_r extend over all the equivalent positions in the unit cell. The summation in $F(h,k,\ell)$ extends over all the different kinds of atoms in the unit cell.

The ordered compound V_6C_5 is based on two interpenetrating lattices one of which is assumed to be completely occupied by V-atoms. The other lattice is divided into two sublattices, the α sublattice being completely occupied by C-atoms and the β sublattice being completely vacant in the ordered state. When the crystal is partially ordered, the probabilities that the α and β sites are occupied are given, respectively by,

$$p_a = \frac{n_a}{rN} = r + S(1-r) \qquad (6.13)$$

and

$$p_b = \frac{n_b}{(1-r)N} = \frac{rN-n_a}{N(1-r)} = r(1-S). \qquad (6.14)$$

In these circumstances the structure factor can be written in the form:

$$|F(h,k,\ell)|^2 = [f_v \sum_v A_v + f_c p_a \sum_\alpha A_\alpha + f_c p_b \sum_\beta A_\beta]^2 + [f_v \sum_v B_v + f_c p_a \sum_\alpha B_\alpha + f_c p_b \sum_\beta B_\beta]^2 = [A]^2 + [B]^2. \quad (6.15)$$

Assuming that the metal atoms are not distorted from their fcc lattice sites, they make no net contribution to the superlattice structure factor which means that,

$$A_v = 0 \quad \text{and} \quad B_v = 0. \quad (6.16)$$

Thus, after substituting (6.13), (6.14), and (6.16) into (6.15) the separate terms of (6.15) become

$$[A]^2 = f_c^2[r(1-S)(\sum_\alpha A_\alpha + \sum_\beta A_\beta) + S \sum_\alpha A_\alpha]^2 \quad (6.17)$$

$$[B]^2 = f_c^2[r(1-S)(\sum_\alpha B_\alpha + \sum_\beta B_\beta) + S \sum_\alpha \beta_\alpha]^2. \quad (6.18)$$

These expressions can be simplified considerably by noting that the factors $(\sum_\alpha A_\alpha + \sum_\beta A_\beta)$ and $(\sum_\alpha B_\alpha + \sum_\beta B_\beta)$ are both identically equal to zero since each factor represents a summation over <u>all</u> the octahedral sites in the unit cell. For superlattice planes (h,k,ℓ) such

summations must vanish and, therefore, equation (6.15) may be written as,

$$|F(h,k,\ell)|^2_{S.L.} = f_c^2 S^2 [(\Sigma_\alpha A_\alpha)^2 + (\Sigma_\alpha B_\alpha)^2] \qquad (6.19)$$

or more simply, as

$$|F(h,k,\ell)|^2_{S.L.} = KS^2. \qquad (6.20)$$

Moreover, the calculations presented in Appendix II indicate that, for the experimental conditions employed, the intensity, I, of a superlattice diffraction spot is proportional to the square of its structure factors to a good approximation. Combining this result with equations (6.9) and (6.20), the variation in intensity of one of these superlattice diffraction spots is then described by the relation

$$d\ell nI/dt = - (12/5) J \sigma_d \bar{\nu}. \qquad (6.21)$$

The cross-section, σ_d, for displacing carbon atoms has been determined on this basis for several energies of the incident electrons, and the results are presented in the following chapter.

REFERENCES

1. F. Seitz and J. S. Koehler, in Solid State Physics, ed. F. Seitz and D. Turnbull, Vol. 2 (Academic Press, New York, 1956).

2. G. J. Dienes and G. H. Vineyard, "Radiation Effects in Solids" (Interscience, London, 1957).

3. J. W. Corbett, J. M. Denney, M. D. Fiske, and R. M. Walker, Phys. Rev., 108, 954 (1957).

4. J. M. Denney, Phys. Rev., 92, 531 (1953).

5. D. Kahn, RIAS, Private communication.

6. W. L. Brown and W. M. Augustyniak, J. Appl. Phys., 30, 1300 (1959).

7. R. M. Walker, in "Radiation Damage in Solids" (Academic Press, New York, 1962) p. 594 ff.

8. W. L. Bragg and E. J. Williams, Proc. Roy. Soc., A151, 540 (1935).

9. "International Tables for X-ray Crystallography," Vol. I edited by N.F.M. Henry and K. Lonsdale. (Kynoch Press, Birmingham, England, 1952.)

CHAPTER SEVEN

THE DISPLACEMENT ENERGY OF CARBON ATOMS IN V_6C_5

7.1 Measurement of E_d

Equation (6.21) does not contain the displacement energy, E_d, directly, however E_d can be obtained once the behavior of σ_d vs E_e is known. Thus, σ_d has been determined for four values of E_e in the range 33 keV to 100 keV by measuring the decay rate of superlattice spot intensities during irradiation by the electron microscope beam.

Both the incident electron flux and the intensity of the superlattice diffraction spots were measured with a Faraday cup positioned in the lower part of the microscope column, fig. 7.1. A grounded shield, which encloses the cup to prevent interference by stray electrons, is coated on top with a phosphor to aid in aligning the beam or the diffraction spot with the hole in the cup. The electron current flow through the cup was measured with a General Radio 1230-A electrometer that is capable of measuring currents as small as 10^{-13} amp.

Two relatively independent methods were employed to measure the incident flux. In the first of these, the central portion of the electron beam was aligned over the hole in the shield.

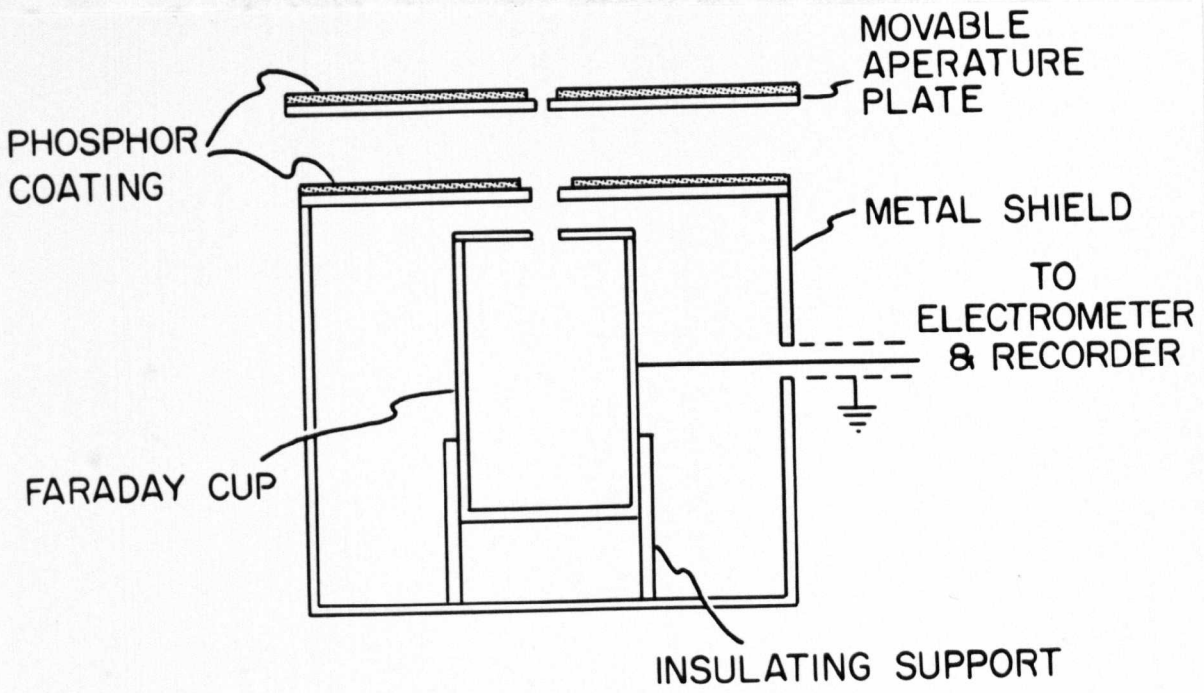

Fig. 7.1. Design of the Faraday cup used to measure electron microscope beam flux and to monitor V_6C_5 superlattice spot intensities during electron bombardment. The cup is positioned centrally in the lower part of the microscope column where phosphor screens, used as aids in aligning beam with aperture or hole in cup, may be observed through normal viewing ports. The metal shield protects the cup from stray electrons, whereas the aperture plate serves to reduce background intensity around superlattice spot.

To prevent undesirable focussing effects due to charging of the phosphor coating, the selected area diffraction blades were positioned to block all radiation except that passing into the Faraday cup. With the sample removed and the aperture plate swung out of the way, measurements were made of the electron flow through the cup. Using the appropriate magnification factor, which was determined with a grating replica, the area of the hole could be translated into a corresponding area at the sample plane. From these measurements the electron current density at the sample plane could be determined.

In the second method, the selected area diffraction blades were used to select only the region of the beam that was determined to be of uniform intensity. (The Faraday cup was utilized as a probe to measure the intensity distribution across the diameter of the beam.) After the area delineated by the blades was measured by means of reference marks inscribed on the phosphor coating, the microscope was switched into the diffraction mode and current measurements were obtained for the sharply focussed electron beam. The effective area in the sample plane contributing to the measured beam intensity was calculated, using the magnification factor established above, and the electron flux was determined from the ratio of the current to the area.

Although consistent values of the flux were obtained from the two methods (within 1-2%), both results would be in error if a significant fraction of the electrons were lost from the beam after leaving the sample plane. To determine the "efficiency" of the microscope lens system a second Faraday cup was placed immediately above the sample plane. The total beam current entering the sample plane was then measured and found to be identical to the total beam current measured in the lower column, indicating that the "efficiency" is close to 100%.

Measurements of the superlattice diffraction spot intensity were made in a manner similar to the second method described for measuring the beam flux. The selected area diffraction blades were positioned to ensure that only the uniformly irradiated portion of the sample within the central area of the beam would contribute to the diffracted intensity. In addition, the movable aperture shown in fig. 7.1 was positioned over the Faraday cup to reduce the background intensity as much as possible. A strip chart recorder, connected to the output of the electrometer was used to record the superlattice diffraction spot intensity during the bombardment.

All quantitative measurements of the rate of disordering were obtained from superlattice spots of the type $20\bar{2}0$ because these spots are well isolated from the primary pattern in the (110)

foils (indices referred to cube axes) used for the experiments. The sample orientation in all cases was adjusted so that $s = 0$ for the primary $30\bar{3}0$ reflection adjacent to the superlattice spot (see fig. 5.1 and II.1). Under these conditions, as shown in Appendix II, the superlattice spot intensity is proportional to the square of its structure factor to a good approximation and equation (6.21) may be employed to analyze the data. In addition, it was necessary to eliminate spurious changes caused by distortion of the sample during bombardment. To accomplish this, Kikuchi lines associated with the primary diffracting planes were constantly monitored on the phosphor coating covering the aperture plate. Any change in the position of the Kikuchi pattern could be corrected by adjusting the goniometer tilt stage.

Radiation damage experiments were performed at four different values of the accelerating potential. Three of these values, nominally 50, 80, and 100 kV, are available on the JEM-7 microscope used for these experiments. The other potential, 33 kV, was obtained by removing two high voltage oscillator tubes (at the suggestion of the manufacturer) and adjusting the span of the intermediate lens current supply to permit focussing the diffraction pattern. Precise values of voltages, i.e. 33.0, 47.3, 79.9, and 100 kV, were measured by means of high resolution diffraction patterns obtained from a gold foil.

Figure 7.2 illustrates a typical result which, in this case, was obtained for 79.9 keV electrons. The plotted intensity is given in terms of the electron current diffracted from the superlattice planes, but corrections have been made for the background intensity contributed by inelastically scattered electrons by subtracting the residual current that remained after the supplemental spots had disappeared. The absolute value of the intensity at t = 0 is not particularly meaningful, because it depends on the thickness of the foil and on its precise orientation relative to the electron beam. The linearity of this plot is typical of results obtained throughout the study, moreover the slopes of similar plots were found to be accurately proportional to the electron flux, as predicted by equation (6.21).

By substituting the measured values for the slope, $d\ell nI/dt = 3.15 \times 10^{-3} sec^{-1}$, and flux, $J = 6.15 \times 10^{18}$ electrons/cm^2sec, and the calculated value of $\bar{\nu} = 1.07$ into (6.21), a displacement cross-section, $\sigma_d = 203$ barns, was obtained from the data shown in fig. 7.2 This value of σ_d is plotted in fig. 7.3 with the other experimental values of the cross-section obtained from measurements at $E_e = 33.0$, 47.3, 79.9, and 100 keV. The values of $\bar{\nu}$ appropriate to these various values of incident electron energies were calculated from relationships (5.17-5.20) and are shown in Table 7.1.

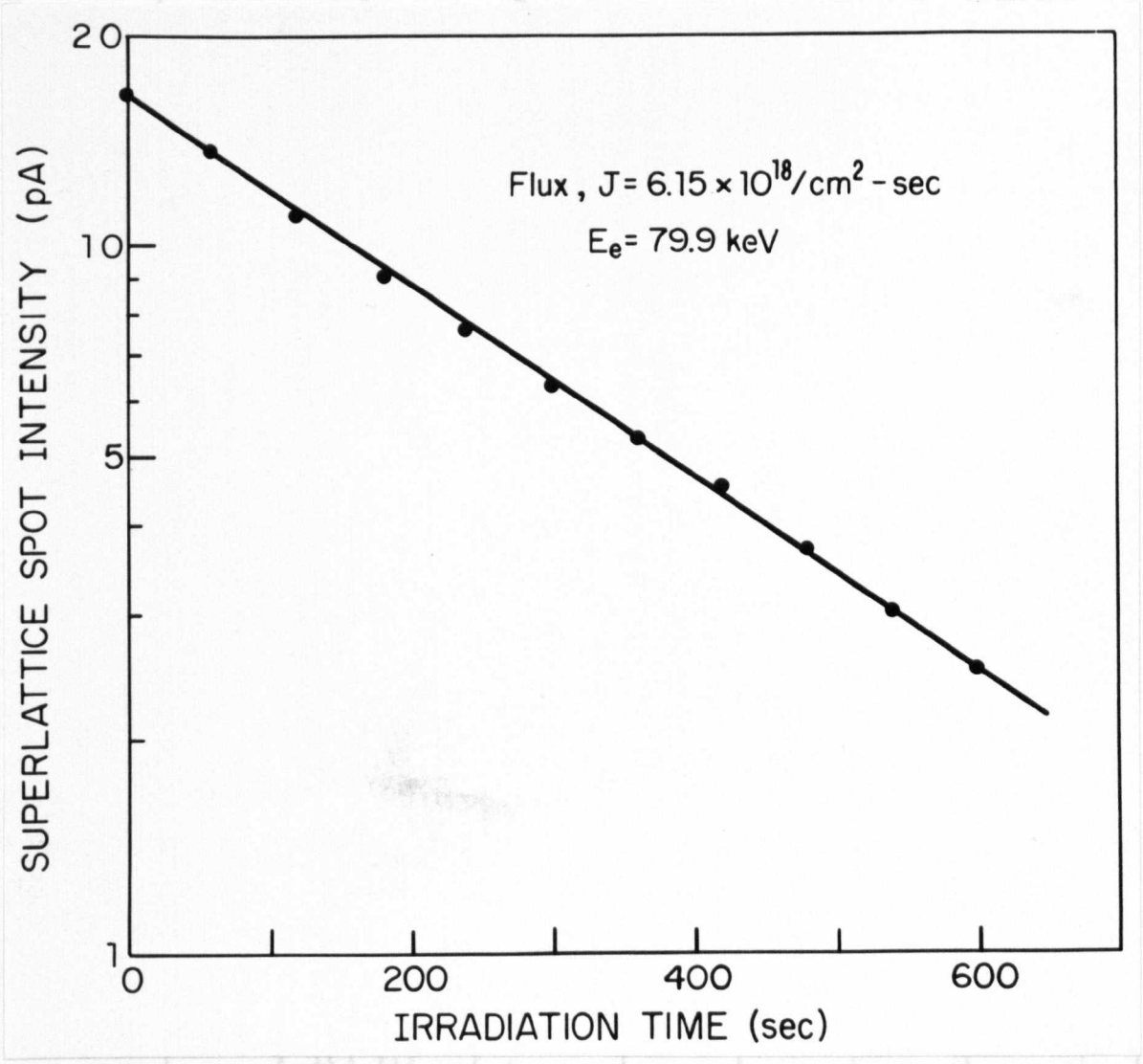

Fig. 7.2. Decay in intensity of a superlattice spot as a function of electron bombardment time. The intensity is given in terms of the current of electrons diffracted from superlattice planes belonging to the form $\{20\bar{2}0\}$. A displacement cross-section σ_d = 203 barns was calculated from this data as described in text.

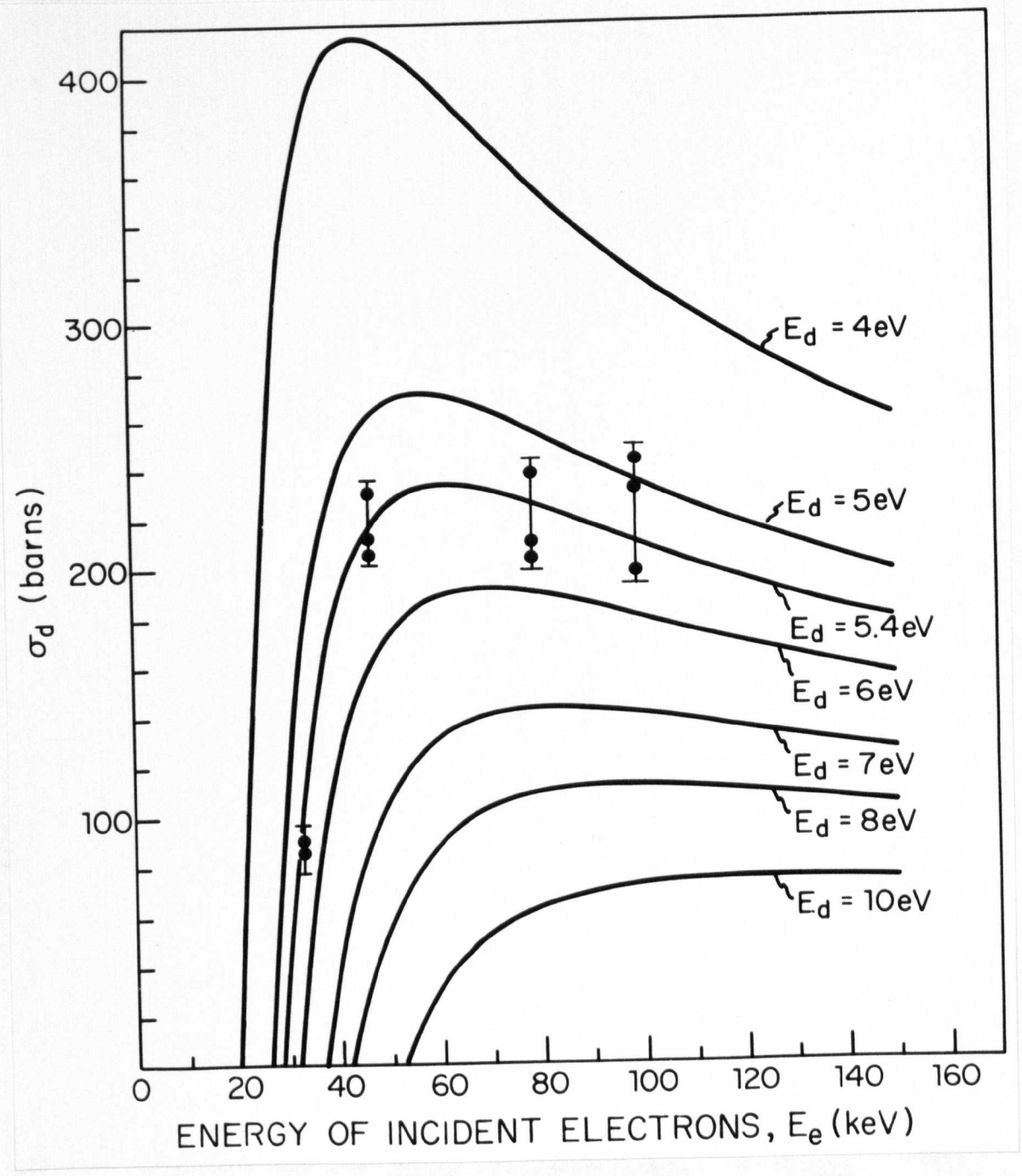

Fig. 7.3. Theoretical curves of the displacement cross-section, σ_d, vs. incident electron energy, E_e, for several values of the parameter E_d. The data points are displacement cross-sections measured for V_6C_5 by means of radiation damage experiments in the electron microscope. The parameter of the curve providing the closest fit to the experimental points indicates that the energy required to displace a carbon atom in V_6C_5 is approximately 5.4 eV.

TABLE 7.1

E_e	E_m	x_m	$\bar{\nu}$
100 keV	20.0 eV	2.72	1.15
79.9	15.7	1.90	1.07
47.3	9.0	.666	1.00
33.0	6.2	.15	1.00

The experimental points are to be compared with the theoretical curves of σ_d vs E_e computed* from equation (5.14) for several values of the parameter E_d. The parameter of the curve providing the best fit to the experimental points indicates that, within the approximations discussed in Chapter Six, the energy required to displace a carbon atom in V_6C_5 is close to 5.4 eV.

7.2 Discussion of results

Rather good agreement is observed in fig. 7.3 between the shape of the theoretical curve for E_d = 5.4 eV and that defined by the measured values of σ_d. This agreement lends support to the original assumption that coulomb encounters between incident electrons and carbon nuclei account for the disordering in V_6C_5, and suggests that the thermal spike displacement process proposed by Seitz and Koehler[1]

*Computer calculations by D. Kahn of RIAS.

for materials containing elements with d-electrons is not applicable in this case. (See discussion in section 5.2.1.) The latter mechanism, in which excited d-electrons come to equilibrium with the lattice in such a manner to form local disorder, would have a cross-section corresponding to an ionization process. Typically, ionization cross-sections increase with decreasing incident electron energy and are expected to exhibit cut-offs only when the energy of the incident electron approaches the appropriate ionization energy. Clearly, the behavior of the data presented in fig. 7.3 is not consistent with such a mechanism.

In spite of the good agreement between data and theory however, two factors may influence the result:

1. If the threshold energy for displacing carbon atoms exhibits a pronounced angular dependence, which has been neglected here, it may modify the energy-dependence of the cross-section and change the effective value of the threhold for different bombarding energies. Such an effect may account for the small positive deviation from the calculated curve of the experimental points at 100 keV. If so, it suggests that a somewhat smaller value of E_d would be determined

from comparable measurements made with the incident beam oriented along crystallographic directions other than the ⟨110⟩ employed here.

2. The arguments presented above suggest that most of the displaced carbon atoms move to vacant sites in the nearest neighbor shell of the carbon sublattice, or return to their original sites. Thus, the probabilities that the displaced atoms move to α or β sites are proportional to the relative numbers of the two kinds of sites in the nearest neighbor shell surrounding the original positions of the atoms. When the mean range of the displaced atoms exceeds the radius of this shell, however, or when the fraction of secondary displaced atoms becomes large, the probabilities become more nearly proportional to the average concentration of the two sites throughout the lattice. Whenever the latter circumstances apply, the values of σ_d obtained by the present analysis would be approximately 20% smaller than the correct values.

It should be noted that these two uncertainties in the values of σ_d have a rather small influence on the value of E_d inferred from the data, and they both suggest that the present estimate, $E_d = 5.4$ eV, is an upper limit to the threshold energy. This value is unexpectedly low in comparison with the values that have been reported in the literature for most other materials, but, as will be discussed in Chapter Nine, the high carbon vacancy concentration (~ 16%) in V_6C_5 may be a factor contributing to the low displacement energy. According to the model for disordering which has been employed to analyze the present data, carbon atoms have a high probability of being permanently displaced only if a vacancy site is accessible in the nearest neighbor shell of the C-lattice. Thus, the minimum impulse of energy which will suffice to generate permanent displacements is that required to remove a carbon atom from its normal lattice site and place it in a nearest neighbor vacant site. This process contrasts to common circumstances expected to apply in monatomic solids, for example, in which the activation energy would be larger by the amount required to form a stable interstitial.

REFERENCES

1. F. Seitz and J. S. Koehler, in "Solid State Physics," ed. F. Seitz and D. Turnbull, Vol. 2, (Academic Press, New York, 1956), p. 377.

CHAPTER EIGHT

FURTHER RADIATION DAMAGE STUDIES

8.1. Search for effect of electron channelling on damage rates in V_6C_5

The effect of channelling on damage rates associated with heavy ion irradiation of gold has been measured by Noggle and Benett[1] who found that the rate in channelling orientations was approximately 10 times less than in random orientations. No analogous experiments have been performed previously for electron damage, but it has been suggested by Makin and Sharp[2] that the channelling which gives rise to the anomalous transmission effect observed in electron microscopy might be accompanied by an anomalously low damage rate. When a sample is oriented for anomalous transmission, a phenomenon which is similar to the Borrmann[3] effect for X-rays and to chanelling for ion beams, the two beam dynamical theory predicts that more of the incident electrons spend time in regions between atomic planes than occurs for other orientations. Since these channelled electrons tend to avoid the atom sites, they should have a reduced probability of interacting with the atomic nuclei to produce displacement damage. In view of the important implications such an orientation dependence would have with respect to electron radiation damage studies, an attempt has been made to determine its magnitude in the ordered compound V_6C_5.

This material offers an unusual opportunity to examine this question experimentally since the full analytical capabilities of the electron microscope can be utilized to resolve the small angular separation between channelling and de-channelling orientations and to measure the respective damage rates in situ.*

The general expression for the wave function describing an energetic electron in a crystalline solid is given by a series of i Bloch waves,(4)

$$\Psi(\bar{r}) = \sum_i \psi^{(i)}(z) \sum_g C_g^{(i)}(\bar{k}^{(i)}) \exp\{2\pi i(\bar{k}^{(i)}+\bar{g}) \cdot \bar{r}\} \exp(-2\pi q^{(i)} z) \quad (8.1)$$

whose excitation amplitudes, $\psi^{(i)}(z)$, are determined by sample orientation and incident electron energy. Because of absorption effects, the waves are damped proportional to $\exp(-2\pi q^{(i)} z)$, where z is the sample thickness and the $q^{(i)}$'s are the absorption coefficients appropriate to each wave. For the two-beam case, where only the zero order beam and one reflection are allowed, two Bloch waves are excited (i = 1,2) and their intensities at the Bragg angle are given by,(4)

$$\begin{aligned} b^{(1)*} \cdot b^{(1)} &= 2 \sin^2 \pi \bar{g} \cdot \bar{r}[\exp(-4\pi q^{(1)} z)] \\ b^{(2)*} \cdot b^{(2)} &= 2 \cos^2 \pi \bar{g} \cdot \bar{r}[\exp(-4\pi q^{(2)} z)]. \end{aligned} \quad (8.2)$$

These expressions illustrate that the waves exhibit different symmetries; Bloch wave (1) peaks in intensity in regions of high

*Prof. P. B. Hirsch, Oxford, first suggested that this technique might be employed to search for channelling effects. (Private communication.)

potential energy between atom planes, whereas Bloch wave (2) has its maximum intensity in regions of low potential energy near the atoms, as illustrated in fig. 8.1. If it were not for absorption effects this result would be trivial; however, since the form of the inelastic potential representing absorption is qualitatively similar to the real potential,[5] it follows that Bloch wave (2) is attenuated more rapidly than the channelled wave, Bloch wave (1), i.e. $q^{(2)} > q^{(1)}$. Thus, because of selective absorption it is primarily the channelled wave that accounts for the transmission of elastically scattered electrons through thick crystals.

The total flux associated with the channelled wave depends upon the amplitude $\psi^{(1)}(z)$, which in turn varies in magnitude as a function of sample orientation. The main effects of taking into account this variation of the Bloch wave excitation are that maximum channelling occurs just outside the Bragg angle, giving rise to anomalous transmission, whereas minimum channelling occurs at the symmetrical position where the transmission is, as a result, anomalously low. At a bend extinction contour, which corresponds to a "rocking curve" about the symmetrical position, these regions of maximum and minimum channelling are delineated by the associated changes in intensity as shown schematically in fig. 8.2. Accordingly, to determine the influence of channelling upon electron damage a

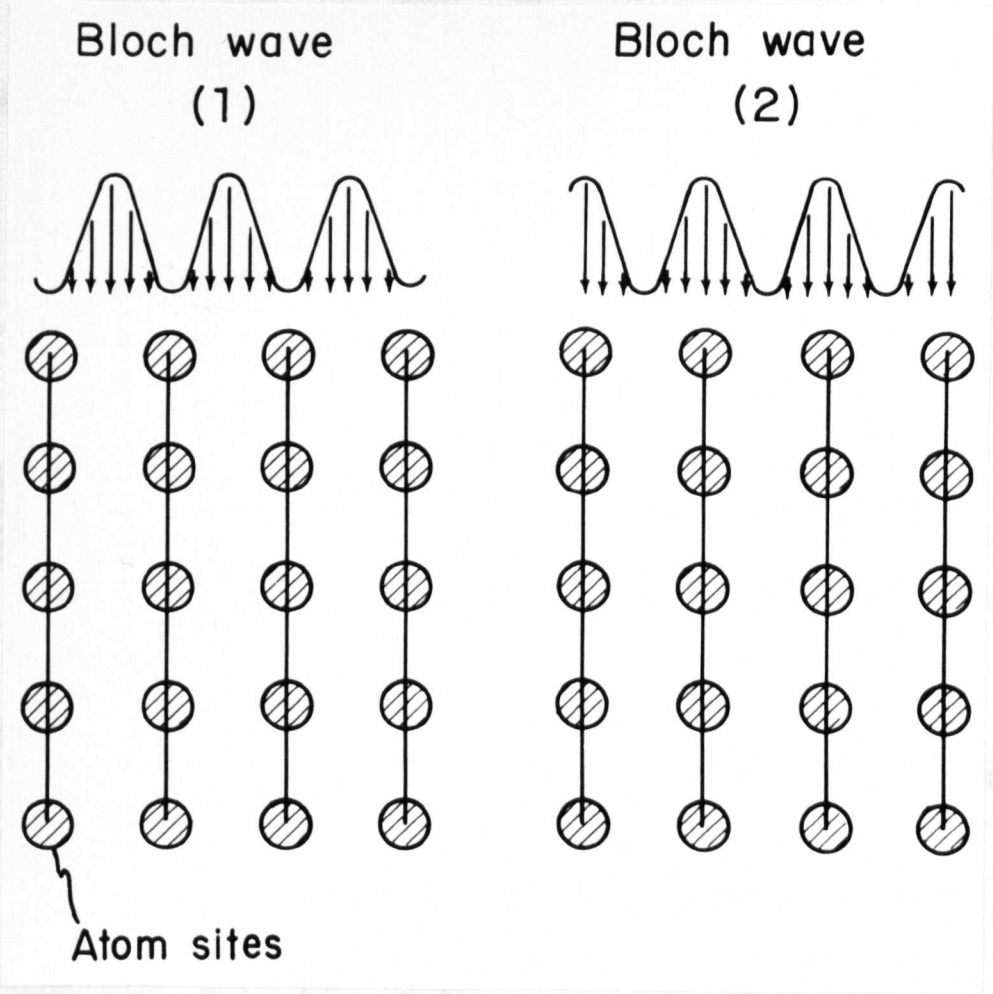

Fig. 8.1. Schematic diagram of the two types of Bloch waves employed in the two-beam dynamical theory of electron diffraction. The current flow vector is parallel to the reflecting planes for both waves. Bloch wave (2) has its maximum intensity at the atom sites, whereas wave (1) has its maxima in the intervening regions. The type (1) wave is "channelled" between the atomic planes and consequently is transmitted more effectively than is the type (2) wave.

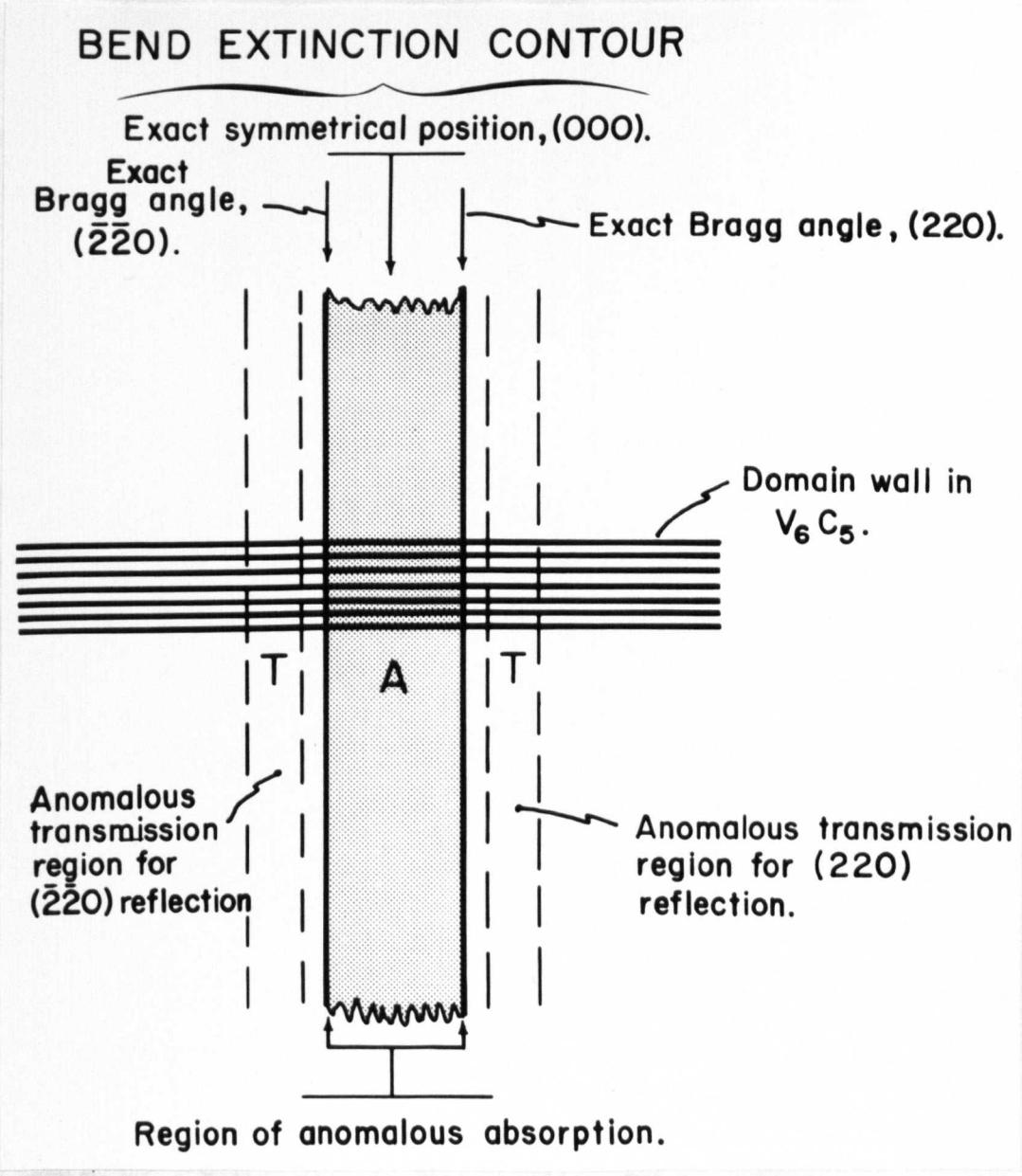

Fig. 8.2. Pictorial representation of method used to search for the influence of electron channelling on damage rates in V_6C_5. The bands associated with the bend extinction contour delineate regions of maximum channelling (anomalous transmission regions) and minimum channelling (anomalous absorption region). In the experiment, a comparison was made between the rate at which the domain wall fringes disappear in the two different regions.

comparison has been made between the damage rate in an anomalous transmission contour with that in an anomalous absorption band.

The experiment was performed by positioning a 220 (indices referred to cube axes) bend extinction contour over a domain wall in a transmission foil of V_6C_5, fig. 8.2. The domain walls arise solely as a result of ordering on the C-lattice so that the intensity of the fringes that make then visible will decrease as the crystal becomes disordered, fig. 5.1. Moreover, the {220} planes satisfy the criterion expressed mathematically in equation (8.2) and schematically in fig. 8.1, that planes of atoms occur only at nodal positions for Bloch wave (1). Thus, after several minutes of irradiation with the electron beam, the fringes should be less intense at A than at T in fig. 8.2 if channelling has influenced the damage rate.

If the effect of electron channelling were as large as that reported for ion beam irradiation,[1] it would be observed readily in this manner, but in these experiments no difference in the damage rate has been detected between the two regions. This result is surprising since the large difference in electron intensities observed experimentally between the anomalous transmission and absorption bands suggests that the effect should be quite pronounced. However, this contrast is somewhat misleading since it is enhanced

by the presence of the objective aperture which serves to remove a substantial background of inelastically scattered electrons. The calculations of Whelan,[6] Howie,[7] and Humphreys and Hirsch,[8] indicate that only one inelastic scattering process, namely phonon scattering, actually contributes to the absorption effects which are responsible for extinction bands. Phonon scattering is sufficiently localized (near atom sites) to selectively attenuate the two Bloch waves, but this is not the case for plasmon, or single electron scattering which exhibit much more diffuse collision zones. Electrons that are inelastically scattered by such non-localized interactions therefore contribute to a general background intensity which can be substantial in thick crystals since the cross-sections for these processes are relatively large.[6,7,9]

Although the effect of background radiation can be suppressed with an aperture to improve the optical contrast, it is clear that the channelling efficiency, i.e., the ratio between the channelled and total flux, will always be degraded if a background is present. Thus, if there is a large background of damage provided by inelastically scattered electrons, the variation in intensity of the channelled electrons with orientation may lead to only a small perturbation in the overall damage rate which could remain undetected even with the rather sensitive techniques employed here. The present

results appear to be consistent with such an hypothesis but as yet no attempt has been made to obtain a direct measurement of the channelling efficiency. Until this is done, no quantitative comparison can be made with the channelling efficiency for ions, but on the basis of these initial studies it would appear that, qualitatively, the influence of channelling upon the production of radiation damage is much less important for electron irradiation than for ions.

8.2 Diffusion of carbon in V_6C_5

Hollox and Venables[10] have demonstrated that the order-disorder transformation temperature of V_6C_5 corresponds rather closely to its brittle-ductile transition temperature, both effects occurring within the range 1250°C to 1300°C*. On the basis of this observation it was suggested that ordering imparts a brittle behavior to the mechanical properties and that significant plastic deformation becomes possible only after the lattice is thermally disordered. Although it is not unreasonable to expect that the ordered structure may place severe restraints upon dislocation motion, perhaps through the necessity to form superdislocations, it is nonetheless possible that the brittle-ductile transition and the order-disorder transformation occur in the same temperature range only because both are determined by the rate at which carbon atoms diffuse through the lattice.

*To be discussed in more detail in Chapter Nine.

Thus, Rowcliffe[11] has proposed a model for slip in the carbides which suggests that dislocation motion is accomplished by means of a synchro-shear process similar to that first suggested by Kronberg[12] to account for deformation in Al_2O_3. If such a model is applicable to the carbides, it implies that dislocations will exhibit appreciable mobilities only at temperatures sufficiently high to permit rapid rates of carbon diffusion. Similarly, significant motion of the carbon atoms must also occur to effect the order-disorder transformation.

To evaluate this alternative proposal, it is necessary to know the rate of carbon diffusion at, or below 1250°C. Unfortunately, the available data on diffusion of carbon in VC were obtained at significantly higher temperatures, 1500°C to 1900°C,[13,14,15] and the possibility remains that the activation energy for carbon diffusion changes with temperature (possibly rather abruptly). Problems are often encountered in measuring diffusion coefficients at low temperatures, but it has now been possible to measure the activation energy for carbon diffusion in V_6C_5 from a study of the kinetics of the ordering process in the temperature range 600°C to 800°C.

In a temperature region sufficiently far below the order-disorder transformation, the time required to achieve a specified degree of order is expected to vary with temperature as[16]

$$\tau = \tau_o \exp W/kT, \qquad (8.3)$$

in which W is the activation energy for thermal motion of a carbon atom into an adjoining vacant site. This activation energy is

expected to be close to the value obtained from a measurement of the bulk self-diffusion coefficient, but in any event, it is the quantity of interest here. Thus, a determination of W can be made by measuring, as a function of temperature, the time required to reorder specimens of V_6C_5 that have been disordered previously under electron bombardment.

Samples of V_6C_5 were disordered in the electron microscope as described previously in Chapter Seven. After imparting a fixed amount of damage to the sample, it was heated in the microscope hot stage and the time required for the superlattice spots to become visible again was measured at various temperatures. The reordering times determined by this procedure are indicated by the solid circles in fig. 8.3. An estimate of the activation energy associated with this reordering can be obtained from the slope of the line through these points,

$$W = k \, d\ell n \, \tau / d(1/T), \qquad (8.4)$$

but the accuracy of this estimate can be improved somewhat by exploiting information derived from the measurements of the specific heat of V_6C_5 by Lowndes et al.[17] In particular, the Debye temperature of V_6C_5 ($721^{\circ}K$) determined from these measurements implies a characteristic atomic vibration frequency, ν_D, of 1.5×10^{13} sec^{-1}, which

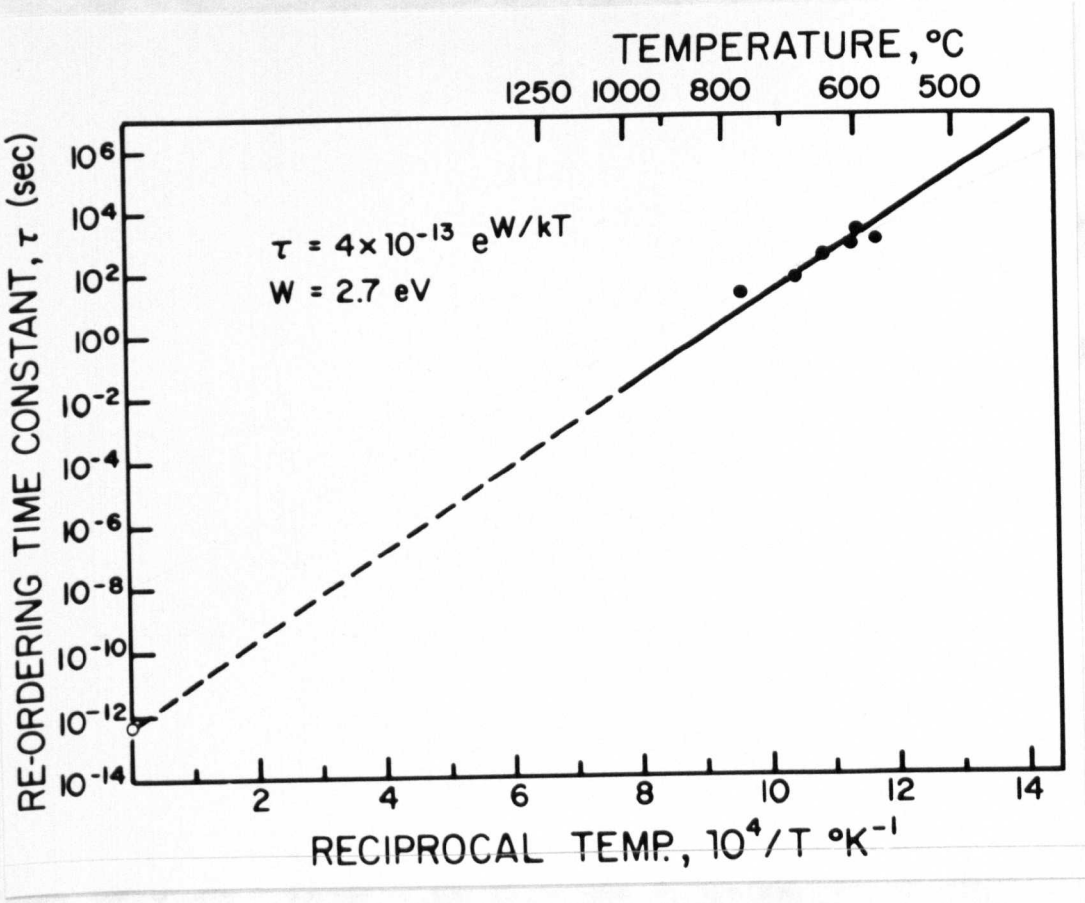

Fig. 8.3. Time constant for thermal re-ordering of V_6C_5 vs reciprocal temperature. The closed circles are data points obtained by monitoring the time, at temperature, required for superlattice diffraction spots to re-appear from a sample that was initially disordered by radiation damage. The open circle is a theoretical point derived from considerations of the Debye temperature of V_6C_5, as described in the text.

will be fully excited at elevated temperatures. Disordered carbon atoms undergoing these vibrations will have one chance in six tries to jump into an ordered position in a nearest-neighbor site of the carbon sublattice since, on the average, 5/6 of the nearest-neighbor sites are already occupied. Thus, the re-ordering time at very elevated temperatures is expected to be approximately $6/\nu_D = 4 \times 10^{-13}$ sec. This re-ordering time is plotted as the open circle at the left ordinate of fig. 8.3.

The straight line through this calculated point and through the points obtained by direct observation of the re-ordering times has a slope corresponding to an activation energy of 2.7 eV, close to the mean of the values, 3.11 eV,[13] 2.9 eV,[14] and 2.52 eV,[15] reported for the activation energy for carbon diffusion at considerably higher temperatures. Thus, these results indicate no significant change in the mechanism for carbon diffusion between the low- and high-temperature regimes. Moreover, the observation that re-ordering does take place very rapidly at temperatures much below 1250°C demonstrates that the order-disorder transformation temperature is established primarily by equilibrium thermodynamic considerations and is not influenced significantly by the kinetics of carbon atom diffusion under readily attainable experimental conditions. Indeed, the present results suggest that the re-ordering time near

the order-disorder transformation temperature is approximately 100μsec, far faster than the cooling times attainable under ordinary circumstances.

On the basis of these observations, it is possible to discount the proposal that the brittle-ductile transition and the order-disorder transformation are correlated only because both are established by the kinetics of carbon atom diffusion. The alternative proposal, that the ordered structure itself severely restricts dislocation motion below the order-disorder transformation, appears to be the more probable explanation, but additional studies will be necessary to elucidate the mechanisms involved.

REFERENCES

1. T. S. Noggle and J. H. Barrett, Phys. Stat. Sol., 36, 761 (1969).

2. M. J. Makin and J. V. Sharp, J. Mat. Science, 3, 360 (1968).

3. G. Borrmann, in "Trends in Atomic Physics," ed. O. R. Frisch, F. A. Paneth, F. Lanes, and P. Rosabud (Interscience, New York, 1959).

4. P. B. Hirsch, A. Howie, R. B. Nicholson, D. W. Pashley, and M. J. Whelan, "Electron Microscopy of Thin Crystals" (Butterworths, London, 1965) p. 208 ff.

5. H. Hashimoto, A. Howie, and M. J. Whelan, Phil. Mag., 5, 967 (1960).

6. M. J. Whelan, J. Appl. Phys., 36, 2099 (1965).

7. A. Howie, Proc. Roy. Soc., A271, 268 (1963).

8. C. J. Humphreys and P. B. Hirsch, Phil. Mag., 18, 115 (1968).

9. R. D. Heidenreich, "Fundamentals of Transmission Electron Microscopy" (Interscience, New York, 1964) p. 52 ff.

10. G. E. Hollox and J. D. Venables, Proc. Intl. Conf. on Strength of Metals and Alloys, Tokyo, in Suppl. Trans. Japan Inst. Metals, 9, 295 (1968).

11. D. J. Rowcliffe, Ph.D. dissertation, "The Mechanical Properties of Transition Metal Carbides," University of Cambridge (1965).

12. M. L. Kronberg, Acta Met., 5, 507 (1951).

13. K. Torkar, H. J. Oel, and A. Illigen, Berg. Deut. Keram. Ges., 43, 162 (1966).

14. V. S. Eremeev and A. S. Panov, Porosh. Met., 7, 65 (1967).

15. L. M. Adelsberg and L. H. Cadoff, J. Am. Ceram. Soc., 51, 213 (1968).

16. T. Muto and Y. Takagi, in "Solid State Physics," ed. F. Seitz and D. Turnbull, Vol. 1 (Academic Press, New York, 1956) p. 251.

17. D. H. Lowndes, L. Finegold, and R. G. Lye, Phil. Mag., 21, 245 (1970).

PART III

AN OVERVIEW

CHAPTER NINE

GENERAL DISCUSSION AND SUMMARY

9.1 Discussion

This investigation has been directed toward obtaining an improved understanding of the unusual physical and mechanical properties that make the transition metal carbides interesting scientifically as well as potentially useful materials for future technology. The emphasis that has been placed on ordering effects grew quite naturally from an initial desire to interpret the complex electron diffraction patterns exhibited by vanadium carbide, but the results have provided much more than a crystallographic description of an ordered structure. Indeed, a rather coherent picture of the relationship between electronic structure, defect structure and mechanical properties emerges when the origins of the ordering are considered in terms of the band structure of vanadium carbide.

Using transmission electron microscopy, electron diffraction and NMR it has been shown that the nominally cubic, isotropic, vanadium carbide structure is modified substantially by ordering in the carbon sublattice when the carbon-to-metal atom ratio is close to the integral composition V_6C_5. In the proposed structure, the vanadium atoms occupy their normal fcc lattice sites, but the carbon

atoms (and carbon vacancies) are distributed on their fcc sublattice in such a manner that all the vanadium atoms have only five nearest neighbor carbon atoms. The observation that ordering in material of this composition leads to a distribution of atoms that is homogeneous on an atomic scale is consistent with the electronic structure of vanadium carbide as it is currently understood.

In particular, Lye[1] has shown that the maximum occupancy of bonding 3d-states is achieved in vanadium carbide when the carbon-to-metal atom ratio is close to 5/6. At this composition the antibonding states are empty, or nearly so, but an increase in the carbon concentration beyond this ratio serves to increase their occupancy with electrons contributed by the carbon atoms in the manner described in Chapter One. Since the electronic interactions between neighboring metal atoms are important in determining the band structure as well as the total cohesive energy of the transition metal carbides, it has been suggested by Lye[1] that the most stable structure would occur when the local concentration of carbon atoms is equal to the integral number five. This condition is not met in VC if the carbon atoms assume a random distribution on their fcc lattice sites even though the carbon-to-vanadium atom ratio is 5/6. In these circumstances the fraction, p, of vanadium sites having $n(n \leq 6)$ nearest neighbor carbon atoms is given by the binomial

distribution function

$$p(n) = C_n^6 (r)^n (1-r)^{6-n} \qquad (9.1)$$

where r is the fraction of the carbon sites that are occupied, and C_n^6 are the binomial coefficients. Thus, for a random distribution, 33% of the vanadium sites will have six nearest neighbor carbon atoms, whereas only 40% will have five. On the other hand, the condition of homogeneity on an atomic scale is readily satisfied without any modification of the metal lattice, if the carbon atoms assume the ordered arrangement which has been deduced for V_6C_5.

Similar arguments also appear to account qualitatively for the ordered structure V_8C_7 which has been described by de Novion et al.[2] In this case the fraction of vanadium sites having six, and five, near neighbor carbon atoms would be 45% and 38% respectively, for a random distribution, but in the ordered structure the corresponding ratios are 25% and 75%. Such an ordered arrangement would be expected to exhibit less stability than V_6C_5 because antibonding d-states are necessarily occupied, but it should clearly be more stable than the random distribution.

In addition, recent NMR experiments by Kahn[3] indicate that this influence of the electronic structure is retained even at low carbon concentrations, imposing short range ordering of the

carbon atoms in $VC_{0.75}$. In this material Kahn finds that the concentration of vanadium atoms having 5 near neighbor carbon atoms (V_1 sites) is very much in excess of that expected on the basis of a random distribution of carbon atoms, whereas the concentration of those having six near neighbor carbon atoms (V_0 sites) is much less. This behavior is consistent with that observed in V_6C_5 and V_8C_7 and it seems reasonable to suppose that it arises from the same cause. In this case, however, the low concentration of the carbon atoms may allow a greater flexibility in their distribution so that the restrictions imposed by the electronic structure may be accommodated by short range order only. This material has not been examined by transmission electron microscopy and therefore it is not known whether long range order is present, but Lye's[1] interpretation of the ordering in terms of the electronic structure suggests that the driving force for long range ordering should be low. The stability of long range ordering may therefore be less in $VC_{0.75}$ than in V_6C_5 or V_8C_7 and the character of the superlattice diffraction pattern may be sensitive to the prior thermal history of the specimens. Clearly, detailed studies will be needed to establish the nature of the ordering in $VC_{0.75}$.

It appears, then, that the ordering effects observed in vanadium carbide are determined by the tendency to avoid occupying the antibonding 3d-states of the band structure with electrons contributed by the carbon atoms. If this interpretation is correct, it provides an example of the way in which the electronic energy band structure of solids can influence their mechanical behavior, because the ordering effects observed in VC appear to account rather well for some of its mechanical properties.

The mechanical behavior of $VC_{0.75}$, $VC_{0.84}$ and $VC_{0.88}$ has been studied by Hollox over a wide temperature range[4]. Figure 9.1 illustrates the temperature dependence of the critical resolved shear stress (CRSS) for slip in these materials, and compares their behavior with that of TiC of equivalent carbon-to-metal ratio. Unlike the situation in TiC, the CRSS of VC does not increase monotonically with increasing carbon content, but passes through a maximum, the strength of $VC_{0.84}$ being higher than that of either $VC_{0.88}$ or $VC_{0.75}$.

The observed strengthening of TiC with increasing carbon content is consistent with Lye's model of the electronic structure. According to Lye,[5,6] the predominant contribution to the cohesiveness of the carbides arises from largely covalent metal-metal bonds. The strength of these bonds increases with carbon content because, (1) the carbon atoms donate electrons to crystal states derived from

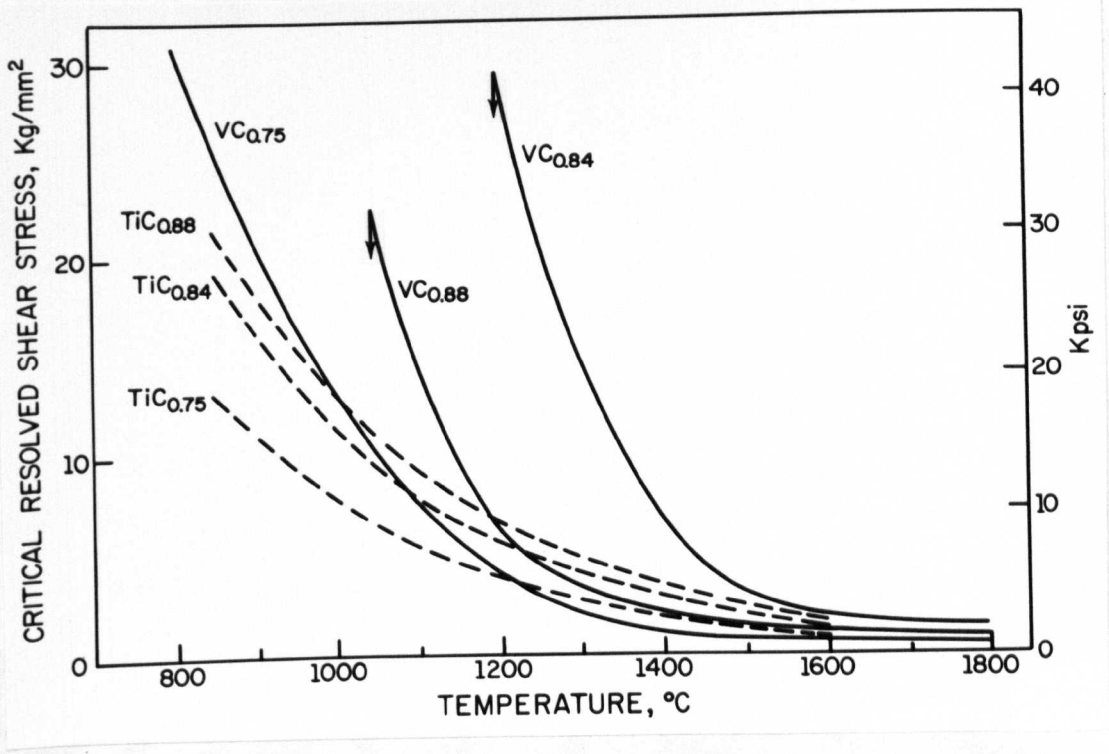

Fig. 9.1. Comparison between the temperature dependence of the critical resolved shear stress for slip in TiC and VC of equivalent carbon-to-metal ratio. Arrows denote brittle-to-ductile transition temperature. (After Hollox[4].)

metal atom wave functions and increase the number of 3-d electrons available for metal-metal bonding, and, more important, (2) the presence of carbon atoms in overlap regions of neighboring metal atom 3d-orbitals introduces a potential that increases the strength of the metal-metal interactions. The complex behavior of VC and the dramatic changes in strength that accompany small variations in stoichiometry cannot be explained directly on this basis but they may be discussed in terms of the electronically induced ordering.

A relationship between ordering effects and the mechanical behavior of V_6C_5 has been established by Hollox and Venables.(7) They determined the order-disorder transformation temperature of this material by measuring the annealing temperature required to induce a permanent change in the domain pattern observed with polarized light. Because a marked change in the pattern was noted when the crystal was annealed above 1300°C, while annealing at 1250°C (or below) did not influence the pattern in any noticeable way, it was concluded that the order-disorder transformation temperature lies between these two limits. Significantly, the lowest temperature for which some ductility is observed in V_6C_5

also lies within this range, fig. 9.1, and for this reason it was inferred that the brittle-ductile transition temperature is determined in whole, or in large part, by the ordering.*

The precise manner in which the ordered structure exerts its influence upon the mechanical properties is not completely understood, but it is not unreasonable to expect that the presence of a superlattice would modify the structure and mobility of dislocations in these materials, leading to the observed hardness and brittleness. It is well known, for example, that in ordered structures slip occurs by the movement of "superdislocations" which are required to avoid the formation of large area antiphase boundaries. Such dislocations are difficult to generate and move,[8] and because they cannot cross glide readily, they are not expected to be very effective in relieving stresses at crack tips.

---

*A similar relationship may also apply for V_8C_7 since recent work by the present author suggests that the order-disorder transition in this material occurs near the brittle-ductile temperature of 1100°C, fig. 9.1. This work was only partially completed at the time of this writing so that a detailed description of the experiment will not be included here. Briefly, however, the disordering temperature was determined by a direct measurement in the electron microscope using the electron beam for heating. The temperature of the hot spot was monitored with a specially constructed pyrometer-microscope attachment, while the degree of order was estimated from an analysis of the superlattice spot intensities in the selected area diffraction patterns.

These specific effects of the ordering are expected to apply up to the order-disorder transformation temperature but the influence of the electronic structure may persist to still higher temperatures imposing short range order on the structure. It is possible, therefore, that the gradual disruption of this short range order may influence the temperature dependence of the strengths of V_6C_5 and V_8C_7 at elevated temperatures. Additional work must be done in this area to establish the nature of the structure above the order-disorder temperature but these arguments appear to account qualitatively for Hollox's[4] observation that V_6C_5 exhibits a consistently higher yield stress than V_8C_7 up to 1800°C, fig. 9.1. The greater stability of the ordering in V_6C_5, which is reflected in its higher order-disorder transformation temperature, appears to extrapolate well into the temperature range in which both V_6C_5 and V_8C_7 deform plastically.

In addition to the ordering effects which have been described in Part I, considerable attention has been focussed on the disordering phenomenon which occurs when V_6C_5 is bombarded with relatively low energy electrons. The value of displacement energy derived from these experiments provides additional insight into the properties of the carbides, but the results appear to have important implication for the general problem of radiation damage in solids as well.

The threshold energy which has been measured for displacing carbon atoms in V_6C_5 is considerably less than that observed in most other materials. The discrepancy is particularly pronounced if the comparison is made on the basis of the argument, proposed initially by Seitz and Koehler,[9] that the displacement energy can be expected to have a value approximately four times the heat of vaporization. For many substances, this qualitative relation holds rather well, although the observed displacement energies often are substantially larger than expected on this basis. For V_6C_5, on the other hand, the displacement energy, E_d = 5.4 eV, is substantially less than the value of E_d = 30 eV expected from the heat of vaporization of carbon from a similar transition metal carbide, ZrC, for which $\Delta H_v \cong$ 170K cal/mole[10].

The low value of the displacement energy for carbon atoms in V_6C_5 may be rationalized in terms of the unusual electronic structure of the carbides by noting that the carbon atoms lose electrons to the 3d-states of the metal atoms according to Lye's band structure calculations.[5,6] Nevertheless, factors other than the electronic structure of the perfect lattice must be expected to play a role in determining the displacement energy. In particular, it was recognized very early in this study that V_6C_5 was somewhat unusual in that every carbon atom had vacant sites available in the nearest neighbor shell

of the carbon sublattice (viewed in terms of the parent rocksalt structure from which V_6C_5 lattice is derived). These vacant positions in the carbon sublattice are available to accept a displaced carbon atom with the expenditure of relatively little energy. Moreover, the carbon atoms displaced to these originally vacant sites are expected to remain trapped at sufficiently low temperatures (i.e. below 550°C, according to the results presented in section 8.2).

For monatomic solids, most displaced atoms will not have a vacant lattice site accessible to them. Furthermore if such an atom becomes trapped momentarily at an interstitial site that is close to the vacant site from which it was displaced, the vacancy-interstitial pair will be unstable and will relax to leave no observable damage. Thus, to produce observable damage, the displaced atom must have sufficient energy to permit transferring the energy pulse for several interatomic distances through the lattice to a position at which the vacancy-interstitial pair is stable. This problem has been studied in considerable detail by Vineyard and coworkers[11,12] and others, using extensive machine calculations to follow the movement of atoms in a model crystal. The results of these studies can be used together with the analysis of the displacement process in V_6C_5, described in Part II, to provide an improved understanding of the displacement threshold energy and its relationship to thermodynamic parameters of this and other materials. In particular, a relatively

simple model of the displacement process appears capable of providing a useful relationship between

1) the energy to form a vacancy,
2) the energy to form an interstitial,
3) the displacement threshold energy(s), and
4) the separation between stable vacancy-interstitial pairs formed at the threshold energy(s).

According to Vineyard and coworkers,[11,12] the effective threshold energy for producing radiation damage is a sensitive function of the original direction of motion of the displaced atom. Some of this variability arises because the displaced atom strikes two atoms simultaneously when it moves in certain directions from its original position. Unless it has an energy large enough to overcome the formidable barrier presented by the two atoms, the displaced atom is reflected back to its original position and no permanent damage is created. A somewhat similar behavior results also when the displaced atom is directed along a path that lies close to certain of the low-index crystallographic directions. For then, the moving atom must have sufficient energy to propagate focussing collisions along the row of atoms in the direction of its initial flight path.

Along most directions, however, the moving atom does not make focussed collisions, nor does it collide with two atoms

simultaneously. The majority of displaced atoms can be considered, therefore, as making hard-sphere collisions with individual atoms. Assuming isotropic scattering for the hard-sphere collisions, it is expected that the energy of the moving atom will diminish by approximately one-half of its initial value on each collision, as confirmed numerically by Vineyard and coworkers[12] for one random direction in bcc iron.

This average energy loss of one-half for each collision will persist only as long as the energy is substantially greater than the binding energy of the atoms in their normal sites (or greater than the energy required to form an interstitial). For simplicity, however, the deviations that occur near the end of the path shall be neglected and it will be assumed, as Vineyard appears to have done, that the propagation of the disturbance terminates when the moving atom has only sufficient energy left to form an interstitial.

On this basis, it is expected that several "threshold displacement energies" will be observed, depending on the number of collisions that are undergone between the original displacement and the site of the (stable) final interstitial. If the energy required to form the initial vacancy is E_v, the energy required to form an interstitial is E_i, and the displacement threshold energies are E_{dn}, then (see fig. 9.2),

$$E_{dn} \cong E_v + 2^n E_i . \qquad (9.2)$$

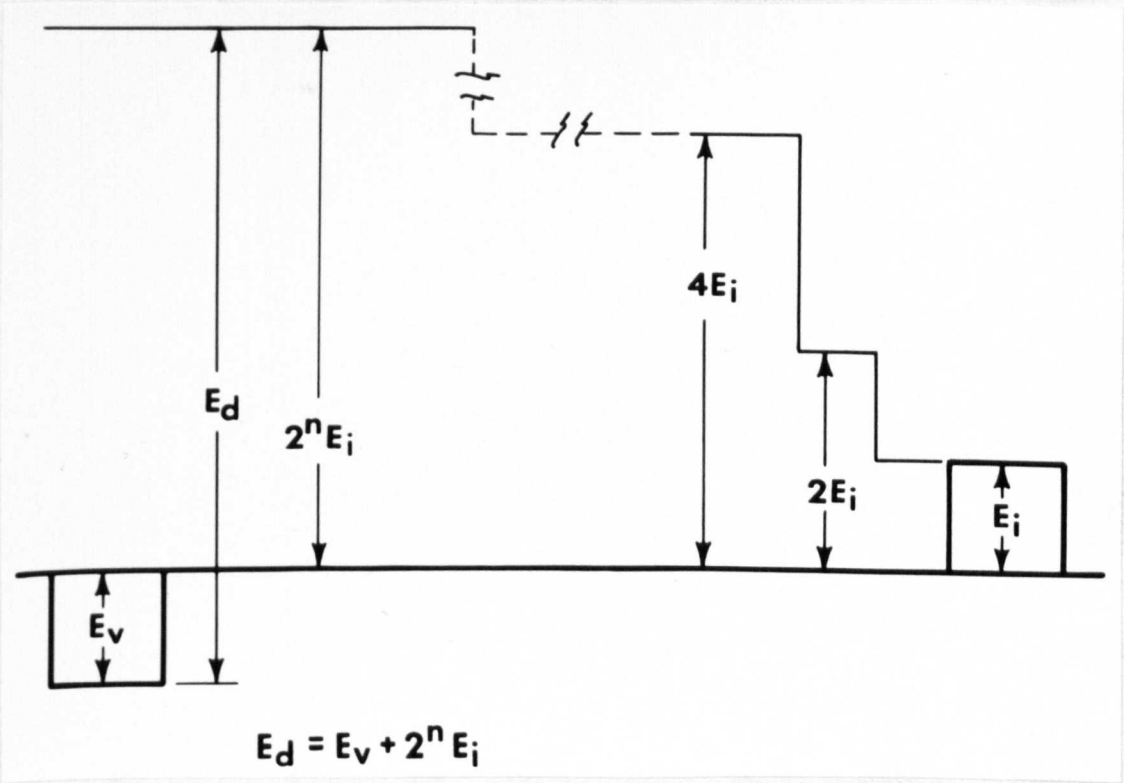

Fig. 9.2. Energy scheme for proposed model of the displacement process in monatomic solids. According to this model, observable damage will occur only if the displaced atom has sufficient energy to (1) create a vacancy of energy E_v, (2) permit transferring the energy pulse for n interatomic distances through the lattice to a position at which the vacancy interstitial pair is stable, and (3) form an interstitial of energy E_i at the terminal point of the disturbance. The energy of the moving atom is expected to decrease by half with each collision so that its initial kinetic energy, after the vacancy is formed, must be $2^n E_i$. For the special circumstances which apply for V_6C_5, $E_i = 0$ and, therefore, $E_d = E_v$.

To test whether this simple model has merit, the behavior predicted by this equation has been compared with a number of observations reported in the literature. R. A. Johnson[13] has calculated the values E_v = 1.49 eV and E_i = 4.08 eV for nickel. Inserting these values in the equation yields the following values for the displacement energies for producing an interstitial after one, two and three collisions (n = 1,2,3)

$$E_{d1} = 9.65 \text{ eV},$$
$$E_{d2} = 17.7 \text{ eV},$$
$$E_{d3} = 34.1 \text{ eV}.$$

These values compare well with displacement energies reported in the literature. For example, Kentworthy and Neely[14] have reported a displacement threshold energy of 34.5 eV, whereas Lucasson and Walker[15] analyzed their results in terms of a probability of displacement that increased from zero near 16.0 eV to unity near 34.0 eV. In terms of the present model, these results can be interpreted as follows: At low energies, the displaced atom forms an interstitial after only one collision, but the proximity of the vacancy to the interstitial makes the configuration unstable and it relaxes to yield no permanent damage.

In the intermediate region, corresponding to the threshold energy E_{d2} = 17.7 eV, increasing numbers of the displaced atoms have sufficient energy to undergo two collisions and have enough energy left to form an interstitial. The resulting interstitial is separated from the vacancy by two or more shells of atoms, and therefore forms a stable configuration.

In the high energy region, some interstitials are still formed within the same distance of the vacancy as in the intermediate energy region, but now an increasingly large fraction of the atoms can undergo three collisions and still have enough energy left to form an interstitial. Most of these interstitials will lie at 3 (or more) interatomic separations from the site of the vacancy, and they will have even greater thermal stability than those formed in the intermediate energy region.

The observations on nickel, therefore, are consistent with the predictions of this simple model, and good agreement is found also with measurements of displacement energies obtained for other materials, as shown in Table 9.1. In addition, further confirmation is provided by the annealing studies of Klontz and MacKay[32] who observed that radiation induced defects in Ge recover in four distinct stages at 20°, 35°, 55° and 67°K. They have suggested that these annealing stages arise from the recombination of vacancies

TABLE 9.1

Element	E_v	E_i	n	E_{dn} (calc.)		E_d (exp.)	
Ni	1.49 eV[a]	4.08 eV[a]	1	9.65			
			2	17.7		16.0[b]	
			3	34.1		34.0[b]	34.5[c]
Ge	1.91[d]	0.93[d]	1	3.77			
			2	5.63			
			3	9.35			
			4	16.8	15.1[e], 15.5[h], 30[j]	14.5[f], 22.3[i]	18.0[g]
			5	31.7			
Si	2.18[d]	1.09[d]	1	4.36			
			2	6.54			
			3	10.9	12.9[k], 21.0[m]	14.0[l], 25.0[n]	
			4	19.6			
			5	37.0			
C (Diamond)	3.68[d]	1.76[d]	1	7.20			
			2	10.7			
			3	18.7			
			4	31.9			
			5	60.0	80[o]		
			6	116.0			
C (Graphite)	10.5[p]	12.9[p]	1	36.4	25[q]		
			2	62.1	60[r]		
			3	113			
Cu	0.71[s]	3.38[s]	1	7.47	[t]		
			2	14.2	[15]	19.0[u]	
			3	27.8	[30]	25.0[v], 22.0[b]	
			4	54.8	[50]		

a) Ref. (13).
b) Ref. (15).
c) Ref. (14).
d) Ref. (16).
e) Ref. (17)
f) Corresponds to onset of damage ref. (18).
g) Mean value required to fit data, ref. (18).
h) Ref. (19).
i) Ref. (20).
j) Ref. (21).
k) Ref. (18) and (22).
l) For n-type, ref. (23).
m) For p-type, ref. (23).
n) Ref. (24).
o) Ref. (25).
p) Ref. (26).
q) D. T. Eggen (c.f. tabulation, ref. (27).
r) Ref. (28).
s) Ref. (11)
t) Three thresholds required to fit data, ref. (29).
u) Ref. (30).
v) Ref. (31).

and interstitials whose radial separation is largest for the 67°K pairs and smallest for the 22°K pairs. The defects which anneal at the three lowest temperatures, however, do not arise as an immediate consequence of electron bombardment because, experimentally, it is shown that they are normally unstable to recombination. Rather, they appear to be formed from the 67°K pairs -- the primary defects -- which can capture an electron and thereby increase the barrier to annihilation for the lower energy interstitial sites in their immediate vicinity. Thus, once a primary defect has formed and has captured an electron, it can relax thermally to one of the other three configurations which anneal at lower temperatures. The relevance of these results to the proposed model for displacement energies is apparent from an examination of the data for Ge presented in Table 9.1. A comparison of the measured thresholds with the calculated values of E_{dn} suggests that the first stable configuration results when the vacancy and interstitial are separated by four shells of atoms. If this configuration is associated with the primary defect referred to by Klontz and MacKay,[32] it leaves precisely three configurations of lower energy to account for the three annealing stages which occur at 20°, 35°, and 55°K.

Thus, as a result of these considerations it appears that the different values determined for the threshold displacement energies by different observers for the same material may reflect truly

distinguishable displacement processes that can be characterized approximately by the number of collisions occurring between the initial impact and the formation of the final stable interstitial. Moreover, the success of this model when applied to rather different classes of solids provides confidence that it may also be used to analyze the observations of radiation damage in V_6C_5. According to the results described in Part II a carbon atom becomes displaced permanently by impinging electrons having energies within the range employed in this study only if a vacancy is available to it in the nearest neighbor shell of the carbon sublattice. Unlike the circumstances in other materials listed in Table 9.1, however, no additional energy is required to insert the atom into an interstitial site. The threshold displacement energy, E_d = 5.4 eV, measured for V_6C_5 is, therefore, approximately the energy required to form a carbon vacancy.

This value for the vacancy formation energy, 5.4 eV, is greater by a factor of two than the activation energy for carbon diffusion measured by studying the kinetics of re-ordering. The factors which determine the diffusional activation energy in VC, however, are different from those that apply in common circumstances where the total energy is equal to the sum of the motional and vacancy formation energies. A large concentration of vacant

carbon sites is always available in VC and diffusion of the carbon atoms can occur without the generation of additional vacancies. Consequently, the measured value for the activation energy of carbon diffusion, 2.7 eV, is expected to correspond to the motional energy alone. It is interesting to note that if no vacant sites were available, the present analysis suggests that the diffusion energy would be larger by 5.4 eV. This conclusion makes it apparent that the high vacancy concentration in non-stoichiometric carbides plays an important role, not only in the displacement process, but also in establishing the energy for carbon self-diffusion.

9.2 Summary

As a result of this investigation into ordering and disordering effects in the refractory hard metal, vanadium carbide, it is concluded that:

(1) At a carbon-to-metal atom ratio corresponding to the integral composition V_6C_5, vanadium carbide exhibits an ordered structure belonging to the trigonal space group $P3_1$, or it enantiomorph, $P3_2$. The nature of the structure has been derived from the results of electron diffraction and NMR studies.

(2) The ordered structure, V_6C_5, is a derivative of the nominal rocksalt structure and arises because of ordering between carbon atoms and carbon vacancies on the fcc carbon sublattice. In the

proposed structure, the distribution of carbon atoms (and vacancies) is such that all the vanadium atoms have only five nearest neighbor carbon atoms. The observation that ordering in a material of this composition leads to a distribution of atoms that is homogeneous on an atomic scale is consistent with the electronic structure of vanadium carbide as it is currently understood. In particular, it appears that the ordering is determined by the tendency to avoid occupation of crystalline anti-bonding 3-d states (derived from d-orbitals of the vanadium atoms) with electrons contributed by the carbon atoms.

(3) As a consequence of the ordering, a domain structure forms which is visible both by electron microscopy and by reflected polarized light. Four domain orientations, corresponding to the alignment of the trigonal superlattice c-axis parallel to each of the four equivalent ⟨111⟩ directions of the primary cell are observed.

(4) The ordering is disrupted by electron microscope beam bombardment even when the electron energy is as low as 33 keV. This effect is interpreted to arise because the carbon atoms are displaced by the incident electrons.

(5) The displacement energy for carbon atoms in V_6C_5 is ~ 5.4 eV. This value was obtained by monitoring the decay rate of superlattice spot intensities with a Faraday cup during bombardment and analyzing

the data in terms of a special model for disordering that has been developed for this material. With only minor modifications the model can be applied to other non-stoichiometric ordered compounds such as V_8C_7.

(6) The unusually small threshold energy for carbon atom displacement in V_6C_5 can be understood in terms of a proposed model for the displacement process that appears to be applicable to many other solids as well. According to this model, observable damage will occur only if the displaced atom has sufficient energy to (1) create a vacancy of energy E_v, (2) permit transferring the energy pulse for n interatomic distances through the lattice to a position at which the vacancy interstitial pair is stable, and (3) form an interstitial of energy E_i at the terminal point of the disturbance. For monatomic solids, and assuming isotropic scattering, these conditions may be expressed by the relation

$$E_d = E_v + 2^n E_i .$$

For the special circumstances which apply for V_6C_5, $E_i \cong 0$ because of the large number of vacancies in the carbon sublattice which are available to accept a displaced atom with the expenditure of very little energy and, therefore, $E_d = E_v = 5.4$ eV.

(7) When the proposed model for the displacement process is applied to other solids, it suggests that the different values determined for the threshold energies by different observers for the same material may reflect truly distinguishable displacement processes that can be characterized approximately by the number of collisions occurring between the initial impact and the formation of the final stable interstitial.

(8) The influence of channelling upon the production of radiation damage in crystalline solids is much less important for electron irradiation than for ions. The fact that V_6C_5 can be disordered by electron microscope beam bombardment has made it possible to compare the rate of disordering in an anomalous transmission band (region of maximum channelling) with that in an anomalous absorption band (region of minimum channelling). If the effect of channelling on the damage rate were as large as that observed for ion beams, it would have been detected easily in this manner. In these experiments, however, no difference in damage rate was detected between the two regions.

(9) The activation energy for carbon diffusion in V_6C_5, measured in the temperature range 550 to 800°C, is ~ 2.7 eV. This determination has been made by studying the kinetics of re-ordering in specimens that have been disordered previously by electron irradiation. Because a large concentration of vacant carbon sites is

always available in V_6C_5, and diffusion of carbon atoms can occur without the generation of additional vacancies, this value is expected to correspond to the activation energy for motion alone.

REFERENCES

1. R. G. Lye, RIAS, private communication.

2. C. H. de Novion, R. Lorenzelli, and P. Costa, Compt. Rend., 263, 775 (1966).

3. D. Kahn, RIAS, private communication.

4. G. E. Hollox, Mat. Science Eng., 3, 121 (1968).

5. R. G. Lye in "Atomic and Electronic Structure of Metals," (ASM, Cleveland, Ohio, 1967).

6. R. G. Lye, G. E. Hollox, and J. D. Venables, in "Anisotropy in Single Crystal Refractory Compounds," Vol. 2, ed. F. W. Vahldiek and S. A. Mersol, (Plenum Press, New York, 1968) p. 445.

7. G. E. Hollox and J. D. Venables, Proc. Intl. Conf. on Strength of Metals and Alloys, Tokyo, in Suppl. Trans. Japan Inst. Metals, 9, 295 (1968).

8. M. J. Marcinkowski and H. Chessin, Phil. Mag., 10, 837 (1964).

9. F. Seitz and J. S. Koehler, in "Solid State Physics," ed. F. Seitz and D. Turnbull, Vol. 2, (Academic Press, New York, 1956) p. 307 ff.

10. E. Storms, in "Fundamentals of Refractory Compounds," ed. H. H. Hausner and M. G. Bowman, (Plenum Press, New York, 1968), p. 90.

11. J. B. Gibson, A. N. Goland, M. Milgram, and G. H. Vineyard, Phys. Rev., 120, 1229 (1960).

12. C. Erginsoy, G. H. Vineyard, and A. Engler, Phys. Rev., 133, A595 (1964).

13. R. A. Johnson, Phys. Rev., 145, 423 (1966).

14. H. M. Kentworthy and H. H. Neeley, North American Aviation Rept. NAA-SR-1580 (Aug. 1, 1956).

15. P. G. Lucasson and R. M. Walker, Phys. Rev., 127, 485 (1962).

16. K. H. Bennemann, Phys. Rev., 137, A1497 (1965).

17. W. L. Brown and W. M. Augustyniak, J. Appl. Phys., 30, 1300 (1959).

18. J. J. Loferski and P. Rappaport, Phys. Rev., 111, 435 (1958). See also J. J. Loferski and P. Rappaport, J. Appl. Phys., 30, 1296 (1959).

19. L. S. Smirnov and P. A. Glazunov, Soviet Phys. Solid State (English Translation), 1, 1262 (1960).

20. V. S. Vavilov, L. S. Smirnov, G. N. Galkin, A. V. Spitsyn, and V. M. Patskevich, Sov. Phys. - Tech. Phys. (English Translation), 1, 1805 (1957).

21. E. E. Klontz and K. Lark-Horovitz, Phys. Rev., 82, 763 (1951); ibid. 86, 643 (1952).

22. J. J. Loferski and P. P. Rappaport, Phys. Rev., 98, 1861 (1951).

23. R. L. Novak, Bull. Am. Phys. Soc., 8, 235 (1963).

24. E. G. Wikner, H. Horiye, and J. W. Harrity, J. Phys. Soc. Japan, 18, Suppl. III, 222 (1963).

25. C. D. Clark, P. J. Kemmey, and E.W.J. Mitchell, Disc. Faraday Soc., 31, 96 (1961).

26. G. J. Dienes, J. Appl. Phys., 23, 1194 (1952).

27. D. S. Billington and J. H. Crawford, "Radiation Damage in Solids," (Princeton Univ. Press, New Jersey, 1961), p. 25.

28. M. W. Lucas and E.W.J. Mitchell, Carbon, 1, 345 (1964).

29. R. v. Jan and A. Seeger, Phys. Stat. Sol., 3, 465 (1963).

30. A. Sosin, Phys. Rev., 126, 1698 (1962).

31. D. T. Eggen and M. Laubenstein, Phys. Rev., 91, 238 (1953).

32. E. E. Klontz and J. W. MacKay, J. Phys. Soc. Japan, 18, Suppl. III, 216 (1963).

APPENDIX I

CRYSTALLOGRAPHIC DATA FOR V_6C_5

Structure factors for the ordered compound V_6C_5 have been calculated using atomic scattering factors for electrons. Some of these structure factors are used in the calculations described in Appendix II, but a more complete list is presented here since it may prove useful for others working in this area.

Two enantiomorphic forms of the V_6C_5 structure are possible, but $P3_1$ has been chosen arbitrarily for the calculations. In this space group, the coordinates of equivalent positions for all atoms are given by:

$$x,y,z;\ \bar{y},\ x-y,\ \frac{1}{3}+z;\ y-x,\ \bar{x},\ \frac{2}{3}+z,$$

where the values of x, y, z are those presented in Table 4.1. The positions of 18 vanadium atoms, 15 carbon atoms, and 3 carbon vacancies contained in a single unit of the triply primitive trigonal cell are shown in Table I.1.

TABLE I.1

Positions of vanadium atoms

0.44444,-0.11111,0.25
-0.22222,-0.44444,0.25
0.11111,0.22222,0.25
-0.22222,-0.11111,0.083333
0.44444,0.22222,0.083333
0.11111,-0.44444,0.0833333
1.11111,0.55555,0.58333
1.44444,0.22222,0.583383
0.77777,-0.11111,0.58333
1.11111,-0.11111,0.41666
0.77777,0.22222,0.41666
1.44444,0.55555,0.41666
0.44444,0.55555,0.91666
0.77777,1.22222,0.91666
1.11111,0.88888,0.91666
1.1111111,1.22222222,0.75
0.77777,0.55555,0.75
0.44444,0.88888,0.75

Positions of carbon atoms

0.11111,-0.44444,0.33333
-0.22222,-0.11111,0.33333
0.44444,0.22222,0.33333
-0.22222,0.22222,0.16666
0.44444,0.55555,0.16666
1.44444,0.55555,0.66666
1.11111,-0.11111,0.66666
0.77777,0.22222,0.66666
0.77777,-0.44444,0.5
0.44444,-0.11111,0.5
0.44444,0.88888,1.0
1.11111,1.22222,1.0
0.77777,0.55555,1.0
1.44444,1.22222,0.833333
1.11111,0.55555,0.83333

TABLE I.1 - cont'd.

Positions of carbon vacancies

0.11111,-0.11111,0.16666
1.11111,0.22222,0.5
0.77777,0.88888,0.83333

Using these atomic positions and the atomic scattering factors for electrons contained in the International Tables for X-Ray Crystallography[1], the structure factors were computed from equation (6.10) with a program generously provided by D. Kahn of RIAS. The results, along with appropriate d spacings, are presented in Table I.2, where the hexagonal indices, H K L, have been used to label all reflections. For some purposes it is convenient to use the cubic indices, h k l, for the primary reflections, in which case the following transformation matrices are useful:

$$\begin{bmatrix} h \\ k \\ l \end{bmatrix} = \begin{bmatrix} -\frac{2}{3} & 0 & -\frac{1}{6} \\ 0 & -\frac{2}{3} & -\frac{1}{6} \\ \frac{2}{3} & \frac{2}{3} & -\frac{1}{6} \end{bmatrix} \cdot \begin{bmatrix} H \\ K \\ L \end{bmatrix}$$

(cubic) (hex.)

$$\begin{bmatrix} H \\ K \\ L \end{bmatrix} = \begin{bmatrix} -1 & \frac{1}{2} & \frac{1}{2} \\ \frac{1}{2} & -1 & \frac{1}{2} \\ -2 & -2 & -2 \end{bmatrix} \cdot \begin{bmatrix} h \\ k \\ l \end{bmatrix}$$

(hex.) (cubic)

TABLE I.2

STRUCTURE FACTORS FOR V_6C_5

(ELECTRON SCATTERING)

H	K	L	D	F(HKL)
0	0	3	4.8000	20.2098
1	0	0	4.4200	11.5120
1	0	1	4.2150	11.4131
1	0	2	3.7950	11.1832
0	0	4	3.6000	0.0000
1	0	3	3.2460	10.7127
0	0	5	2.8800	0.0000
1	0	4	2.7880	9.7923
1	1	0	2.5450	0.0016
1	1	1	2.5060	0.0023
1	1	-1	2.5060	15.6907
1	0	5	2.4110	8.8047
1	1	2	2.4000	163.1550
0	0	6	2.4000	163.1550
1	1	3	2.2480	0.0021
1	1	-3	2.2480	0.0035
2	0	0	2.2040	8.1755
2	0	1	2.1800	8.0979
1	0	6	2.1080	7.8428
2	0	2	2.1080	7.8425
1	1	4	2.0780	0.0013
1	1	-4	2.0780	270.1859
0	0	7	2.0570	0.0000
2	0	3	2.0030	7.4432

TABLE I.2 (cont'd.)

H	K	L	D	F(HKL)
1	1	5	1.9070	12.2576
2	0	4	1.8800	6.9674
1	0	7	1.8640	6.9001
0	0	8	1.8000	0.0000
2	0	5	1.7500	6.3899
1	1	6	1.7460	0.0013
1	1	-6	1.7460	0.0013
2	1	0	1.6666	5.9759
1	0	8	1.6666	5.9741
2	1	1	1.6555	5.9239
2	1	2	1.6230	5.7816
2	0	6	1.6230	5.7833
1	1	7	1.6000	0.0023
0	0	9	1.6000	9.8355
1	1	-7	1.6000	9.8302
2	1	3	1.5740	5.5555
2	1	4	1.5120	5.2409
1	0	9	1.5040	5.1999
2	0	7	1.5040	5.1987
1	1	8	1.4690	177.5514
3	0	0	1.4690	177.5514
3	0	1	1.4620	0.0036
3	0	-1	1.4620	0.0036
2	1	5	1.4420	4.8584
3	0	2	1.4400	0.0018
0	0	10	1.4400	0.0000
3	0	-2	1.4400	0.0018
3	0	3	1.4050	8.0839
2	0	8	1.3940	4.6185
1	0	10	1.3690	4.4961
2	1	6	1.3690	4.4959
3	0	4	1.3600	0.0014
3	0	-4	1.3600	0.0014
1	1	-9	1.3540	0.0011
1	1	9	1.3540	0.0019
3	0	5	1.3090	0.0019
3	0	-5	1.3090	0.0019
2	1	7	1.2950	4.1036
2	0	9	1.2950	4.1057
2	2	0	1.2725	0.0014
2	2	1	1.2676	6.8402
1	1	10	1.2533	0.0009

TABLE I.2 (cont'd.)

H	K	L	D	F(HKL)
1	1	-10	1.2533	76.0302
2	2	2	1.2531	0.0017
3	0	6	1.2531	76.0151
-3	0	6	1.2531	76.0151
2	2	2	1.2531	0.0017
3	0	6	1.2531	76.0151
2	2	3	1.2300	0.0033
2	1	8	1.2227	3.7148
3	1	10	1.2226	3.7142
3	1	1	1.2182	3.6911
2	0	10	1.2055	3.6297
2	0	10	1.2055	3.6297
3	1	2	1.2053	3.6303
3	1	2	1.2053	3.6303
0	0	12	1.2000	134.8800
2	2	4	1.1997	134.8331
3	0	7	1.1957	0.0017
3	0	7	1.1957	0.0017
3	1	3	1.1847	3.5227
2	2	5	1.1639	0.0030
3	1	4	1.1576	3.3804
2	1	9	1.1540	3.3600
3	0	8	1.1383	0.0011
3	1	5	1.1254	3.2015
2	2	6	1.1242	0.0015
4	0	0	1.1020	3.0756
0	4	1	1.0988	3.0582
4	0	1	1.0988	3.0589
2	1	10	1.0895	3.0165
3	1	6	1.0894	3.0143
4	0	2	1.0893	3.0154
3	0	10	1.0824	0.0012
3	0	9	1.0822	5.1638
2	2	7	1.0822	5.1606
4	0	3	1.0741	2.9403
4	0	4	1.0537	2.8375
3	1	7	1.0510	2.8246
2	2	-8	1.0391	108.7093
2	2	8	1.0391	0.0011
2	2	8	1.0391	0.0011
4	0	5	1.0292	2.7099

TABLE I.2 (cont'd.)

H	K	L	D	F(HKL)
3	1	8	1.0113	2.6101
3	2	0	1.0113	2.6092
3	2	1	1.0088	2.5961
3	2	2	1.0014	2.5542
2	2	9	0.9959	0.0015
3	2	3	0.9896	2.5011
3	2	4	0.9736	2.4334
3	1	9	0.9714	2.4252
4	1	0	0.9619	0.0013
3	2	5	0.9542	2.3452
3	2	5	0.9540	2.3443
2	2	10	0.9535	54.3587
4	1	2	0.9534	54.3508
3	1	10	0.9320	2.2425
3	1	10	0.9320	2.2425
-3	0	-12	0.9294	91.0313
4	1	4	0.9293	0.0012
-2	1	-16	0.8485	78.6624
0	0	-18	0.8000	41.8050
-4	2	-14	0.7999	41.7959
3	3	-12	0.6930	55.0439

REFERENCES

(1). "International Tables for X-Ray Crystallography," Vol. I, ed. N.F.M. Henry and K. Lonsdale (Kynoch Press, Birmingham, England, 1952).

APPENDIX II

RELATIONSHIP BETWEEN THE INTENSITY OF A SUPERLATTICE DIFFRACTION SPOT AND ITS STRUCTURE FACTOR

In Chapter Six, a relationship describing intensity changes of a V_6C_5 superlattice spot during electron microscope beam bombardment was derived under the assumption that the intensity of a diffracted beam, I_g, is proportional to the square of the structure factor, F_g, appropriate to the particular reflection, g, employed:

$$I_g \alpha |F_g|^2. \qquad \text{(II.1)}$$

Although (II.1) is correct for X-ray diffraction, its applicability for electron diffraction must be justified for the relevant experimental conditions. Accordingly, the dynamical theory of electron diffraction has been employed to calculate superlattice spot intensities for a V_6C_5 crystal under conditions which simulate radiation induced disordering.

All quantitative measurements of the disordering rate were obtained from superlattice spots of the type 200 (indices referred to hexagonal axes). In each case, the sample orientation was adjusted to satisfy the condition that the deviation parameter $s = 0$ for an adjacent 300 primary reflection as shown in fig. II.1. Under these

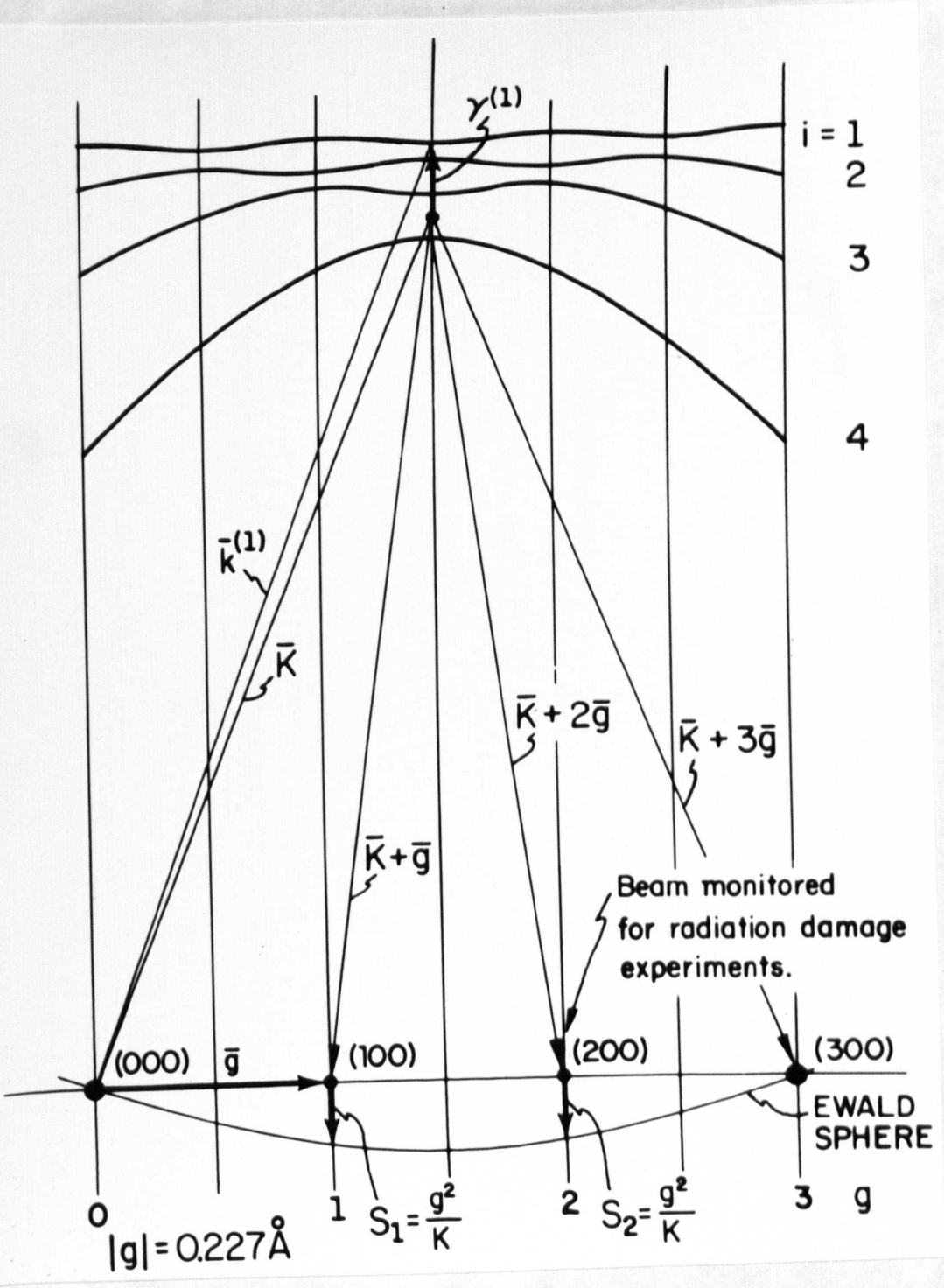

Fig. II.1. Dispersion surface and reflecting sphere construction corresponding to the four beams excited during radiation damage experiments.

circumstances, the four beams shown in the figure exhibit appreciable intensities and must therefore be included in the calculations. The general matrix formulation of many beam theory[1] provides a convenient method for handling such computations.

In this formulation, an eigenvalue equation of the form

$$AC^{(i)} - \gamma^{(i)}C^{(i)} = 0 \qquad \text{(II.2)}$$

expresses the relationship between (1) the $C_g^{(i)}$ Bloch wave amplitudes contained in the column vector $C^{(i)}$, (2) the dynamical scattering potentials $A_{gh} = U_{g-h}/2K$ (K is the incident wave vector) which appear as the off-diagonal elements of the square matrix A, (3) the deviation parameters which appear as the diagonal components, $A_{gg} = s_g$, and (4) the eigenvalues, $\gamma^{(i)} \simeq k_z^{(i)} - K$, where $k_z^{(i)}$ is the z component of the zero order wave vector associated with the i^{th} Bloch wave as shown in fig. II.1. Solutions to equation II.2 may be used to compute the intensity of the g^{th} diffracted beam from the relationship,

$$I_g = \sum_i \left(C_o^{(i)} C_g^{(i)}\right)^2 + \sum_{j \neq i} \sum_i \left(C_o^{(i)} C_g^{(i)}\right)\left(C_o^{(j)} C_g^{(j)}\right) \cos 2\pi\left(\gamma^{(i)} - \gamma^{(j)}\right)t \qquad \text{(II.3)}$$

where the summations in both i and j are over the Bloch wave indices, and t is the sample thickness.

The proportionality between the dynamical potentials and structure factors, $U_g = F_g/\pi V_c$, where V_c is the volume of the unit cell, makes it evident that the validity of II.1 may be tested by examining the relationship between I_g and U_g. Thus, the intensity of the 200 superlattice reflection, I_2, has been calculated as a function of the dynamical potential, U_2, over the range of intensities encountered in the radiation damage experiments.

The matrix, A, which corresponds to the four beam case depicted in fig. II.1 is given by

$$A = \begin{bmatrix} 0 & U_1/2K & U_2/2K & U_3/2K \\ U_1/2K & s_1 = g^2/K & U_1/2K & U_2/2K \\ U_2/2K & U_1/2K & s_2 = g^2/K & U_1/2K \\ U_3/2K & U_2/2K & U_1/2K & 0 \end{bmatrix}$$

where the substitution $U_g = U_{-g}$ follows from symmetry considerations. As a starting point for the calculations, values of U_1, U_2, and U_3 were determined from the structure factors tabulated in Table I.2 and I_2 was computed for the perfectly ordered structure. To simulate disordering, the values of the superlattice potentials, U_1 and U_2, were reduced in proportion by small increments while the value of the primary potential, U_3, was held fixed. (The magnitude of U_3 changes by less than 4% when the long range order paramenter is

reduced from one to zero.) Since the range of the measured intensities extends over an order of magnitude, the computations were continued until the calculated intensity was decreased to one-tenth of its initial value.

Using estimated sample thicknesses of t = 1000 Å for 33.0 and 47.3 kV, and t = 2000 Å for 79.9 and 100 kV, the relationship between I_2 and U_2 was determined in this manner for the four values of incident electron energies used in the measurements. The resulting curves, shown in fig. II.2, exhibit slight deviations from a square-law dependence, however their average slopes correspond closely to a value of two. Because only the average values of the slopes are important for the radiation damage experiments (see fig. 7.2), it is concluded that the proportionality assumed between the intensity of the 200 superlattice spot and the square of its structure factor is a valid approximation for the experimental conditions employed.

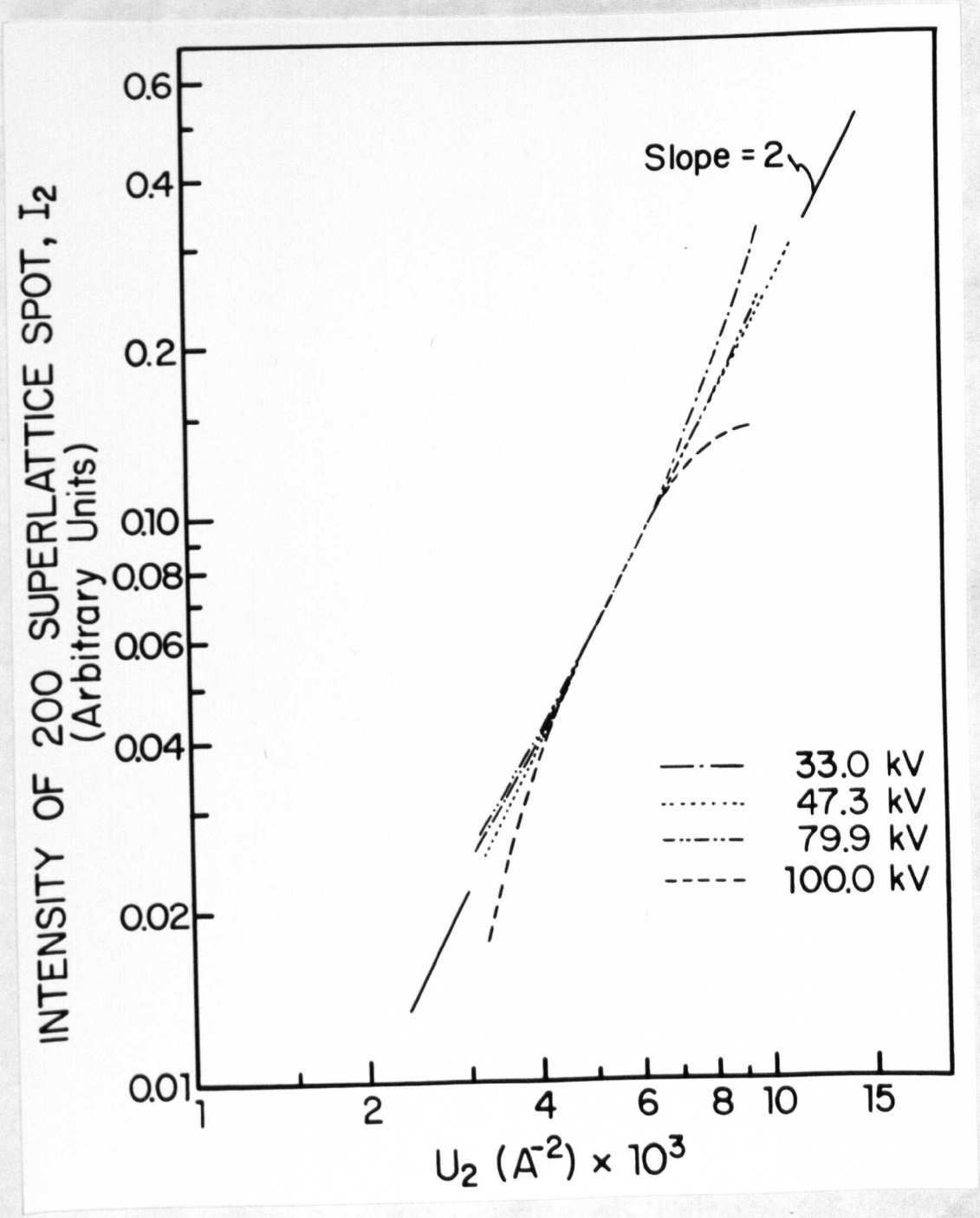

Fig. II.2. Calculated intensity of the 200 superlattice reflections, I_2, as a function of the dynamical potential U_2. The curves, which span the range of intensities encountered in the radiation damage experiments, have been normalized to an intensity of 0.10.

REFERENCES

1. P. B. Hirsch, A. Howie, R. B. Nicholson, D. W. Pashley, and M. J. Whelan, "Electron Microscopy of Thin Crystals," (Butterworths, London, 1965).

APPENDIX III

BIBLIOGRAPHY

Adelsberg, L. M. and Cadoff, L. H., J. Am. Ceram. Soc., 51, 213 (1968).

Amelinckx, S., in "Radiation Damage in Solids," ed. D. S. Billington, (Academic Press, New York, 1962).

Bennemann, K. H., Phys. Rev., 137, A1497 (1965).

Billington, D. S. and Crawford, J. H., "Radiation Damage in Solids," (Princeton Univ. Press, New Jersey, 1961).

Bilz, H., Z. Physik, 153, 338 (1958).

Borrmann, G., in "Trends in Atomic Physics," ed. O. R. Frisch, F. A. Paneth, F. Lanes, and P. Rosabud (Interscience, New York, 1959).

Bragg, W. L. and Williams, E. J., Proc. Roy. Soc., A151, 540 (1935).

Brown, W. L. and Augustyniak, W. M., J. Appl. Phys., 30, 1300 (1959).

Childs, W. J., Phys. Rev., 156, 71 (1967).

Clark, C. D., Kemmey, P. J., and Mitchell, E.W.J., Disc. Faraday Soc., 31, 96 (1961).

Corbett, J. W., in "Solid State Physics," ed. F. Seitz and D. Turnbull, supplement to Vol. 7, (Academic Press, New York, 1956).

Corbett, J. W., Denney, J. M., Fiske, M. D., and Walker, R. M., Phys. Rev., 108, 954 (1957).

Denney, J. M., Phys. Rev., 92, 531 (1953).

de Novion, C. H., Lorenzelli, R., and Costa, P., Compt. Rend., 263, 775 (1966).

Dienes, G. J., J. Appl. Phys., 23, 1194 (1952).

Dienes, G. J. and Vineyard, G. H., "Radiation Effects in Solids," (Interscience, London, 1957).

Dobson, P. S., Kritzinger S., and Smallman, R. E., Phil. Mag., 17, 769 (1968).

Eggen, D. T. and Laubenstein, M., Phys. Rev., 91, 238 (1953).

Eremeev, V. S. and Panov, A. S., Porosh. Met., 7, 65 (1967).

Erginsoy, C., Vineyard, G. H., and Engler, A., Phys. Rev., 133, A595 (1964).

Froidevaux, D. and Rossier, D., J. Phys. Chem. Solids, 28, 1197 (1967).

Gevers, R., Van Landuyt, J., and Amelinckx, S., Phys. Stat. Sol., 11, 689 (1965).

Gibson, J. B., Goland, A. N., Milgran, M., and Vineyard, G. H., Phys. Rev., 120, 1229 (1960).

Goldschmidt, H. J., "Interstitial Alloys," (Plenum Press, New York, 1967).

Gorbunov, N. S., Shishakov, N. A., and Saidkov, C. G., Izv. Akad. Nauk. SSSR, 11, 2093 (1961).

Goretzki, H., Phys. Stat. Sol., 20, K141 (1967).

Harrison, W. and Seitz, F., Phys. Rev., 98, 1530 (1955).

Hashimoto, H., Howie, A., and Whelan, M. J., Phil. Mag., 5, 967 (1960).

Hashimoto, H., Howie, A., and Whelan, M. J., Proc. Roy. Soc., A269, 80 (1962).

Heidenreich, R. D., "Fundamentals of Transmission Electron Microscopy," (Interscience, New York, 1964).

Hirsch, P. B., Howie, A., Nicholson, R. B., Pashley, D. W., and Whelan, M. J., "Electron Microscopy of Thin Crystals," (Butterworths, London, 1965).

Hollox, G. E., Mat. Science Eng., 3, 121 (1968).

Hollox, G. E. and Venables, J. D., Proc. Intl. Conf. on Strength of Metals and Alloys, Tokyo, in Suppl. Trans. Japan. Inst. Metals, 9, 295 (1968).

Howie, A., Proc. Roy. Soc., A271, 268 (1963).

Humphreys, C. J. and Hirsch, P. B., Phil. Mag., 18, 115 (1968).

"International Tables for X-ray Crystallography," Vol. I, edited by N.F.M. Henry and K. Lonsdale. (Kynoch Press, Birmingham, England, 1952.)

Johnson, R. A., Phys. Rev., 145, 423 (1966).

Kentworthy, H. M. and Neeley, H. H., North American Aviation Rept. NAA-SR-1580 (Aug. 1, 1956).

Kieffer, R. and Benesovsky, F., "Hartsoffe," (Springer-Verlag, Vienna, 1963).

Klontz, E. E. and Lark-Horovitz, K., Phys. Rev., 82, 763 (1951).

Klontz, E. E. and Lark-Horovitz, K., Phys. Rev., 86, 643 (1952).

Klontz, E. E. and MacKay, J. W., J. Phys. Soc. Japan, 18, Suppl. III, 216 (1963).

Kronberg, M. L., Acta Met., 5, 507 (1951).

Loferski, J. J. and Rappaport, P., Phys. Rev., 82, 763 (1951).

Loferski, J. J. and Rappaport, P., Phys. Rev., 111, 435 (1958).

Loferski, J. J. and Rappaport, P., J. Appl. Phys., 30, 1296 (1959).

Lowndes, D. H., Finegold, L., and Lye, R. G., Phil. Mag., 21, 245 (1970).

Lucas, M. W. and Mitchell, E.W.J., Carbon, 1, 345 (1964).

Lucasson, P. G. and Walker, R. M., Phys. Rev., 127, 485 (1962).

Lye, R. G., in "Atomic and Electronic Structure of Metals," (ASM, Cleveland, Ohio, 1967).

Lye, R. G., Hollox, G. E., and Venables, J. D., in "Anisotropy in Single Crystal Refractory Compounds," Vol. 2, ed. F. W. Vahldiek and S. A. Mersol, (Plenum Press, New York, 1968).

Lye, R. G. and Logothetis, E. M., Phys. Rev., 147, 622 (1966).

Makin, M. J. and Sharp, J. V., J. Mat. Science, 3, 360 (1968).

Marcinkowski, M. J. and Chessin, H., Phil. Mag., 10, 837 (1964).

McKinley, W. A. and Feshbach, H., Phys. Rev., 74, 1759 (1948).

McLaren, A. C. and Phakey, P. P., Phys. Stat. Sol., 13, 413 (1966).

Mott, N. F., Proc. Roy. Soc., A124, 426 (1929).

Muto, T. and Takagi, Y., in "Solid State Physics," ed. F. Seitz and D. Turnbull, Vol. 1 (Academic Press, New York, 1956).

Neufeld, J. and Snyder, W. S., Phys. Rev., 99, 1326 (1955).

Noggle, T. S. and Barrett, J. H., Phys. Stat. Sol., 36, 761 (1969).

Novak, R. L., Bull. Am. Phys. Soc., 8, 235 (1963).

Pashley, D. W. and Presland, A.E.B., J. Inst. Metals, 87, 419 (1959).

Pashley, D. W. and Presland, A.E.B., Phil. Mag., 6, 1003 (1961).

Precht, W. and Hollox, G. E., J. Crystal Growth, 3,4, 818 (1968).

Robins, D. A., Powder Metallurgy, No. 1/2, 172 (1958).

Rowcliffe, D. J., Ph.D. dissertation, "The Mechanical Properties of Transition Metal Carbides," University of Cambridge (1965).

Rutherford, E., Phil. Mag., 21, 669 (1911).

Schulman, J. H. and Compton, W. D., "Color Centers in Solids," (Pergamon Press, New York, 1962).

Schwartzkopf, P. and Kieffer, R., "Refractory Hard Metals," (The Macmillan Co., New York, 1958).

Seitz, F., Rev. Mod. Phys., 26, 81 (1954).

Seitz, F. and Koehler, J. S., in "Solid State Physics," ed. F. Seitz and D. Turnbull, Vol. 2 (Academic Press, New York, 1956).

Smirnov, L. S. and Glazunov, P. A., Soviet Phys. Solid State (English Translation), 1, 1262 (1960).

Snyder, W. S. and Neufeld, J., Phys. Rev., 97, 1636 (1955).

Sosin, A., Phys. Rev., 126, 1698 (1962).

Storms, E. K., "The Refractory Carbides," (Academic Press, New York, 1967).

Storms, E. K., in "Fundamentals of Refractory Compounds," ed. H. H. Hausner and M. G. Bowman, (Plenum Press, New York, 1968).

Thomas, G., Trans. Metall. Soc. A.I.M.E., 233, 1608 (1965).

Torkar, K., Oel, H., and Illingen, A., Berichte der Deutchen Keramischen Gesellshaft, 43, 162 (1966).

v. Jan, R. and Seeger, A., Phys. Stat. Sol., 3, 465 (1963).

van Landuyt, J., Gevers, R., and Amelinckx, S., Phys. Stat. Sol., 7, 519 (1964).

van Landuyt, J., Gevers, R., and Amelinckx, S., Phys. Stat. Sol., 13, 467 (1966).

Varley, J.H.O., J. Nuclear Energy, 1, 30 (1954).

Vavilov, V. S., Smirnov, L. S., Galkin, G. N., Spitsyn, A. V., and Patskevich, V. M., Sov. Phys. - Tech. Phys. (English Translation), 1, 1805 (1957).

Walker, R. M., in "Radiation Damage in Solids," (Academic Press, New York, 1962).

Watenabe, M., Someya, T., and Nagahama, Y., "Fifth Intl. Congress for Electron Microscopy," Paper A-8, (Academic Press, New York, 1962).

Whelan, M. J., J. Appl. Phys., 36, 2099 (1965).

Wikner, E. G., Horiye, H., and Harrity, J. W., J. Phys. Soc. Japan, 18, Suppl. III, 222 (1963).

Williams, W. S., Science, 152, 34 (1966).

Williams, W. S. and Schaal, R. D., J. Appl. Phys., 33, 955 (1962).

Zubkov, V. G., Dubrovskaya, L. B., Gel'd, P. V., Tskhai, V. A., and Dorafeev, Y. A., Dokl. Akad. Nauk. SSSR, 184, 874 (1969).